DISS. ETH NO. 25762

Wood-Based and Wood-Templated Materials with Special Wettability

A thesis submitted to attain the degree of

DOCTOR OF SCIENCES of ETH ZURICH

(Dr. Sc. ETH Zurich)

presented by

Yaru Wang

M. Sc. Materials Science, Sichuan University

born on 13/07/1989

citizen of the People's Republic of China

accepted on the recommendation of

Prof. Dr. Ingo Burgert, ETH Zürich, examiner

Prof. Dr. Christoph Neinhuis, TU Dresden, co-examiner

Prof. Dr. Cordt Zollfrank, TU München, co-examiner

2019

Learn as if you were to live forever.

- Mahatma Gandhi

Abstract

The affinity of water to wood originates from the hygroscopic lignocellulose composition of wood. In addition, wood has capillaries and pores at the micro- and nanoscale, which promote the absorption of large quantities of water. The interactions between water and wood have great impacts on various properties of wood, such as dimensional stability, biodegradability, mechanical strength, and consequently the service life. Changing the wettability of wood is not only necessary to guarantee its durability and reliability as a construction material. It may also be of interest when expanding the application scope of wood, from traditional building materials to functional wood materials. Based on a smart utilization of both, wood chemistry and wood structure, the aim of this thesis is to develop wood-based and wood-templated materials with special wettabilities.

In nature, a multitude of plants and animals have developed special wetting phenomena fulfilling various functions. Understanding and mimicking the wetting principles of the biological models allow for fabricating wettability related functional materials. Here, we considered four biological wetting models to transfer to wood: the slippery surface of the pitcher plant, the wettability patterns of the desert beetle, the directional flow of water on the rice leaf, and the superhydrophobic surface of the lotus leaf.

The first part of this thesis addresses the water repellency of wood and the improvement of the durability of this highly hygroscopic material through the creation of a slippery wood surfaces inspired by pitcher plants. The approach focuses on the covalent attachment of liquid-like polymer chains upon a wood surface, previously coated with a conformal layer of silica. By avoiding the metastable Cassie-Baxter state, the modified slippery wood surface showed an improved underwater durability when compared to a classical superhydrophobic wood coating. Furthermore, the slippery wood surfaces exhibit low adhesion to protein, smudge, and bacteria.

The second part of the thesis is referring to the desert beetle and rice leaf models, to fabricate a wood composite with wetting patterns and directional flow of water (which is achieved through creating anisotropic wettability). It is shown that by taking advantage of wood anatomical structure, wettability patterns can be built upon spruce wood cross-sections through selective chemical modification: the sol-gel-derived ZnO micro-rods predominantly grow on early wood regions. Consequently, the early and late wood wettabilities differ due to the different chemical patterns. Anisotropic wetting is observed for droplets deposited on latewood because the water spreading across the growth ring is constrained by the hydrophobic early wood domains. This

part further includes a discussion on the potential applications of wood with wetting patterns and anisotropy in designing biphasic materials and controlling water droplet movement.

In the third part of this thesis, we demonstrate how the anatomical structure of beech wood can be exploited to design templates for the fabrication of superhydrophobic polydimethylsiloxane (PDMS) surfaces (lotus leaf wetting model). By taking advantage of the open pores of wood cross-sections, the hydrophobization of polymer surfaces is achieved through structuration by templating. The obtained polymer negative replica is structured with pillars of different aspect ratios, and the pillar heights correlate with the wettability of the structured PDMS surface. With an appropriate pillar size, the surface can achieve superhydrophobicity. This part emphasizes the role of wood structure in the fabrication of functional materials.

In this thesis, by combining bioinspiration and bio-based materials, and by exploiting the wood anatomical structure and the possibilities offered by chemical modification, we fabricated wood-based and wood-templated materials with special wettabilities. The development of new methods to control the wettability of wood materials can not only be used in traditional wood applications, but is also quite promising for developing innovative functional materials for fog collection, microfluidic manipulation, or antifogging glass.

Zusammenfassung

Die Affinität des Holzes gegenüber Wasser entspringt seiner Zusammensetzung aus hygroskopischer Lignocellulose. Zusätzlich begünstigen Holzporen und -kapillaren auf der Mikro- und Nanoskala die Adsorption von grossen Wassermengen. Die Wasser-Holz Interaktionen beeinflussen Holzeigenschaften wie Dimensionsstabilität, Bioabbaubarkeit, mechanische Stabilität sowie die daraus resultierende Lebensdauer verschiedener Holzprodukte. Durch Veränderungen des Benetzungsverhaltens können nicht nur Dauerhaftigkeit und Zuverlässigkeit erhöht, sondern auch die Bandbreite und Einsatzmöglichkeiten von Holz erweitert werden, sei es als Baustoff oder funktionales Material. Basierend auf einer intelligenten Nutzung des Holzes ist es das Ziel dieser Arbeit, holzbasierte Materialien mit speziellen Benetzbarkeiten zu entwickeln.

In der Natur finden sich verschiedene Tier- und Pflanzenarten, welche spezielle Benetzbarkeiten in Hinsicht auf verschiede Funktionen entwickelt haben. Das Verständnis und die Übertragung dieser biologischen Prinzipien in technische Anwendungen, erlaubt es, neue funktionale Materialien in Bezug auf die Benetzbarkeit herzustellen. In dieser Arbeit sollen Prinzipien von vier biologischen Vorbildern auf Holz angewendet werden: Die glatte Oberfläche von Kannenpflanzen, das Benetzungsmuster von Wüstenkäfern, der anisotrope Tropfenablauf der Blätter der Reispflanze und die superhydrophobe Oberfläche des Lotusblattes.

Im ersten Teil der Arbeit wird das Wasserabweisungsvermögen von Holz und die Erhöhung seiner Dauerhaftigkeit durch das Erschaffen rutschiger Oberflächen, inspiriert durch Kannenpflanzen, untersucht. Dieser Ansatz basiert auf einer kovalenten Bindung von Polymerketten auf eine zuvor mit Siliziumdioxid beschichtete Holzoberfläche. Das Verhindern eines metastabilen Cassie-Baxter Zustandes resultiert in einer glatten Holzoberfläche mit erhöhter Unterwasser-Dauerhaftigkeit im Vergleich zu herkömmlichen superhydrophoben Holzbeschichtungen. Die rutschigen Oberflächen verhindern des Weiteren die Adhäsion von Proteinen, Schmutz oder Bakterien.

Im zweiten Teil der Arbeit werden Holz-Komposite mit verschiedenen Benetzungsmustern und anisotroper Benetzbarkeit nach Vorbild eines Wüstenkäfers und von Reispflanzenblättern untersucht, welche einen gerichteten Flüssigkeitsablauf begünstigen sollen. Durch die Nutzung des anatomischen Holzaufbaus werden durch selektive chemische Modifikation, verschiedene Benetzungsmuster auf der Querschnittsfläche von Fichte erzeugt. Sol-Gel basierte Verfahren erlauben es, ZnO-Mikrostäbe auf Früholzregionen der Fichte wachsen zu lassen. Als

Konsequenz unterscheidet sich die Benetzbarkeit von Früh- und Spätholz dank der nun unterschiedlichen Oberflächenchemie. Anisotrope Benetzbarkeit von Wassertropfen, welche auf Spätholz aufgesetzt werden, konnte zudem beobachtet werden. Die hydrophoben Frühholzbereiche zwängen dabei den Wassertropfen ein. Des Weiteren wird im zweiten Teil über die mögliche Nutzung von Holz mit lokal verschiedenen Benetzbarkeitsmustern und Anisotropie als zweiphasiges Material diskutiert, welches die potentielle Fähigkeit besitzt, Wassertropfenbewegung an der Oberfläche zu steuern.

Im dritten Teil der Arbeit wird aufgezeigt, wie die Struktur von Buchenholz genutzt werden kann, um negative Template für superhydrophobe Polydimethylsiloxane (PDMS) Oberflächen, nach dem Vorbild von Lotusblättern, herzustellen. Die offenporige Struktur des Holzquerschnittes erlaubt es, beim negativen Replikat eine strukturierte Hydrophobierung der Polymeroberfläche zu erschaffen. Das Polymer-Negativ wird dabei mit Stäben unterschiedlicher Schlankheit ausgestattet, deren Höhen mit der Benetzbarkeit von strukturierten PDMS Oberflächen korrelieren. Mit der richtigen Stabhöhe kann auch eine Superhydrophobierung erreicht werden. In diesem dritten Teil werden besonders die Holzstruktur und ihre Rolle bei der Herstellung von funktionalen Materialien hervorgehoben.

Die Kombination von bio-inspirierten Ansätzen und bio-basierten Materialien sowie die spezifische Nutzung der holzanatomischen Struktur und deren chemische Modifikation, ermöglicht es, holzbasierte Materialien mit speziellen Benetzbarkeiten herzustellen. Die Entwicklung neuer Methoden zur Kontrolle der Benetzbarkeit von Holzmaterialien kann nicht nur in traditionellen Holzanwendungen von Vorteil sein, sondern ist auch vielversprechend für innovative und funktionale Anwendungen wie die Sammlung von Kondenswasser, die Mikrofluidik oder beschlagfreie Materialien.

Table of Contents

Abbreviation

ATRP: atom transfer radical polymerization

CA: contact angle

CAH: contact angle hysteresis

CML: compound middle lamella

DMDEOS: dimethyldimethoxysilane

EW: early wood

FITC-albumin: albumin fluorescein isothiocyanate conjugate

LBL: layer by layer

LW: late wood

ML: middle lamella

PDMS: polydimethylsiloxane

PEI-PDA: (polydopamine/polyethyleneimine)

PFDTS: perfluorodecyltriethoxysilane

PFPE: perfluoropolyether

PMMA: poly(methyl methacrylate)

POTS: 1H, 1H, 2H, 2H-Perfluorooctyltriethoxysilane

PS: polystyrene

SA: sliding angle or steric acid

SLIPS: slippery liquid-infused porous surface(s)

TEOS: tetraethyl orthosilicate

1. Introduction

1.1 Motivation and objectives

There is an urgent demand to develop sustainable materials substituting petroleum-based products,[1] to contribute to the sustainable development of our society. Biomass-based renewable raw materials will be undoubtedly part of the solution. Wood, consisting of the most abundant biopolymers on earth, has become one of the most promising materials for replacing non-renewable engineering materials manufactured with energy intensive processes.

For millennia, wood has been used as a building material by mankind. As a traditional construction and furniture material, wood is protected by various techniques to overcome its intrinsic limitations such as low resistance against microorganisms, dimensional instability, flammability and UV induced degradation.[2] Nowadays, research and application of wood materials involve a multidisciplinary effort with state of the art technologies to develop new opportunities. Modifying and functionalizing wood at nano- and microscales aims to develop bio-based functional materials of high-added value.[3] Consequently, the utilization of wood has been expanded from traditional construction materials to actuators,[4] wastewater treatment,[5, 6] semi-conductive wood,[7, 8] templates for ceramics,[9, 10, 11] magnetic wood,[12] light-transmitting materials, and transparent solar cell windows.[13]

In this thesis, we focus on an interesting research and application potential, namely the wettability of wood-based and wood-templated materials and their related functions. Wettability is a fundamental property of solids[14] and plays an important role in both academia and industry, related to ink printing, adhesives, textile and clothing, anticorrosion surfaces, antifouling coatings, mining or anti-icing of airplane surfaces.[15] Studying and developing special wettabilities on synthetic and bio-based materials is of high relevance. Water is a key ingredient of biological tissues, as it supports the functions and the properties of the living tissues. When the tissues die, water can still interact with the biological materials and have an impact on their properties and final applications. For wood, wetting properties are especially important as uptake and evaporation of moisture induce dimensional instability of wood. Additionally, microorganisms can attack wood when it has a certain water content.[2] For advanced wood-based materials, the interaction with water can be used advantageously: changes in relative humidity can act as a stimulus for wood bilayer actuation,[4] water-saturated wood can be used as an oil/water separating membrane,[5] or, due to the ability of the wood

structure to transport water through various anatomical features, filtering out bacteria to obtain drinkable water can be envisaged.[16]

In this thesis, the focus is on transferring bioinspired wetting models to wood materials, in order to improve the quality of the wood-based materials in traditional engineering fields and to expand their application scope to advanced functional materials. Some pioneering work on bioinspired wood mineralization[17] and bioinspired wood hydro-actuation[4] have ingeniously shown the potential of a transfer of the design principles from nature to wood materials, highlighting the advantages of the combination of "bioinspired concepts" and "bio-based resources". In this thesis, four biological models were considered, and the objectives described below were pursued.

Pitcher Plant inspired slippery surfaces

The carnivorous pitcher plant (*Nepenthes*) is known to have a slippery lubricated surface,[18] causing insects to slide down into the pitfall traps containing a digestive liquid.[19] Inspired by this model, Wong *et al*.,[20] developed "slippery liquid-infused porous surface(s)" (SLIPS) which can repel a wide range of low surface energy liquids and exhibit optical transparency, self-repairing ability, and pressure stability. Guo *et al.*[21] transferred SLIPS to wood by growing ZnO nanorods on wood surfaces and infusing the surface texture with a fluoro-lubricant. However, SLIPS faces the problem of lubricant depletion. To circumvent this issue, we aimed at modifying wood surface through the covalent bonding of lubricating agents, to achieve a slippery surface with water repellency and improved durability.

Desert beetle inspired wettability pattern

Tenebrionid beetles (*Stenocara sp.*) can collect water from fog due to ingenious wettability patterns on their back.[22] The integration of hydrophobic-hydrophilic regions on the same surface in close vicinity contributes to a fast water droplet nucleation and an efficient water drainage. The research on wettability patterns still needs further efforts in building up new fabrication approaches and exploring new applications. By exploiting the selective modification of early- and latewood on wood cross-sections, we have taken advantage of the specific wood growth ring structure to build up wetting patterns.

Rice leaf inspired directional flow of liquid

Due to its directional arrangement of micropapillae, [23] the rice leaf surface structure facilitates the rolling of water droplets in a preferred direction - along the leaf edge.[24] Manmade material

surfaces with artificial directional liquid rolling properties are often achieved by anisotropic wetting behavior, because both anisotropic wetting and the directional liquid flow can be generated by an aligned surface structure such as grooved channels. New developments of surfaces with special wettabilities offer many promises to further exploit the fabrication of surfaces with anisotropic wetting and liquid directional flow properties with scaling-up potential, low cost, and bio-compatibility.[25] With its natural anisotropy, the wood scaffold could be a potential substrate to create anisotropic wetting and possibly generate a directional rolling of water droplets. Using the wetting abovementioned patterns, we could also introduce anisotropic wettability on wood surfaces, and we explored the formation and application potentials of the anisotropic wetting.

Lotus leaf inspired superhydrophobic surfaces

The lotus leaf is the most well-known biological role model for superhydrophobic surfaces.[26] It exhibits a high water contact angle and a low contact angle hysteresis leading to a self-cleaning effect, obtained by the hierarchical surface roughness and hydrophobic waxes. Bioinspired superhydrophobic surfaces for technical applications face many challenges, such as surface mechanical robustness or fabrication costs.[27] Wood cross-sections can be interpreted as porous surfaces composed by bundles of open capillaries (cut wood cells). The idea was to create superhydrophobic polymer surfaces through structuration using wood cross-sections as templates. By controlling the polymer flow inside wood cell lumina, variable surface feature sizes could be achieved. These preliminary tests were aiming at a facile way for producing large superhydrophobic surfaces.

In summary, we aimed at developing the wood-based and wood-templated materials with special wettabilities, inspired by various biological role models:

- Pitcher plant-inspired slippery wood surface for wood protection against water,
- Desert beetle-inspired wood surface with wettability patterns,
- Rice leaf-inspired wood surface where water flows in a certain direction,
- Lotus leaf-inspired superhydrophobic polymer surfaces by wood templating.

The potential applications ranging from traditional building materials to functional materials such as fog collection panels or anti-wetting surfaces.

1.2 Outline of the thesis

This cumulative thesis mainly consists of three articles aiming at developing wood-based and wood-templated materials with bioinspired wetting properties/approaches. Prior to the three main manuscripts in Chapter 2, a brief introduction to wood anatomy and chemical composition is given in Chapter 1. Additionally, fundamentals about surface wetting and the special wetting phenomena of the respective biological role models are presented.

In Subchapter 2.1, the first article "Liquid-like SiO_2-g-PDMS coatings on wood surfaces with underwater durability, anti-fouling, anti-smudge, and self-healing properties"[28] is presented. In this study surfaces of wood veneers were modified for improved water resistance, antifouling, and self-healing properties.

In Subchapter 2.2, the second article "Wood composites with wettability patterns prepared by controlled and selective chemical modification of a three-dimensional wood scaffold"[29] shows the combination of structuration and chemical modification, to generate wettability patterns and anisotropic wettability, which leads to a directional flow of water (microfluidic manipulation).

In Subchapter 2.3, the third article "Beech cross-sections as a natural template to fabricate superhydrophobic surfaces"[30] is exploiting the wood scaffold as a template to manufacture superhydrophobic polymer surfaces.

A general discussion addressing the outcome and relevance of the publications and the future research possibilities is given in Chapter 3.

1.3 Wood structure and chemical composition

1.3.1 Hierarchical structure of wood

A tree trunk cross-section reveals a concentric arrangement of different tissues (Figure 1). From outside towards the center, it is composed of bark, cambium, sapwood, heartwood, and pith. Cambium is a thin layer of living cells that can divide outwards and inwards, differentiating into phloem tissue (bark) and xylem tissue (wood). Sapwood is the outer part of the wood. It transports water from the roots to the leaves.[2] The completely dead xylem in the center of the tree, often showing a darker color, belong to the so-called heartwood. The most central part of the tree is the pith, which is the remain from the early growth of the tree.

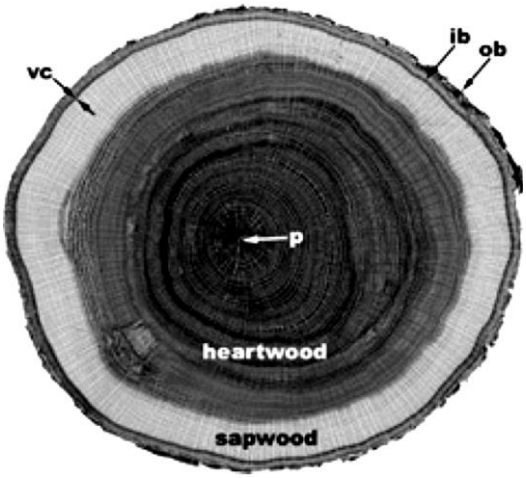

Figure 1. Cross-section of an oak (Quercus alba) trunk: from outside in, the image shows outer bark (ob), inner bark (ib), vascular cambium (vc), sapwood, heartwood and pith (p).[2]

As shown in Figure 2, wood possesses an anisotropic and hierarchical anatomical structure.[31] Wood can be considered as a cellular solid[32] composed of parallel capillaries (cells). Wood cells consist of lumen and wood cell walls. The cell morphologies vary in soft- and hardwood species. The wood cell wall is composed of concentric cell wall layers, which are characterized by different chemical compositions and orientations of the structural elements.[33]

In this section, the wood structures of particular relevance in this thesis are introduced, including the cell morphologies and their distributions, and the cell wall structure and its chemical composition.

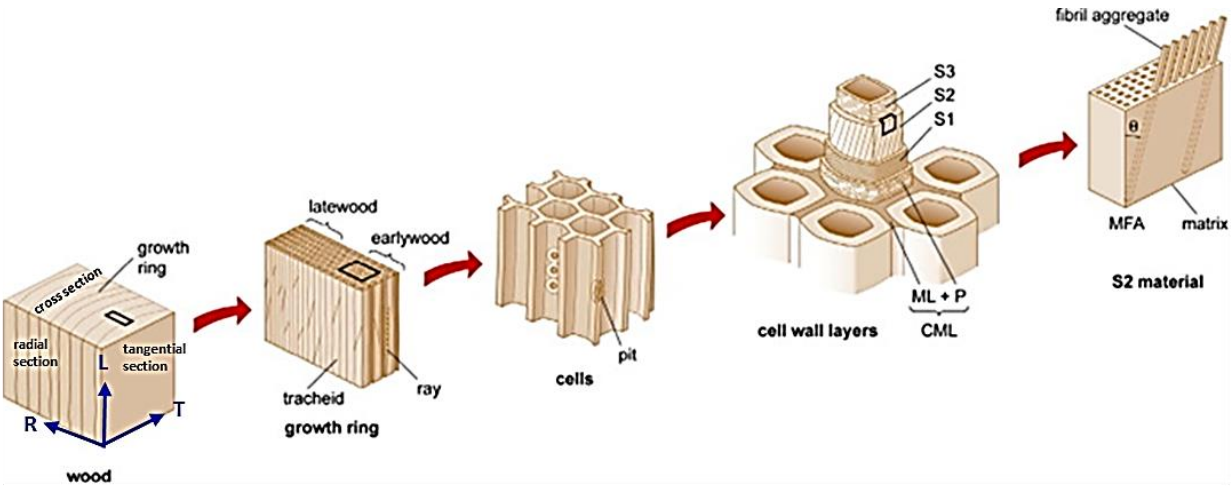

Figure 2. The hierarchical structure of wood. The picture is adapted from Rafsanjani et al.[34]

1.3.2 Wood cells

Cell types of hardwoods and softwoods

Softwoods are gymnosperms, while hardwoods are angiosperms. Microscopically, softwoods and hardwoods have different cell types (Figure 3).

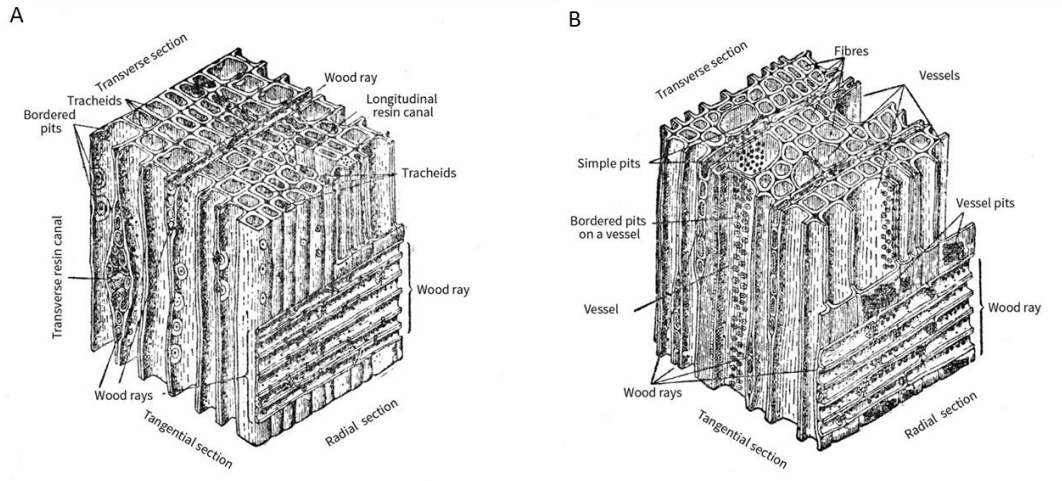

Figure 3. The a) soft- and b) hardwood tissues with different cell types.[35]

In softwoods, 90 to 95% of the cells are tracheids. Tracheids are tens of micrometers in diameter, several millimeters long and are mostly arranged along the longitudinal direction in the stem. Tracheids have two functions: transporting water from roots to leaves and supporting the wood mechanically.[36] Besides tracheids, some softwood species also have axial parenchyma cells (with smaller diameters when compared to tracheids). Radially, softwoods contain rays, which consist of ray parenchyma cells and in some species also ray tracheids. Rays are mainly

responsible for radial transport and storage. Some softwoods additionally possess resin canals with epithelial cells, which can secrete resins.[36]

Hardwoods (Figure 3b and Figure 4b) have different cell types than softwoods (Figure 3a and Figure 4a). The hardwood consists of fibers (15-50 µm in diameter),[37] vessels constructed from vessel elements (typically 50 up to 200 µm in diameter[2]), and axial parenchyma cells. The radial system of hardwood consists of ray parenchyma cells. As opposed to softwood rays, which are uniseriate, many hardwoods have both small rays and multiseriate rays. As a result, the rays of many hardwood species are easily detectable with naked eye.[38] Vessels are responsible for water conduction, the fibers in hardwood act as mechanical support and the parenchyma cells serve as storage cells.

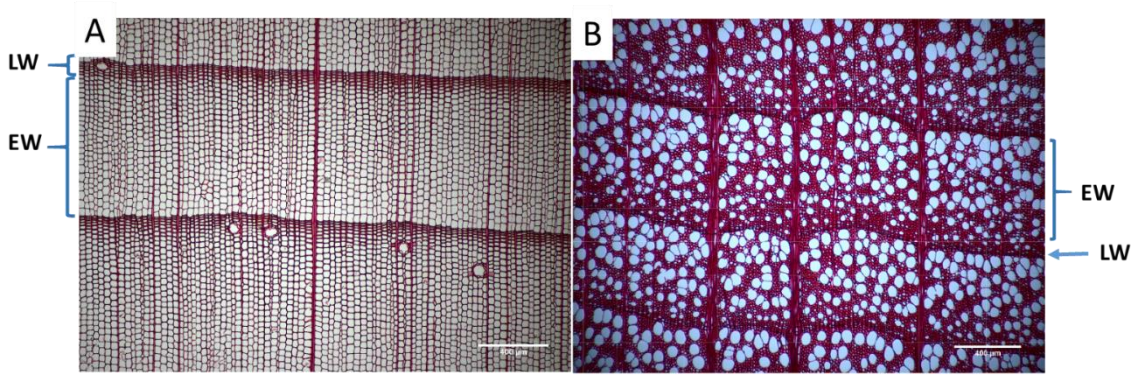

Figure 4. The early- and latewood of a) spruce (Picea abies) and b) beech (Fagus sylvatica). Pictures are adapted from Wang et al.[30]

The cells in wood are interconnected. For example, in both hardwood and softwood, the cell wall is decorated with pits (as shown in Figure 5). According to their structures, they can be classified as: simple pits (Figure 5b), bordered pits (Figure 5a), and half bordered pits. Pits are responsible for water transport in between adjacent cells. Vessel elements forming a vessel are connected by perforations which can be completely open (simple perforation plate) or appear as a plate with holes (scalariform perforation plate) (Figure 5c). Water can pass through the perforations to travel to another vessel element.

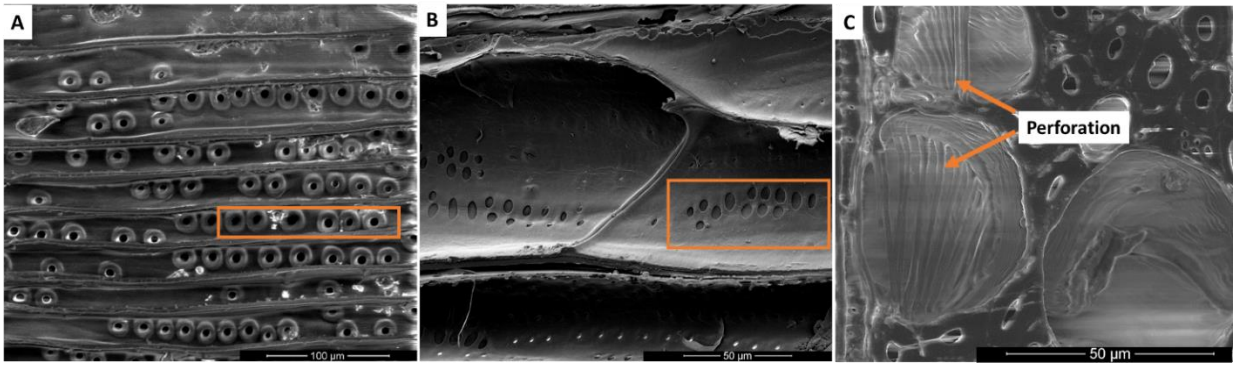

Figure 5. SEM images showing pits on the radial section of a) spruce (Picea abies) and b) beech (Fagus sylvatica), and c) the scalariform perforation plates of beech.

Cell morphologies and distribution in early and late wood

The new cells formed by the tree during one growth period are arranged in concentric rings called growth rings. Anatomical structure and volume of wood in one growth ring not only depend on the wood species, but also on the ecological factors from the tree environment, such as temperature and humidity. Growth rings can be divided into early wood (EW) and late wood (LW).

According to the vessel arrangement and distribution across the growth ring, hardwoods can be divided into three types: ring-porous wood, diffuse-porous wood and semi-ring-porous wood. In ring-porous wood, the EW forms a band of large vessels, while the vessels in LW are smaller. In a diffuse-porous wood (Figure 4b), vessels are distributed homogeneously over one growth ring. In semi-ring-porous wood, no obvious vessel bands are formed, but there is a gradual pore size change from larger vessels in the EW to smaller vessels in the LW.

For softwoods (Figure 4a), EW cells have a wide lumen and a thin cell wall, while LW cells have a narrow lumen and a thick cell wall. The EW to LW transition can be either abrupt or gradual. Besides the differences in cell morphologies, EW and LW have also different contents of holocellulose (cellulose and hemicelluloses) and lignin.[39] In terms of function, EW is mainly responsible for water transport while LW is responsible for mechanical support.[36]

1.3.3 Wood cell walls

Cell wall structure

Wood cell walls are divided into middle lamella (ML), primary cell wall and secondary cell wall (S1, S2, and S3 layers). Besides their spatial arrangement (see Figure 2), these tissues can

be differentiated by the orientation of cellulose fibrils (described by the microfibril angle, MFA) and the fractions of the biopolymers.[40]

The middle lamella and primary cell wall collectively are called compound middle lamella (CML). The middle lamella is 0.5-1.5 μm thick[41] and functions as binder between cells. The primary cell wall is 0.1-0.2 μm thick and the microfibrils form a random network in the outer layer, while in the interior layer, the microfibrils align nearly perpendicularly to the cell axis orientation.[42] The S1 layer in the secondary cell wall is an intermediate layer between the primary cell wall and the S2 layer. The S1 layer has a thickness of 0.1-0.35 μm with MFA of 60-80°.[41] The S2 layer is the thickest of all layers (1 - 10 μm in thickness). The microfibril angle in this layer is 5-30° or can be even higher in some specific wood tissues (e.g. compression wood).[41] The S3 layer directly facing the lumen has a thickness of around 0.1 μm with a MFA around 50-90°.[42]

Cell wall chemical composition

Wood is essentially composed of biopolymers, including cellulose (40-50%), hemicellulose (25-35%) and lignin (18-35%) and the rest being extractives and ashes (4-10%).[43] The cellulose microfibrils are coated with amorphous hemicellulose and embedded into lignin matrix.[44]

Cellulose

Cellulose, a polysaccharide of thousands of units of β (1→4) linked D-glucose (Figure 6), is the major component of wood cell walls.[33] The cellulose chains tend to form intra- and inter-molecular hydrogen bonds and are aggregated together, forming microfibrils.[42] These microfibrils can aggregate into macrofibrils in the cell wall.[45] Spaces between microfibrils are occupied by matrix substances.[46] Cellulose in wood is partially crystalline, it contains both crystalline regions and amorphous regions.

Natural cellulose is cellulose I in which cellulose chains are packed in parallel orientation whereas cellulose II has antiparallel packing.[47] Cellulose II is the most stable crystalline form[47] and cellulose I can be easily transformed into cellulose II by regeneration and mercerization.[48] There are also celluloses III and IV, which can be produced by certain chemical treatments and heating of celluloses I and II.[42]

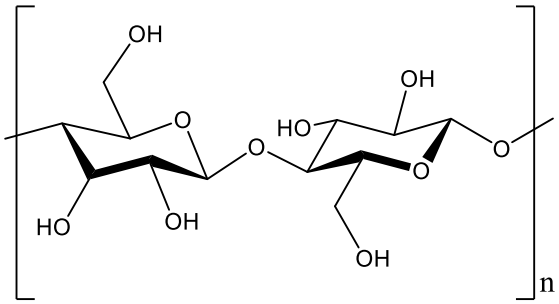

Figure 4. The molecular structure of cellulose.

Hemicelluloses

Hemicelluloses are generally branched heteropolymers that contain more than one type of monomeric sugar or sugar derivatives. The main monomeric components of hemicellulose are pentoses (D-xylose, L-arabinose, and L-rhamnose), hexoses (D-mannose, D-galactose, and D-glucose), and uronic acids.[36, 49] Their polymerization degree is lower than cellulose, usually around 100-200,[31] and the backbone can have multiple side chains as shown in Figure 7. Hemicelluloses are different in soft- and hardwoods. In softwoods, O-acetyl-galactoglucomannan is the principal hemicellulose component whereas the major components found in hardwoods are glucuronoxylans.[42] Hemicelluloses tether cellulose microfibrils to strengthen the cell wall.[50] Hemicelluloses are soluble in alkalis and thus can be removed from wood components by base extraction.

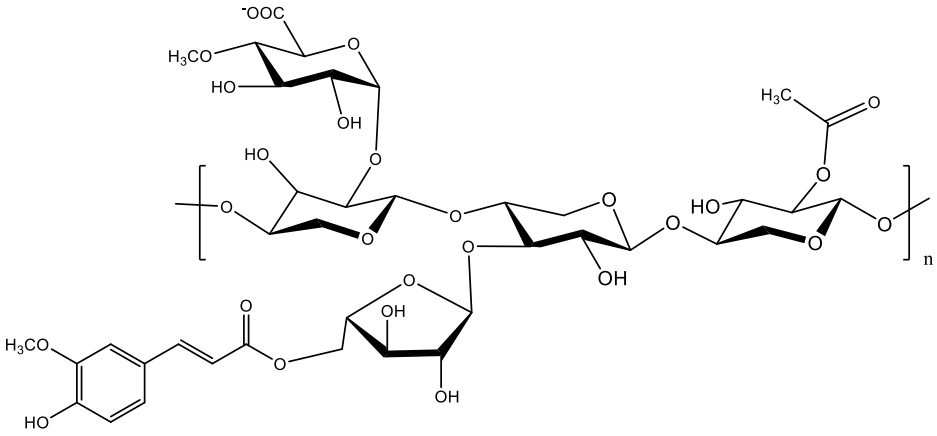

Figure 5. An example of hemicellulose (xylan).

Lignin

Lignin is a polyaromatic polymer composed of phenylpropane-based monomers with hydroxy- and methoxy-substitutions. The basic monolignols are paracoumaryl alcohol, sinapyl alcohol and coniferyl alcohol (Figure 8) which are bonded by alkyl-aryl ether or carbon-carbon bonds.

Lignin can reduce the water penetration into cell walls and make them more rigid.[51] Lignin is fragile towards oxidizing agents, which are typically used in delignification processes.

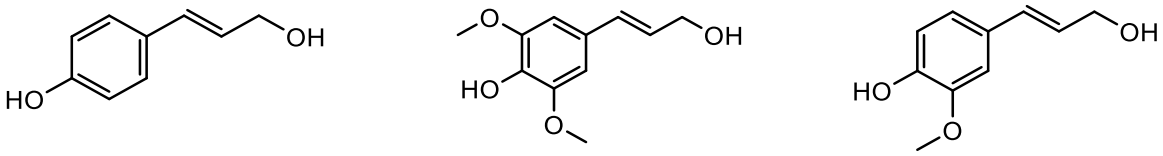

Figure 6. Three common monolignols: paracoumaryl alcohol, sinapyl alcohol, and coniferyl alcohol.

Extractives and ash

Wood also contains some minor amount of organics and inorganics, namely, extractives and ashes. Extractives comprise fats, waxes, alkaloids, proteins, phenolics, simple sugars, mucilages, gums, resins, terpenes, starches, glycosides, saponins, and essential oils.[43] Extractives are responsible for wood's color, odor, and decay resistance. They can be usually removed from wood by solvents using Soxhlet extraction.

Ash corresponds to the inorganic minerals in wood. It constitutes less than 1% of wood from temperate zones, slightly higher contents are found in tropical woods.[43]

1.4 Surface wetting fundamentals

1.4.1 Fundamental conceptions

Surface tension

The liquid molecules at the interface of liquid/air are different from the inner liquid molecules (shown in Figure 9). The surface liquid molecules have little attraction from the air molecules, and this cannot balance the strong attractions from the surrounding liquid molecules. Since the interface or surface molecules are not in a favorable energy state, the liquid adopts a shape resulting in the smallest surface area, in order to minimize the interactions with air. The surface tension is used to quantify the energy required to increase a unit surface area of a liquid isothermally and reversibly.[52] The surface tension of water at 20 ^{o}C is 72.8 mN·m^{-1}, which is higher than most other liquids because water molecules can form hydrogen bonds,[53] which increases the cohesion of water molecules. Contrarily, oils usually have low surface tensions. As an example, silicon oil has a surface tension around 20 mN·m^{-1} at 20 ^{o}C, while extremely low surface tension liquids such as fluoro-lubricants can have surface tensions below 20 mN·m^{-1} at 20 ^{o}C.

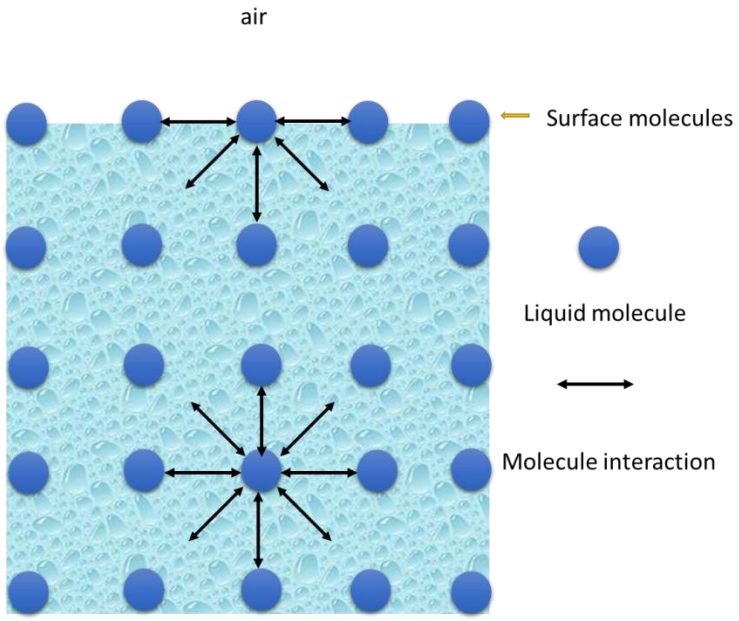

Figure 7. The origin of surface tension.

Surface energy

Surface energy can be understood as the work needed to create a new surface area or the energy difference between the bulk of the material and the surface of the material. Surface energy and surface tension have the same units[54] but surface tension is commonly used for liquids, while surface energy is used for solids. Some features of high and low surface energy surfaces are shown in table 1.

Table 1. High and low surface energy.

Surface energy	Energy Range	Chemical Group Types[55]	Examples[55]
High surface energy	500 - 5000 mN/m	Hydrophilic groups: polar group, H-bonding, ionized group	-OH, -NH_2, -COOH, -OSO_3H
Low surface energy	10 - 50 mN/m	Hydrophobic groups: non-polar	Hydrocarbons, silicones, fluorocarbons

Capillary action

Liquids can flow in narrow spaces, e.g. hollow spaces in porous materials, without the assistance of external forces. This phenomenon is called capillary action, and is related to cohesive and adhesive forces.[56]

Cohesion forces are the intermolecular forces of the liquid causing molecules to stick together, while adhesion forces are the forces governing the interaction between dissimilar molecules (such as a liquid and a solid substance, as shown in Figure 10). The capillary action is due to the fact that the liquid adhesion to the walls of the narrow capillary is stronger than the cohesive forces inside the liquid molecules. The capillary flow of liquids inside a porous material can be described with the Lucas-Washburn law:[57]

$$L^2 = \frac{\gamma \cos(\theta) r}{2\eta} t \qquad \textit{Eq. 1}$$

Where L is the liquid penetration length in the capillary, γ is the surface tension of the liquid, θ its contact angle with the capillary material, r is the capillary radius, η is the dynamic viscosity of the liquid, and t is the time of penetration.

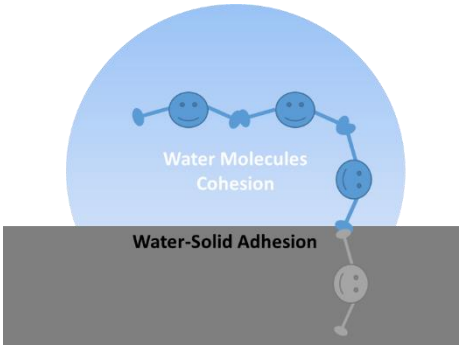

Figure 8. The difference between adhesion and cohesion.

1.4.2 Surface wetting and wetting modes

Wetting defines the solid-liquid intermolecular interaction when they are brought together.[58] Whether a solid can be wetted by liquids can be judged from the spreading parameter S:

$$S = \gamma_{SV} - (\gamma_{SL} + \gamma_{LV}) = \; k(\alpha_S - \alpha_L)\alpha_L \qquad \textit{Eq. 2}$$

Where γ_{SV} is the surface energy of the solid, γ_{LV} the surface tension of the liquid, and γ_{SL} the interfacial tension of the solid and liquid, k is a constant, α_S and α_L are the polarizability of the solid and liquid respectively.

If $S < 0$, the surface is partially wetted, and if $S > 0$, the surface is totally wetted. This equation also indicates that the surface tension of the liquid is not sufficient to predict the wettability: the surface energy of the solid surface and the liquid-solid interface tension also need to be taken into account. According to Eq. 2, one can judge the partial or total wetting from comparing the polarizabilities of the solid and liquid molecules. If the liquid is less polarizable than the solid, it will wet the solid completely.[59]

Ideal condition - Young's equation

The first mathematical description of surface wetting was proposed by Young in 1850:[60]

$$\gamma_{SV} = \gamma_{LV} \cdot \cos\theta_Y + \gamma_{SL} \qquad \textit{Eq. 3}$$

Where θ_Y is the static contact angle (or the equilibrium contact angle or the Young's contact angle).

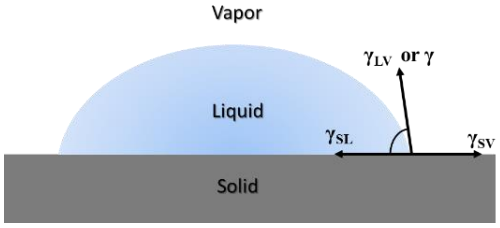

Figure 9. The equilibrium of the three surface tensions.

Young's equation[60] describes the equilibrium of the forces acting along the three-phase contact line shown in Figure 11. One needs to know that this basic model only applies to an ideal surface which is perfectly flat, rigid, chemically homogenous, and not interacting with the liquid.[61] However, in reality, solid surfaces are usually both rough and heterogeneous. Therefore, the Wenzel[62] and Cassie-Baxter[63] models were put forward to include the effects of surface roughness and chemical heterogeneity, respectively.

Wenzel State

The wetting of liquid on rough surfaces shown in Figure 12, was first described by Wenzel:[62]

$$\cos\theta^* = r\cos\theta_Y \qquad \textit{Eq. 4}$$

Where θ_Y is the Young's contact angle from Eq. 3 in ideal conditions, θ^* is the apparent contact angle (considering roughness), r is the roughness, defined as the ratio between the real surface area and the projected surface area. From this equation, we can get the following categories:

- $r \geq 1$ describes non-ideal surfaces. When r =1, we obtain the Young's equation.
- For an intrinsically hydrophobic material ($\theta > 90°$) when r ↑ , θ^* ↑ . Conversely, for an intrinsically hydrophilic material ($\theta < 90°$), when r ↑ , θ^* ↓ . Therefore, this equation predicts that the wettability effect (hydrophilicity or hydrophobicity) is enhanced by surface roughness.

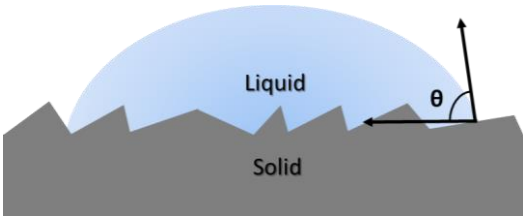

Figure 10. Droplet on a rough surface.

Cassie-Baxter State

Eight years after Wenzel, Cassie and Baxter described the wetting of liquids on porous surfaces (Figure 13).[63] Cassie-Baxter model deals with the liquid wetting of flat surfaces with chemical heterogeneity.[64] Such surfaces can be understood as chemical heterogeneous surfaces comprised of air and solid.

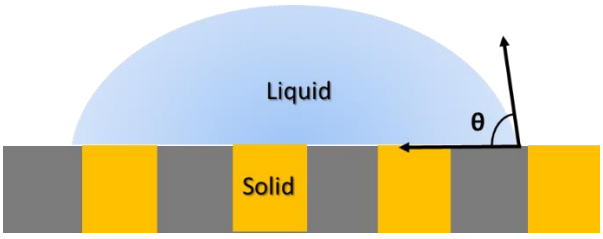

Figure 11. Droplets on a surface composed of constituents with different chemical properties (yellow and gray represent the different chemical species).

For example, the apparent CA of a surface containing composition 1 and 2 can be expressed as:

$$\cos\theta^* = f_1 \cos\theta_1 + f_2 \cos\theta_2 \qquad \textit{Eq. 5}$$

Where θ_1 and θ_2 are the Young's contact angles of the liquid on constituent 1 and 2 respectively, θ^* is the contact angle considering chemical heterogeneity, f_1 and f_2 are area fractions of constituent 1 and 2. If the second constituent is air, then θ_2 is 180° (perfectly non-wetting situation), and considering that $f_1 + f_2 = 1$, equation 5 becomes:

$$\cos\theta^* = f_1 \cos\theta_1 + (f_1 - 1) \qquad \textit{Eq. 6}$$

According to this equation, for intrinsically hydrophobic materials as well as intrinsically hydrophilic materials, if $f_1 \downarrow$, $\theta^* \uparrow$, indicating that the larger the air fraction, the larger the contact angle.

Wetting transition

As described above, the Cassie-Baxter state is usually obtained with structured surfaces allowing air entrapment. The Cassie-Baxter (Figure 14b) to Wenzel (Figure 14a) transition describes the invasion of the liquid into the rough surface to replace the trapped air.[65] The mechanism of the Cassie-Baxter to Wenzel transition is not fully understood. From Gibbs energy considerations, the Cassie-Baxter state is often metastable. The droplets can easily impale into the surface structure with perturbation such as hydraulic pressure[66] or vibration.[67] This transition is not desired for a stable superhydrophobic surface. In order to avoid this transition, the surface structures can be designed with hierarchical roughness and geometry to pin the solid-liquid-air triple phase line which can hinder the further penetration of liquid into the air pockets and enhance the stability.[68, 69] Vice versa, Wenzel state to Cassie-Baxter state is also possible, with the assistance of heating[70] or during droplet impingement.[71]

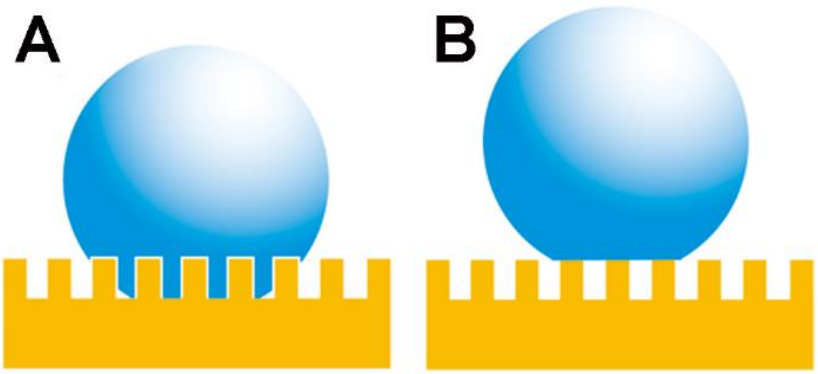

Figure 12. A) Wenzel model and B) Cassie-Baxter model.[72]

Combining equation 4 and 6, one can get the critical angle for Cassie-to-Wenzel transition:

$$\Phi \cos\theta_c + (\Phi - 1) = r \cos\theta_c \qquad \textit{Eq. 7}$$

In another form, $\cos\theta_c = \frac{\Phi - 1}{r - \Phi}$, where Φ is the solid fraction. When $\theta_Y > \theta_c$, the Cassie-Baxter mode is obtained. In Figure 15, this relation is illustrated in a plot.

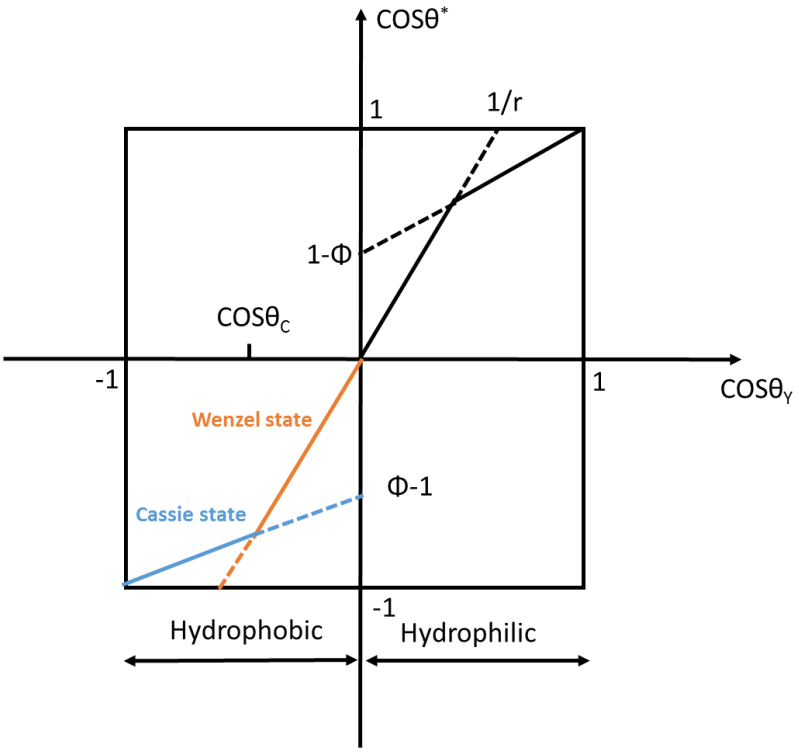

Figure 13. The relation between apparent contact angle and Young's contact angle.

1.4.3 Characterization methods

Quantities

The common characterization of surface wetting includes contact angle (CA), sliding angle (SA), advancing angle, receding angle and contact angle hysteresis (CAH).

Contact angle (obtained with drop shape analyzers) is used to quantitatively characterize the wetting of a solid by a liquid and has become a common and facile measure to study surface wettability.[15] Contact angle is a line property. This point is also shown later in Subchapter 2.2. Though the thermodynamic approach optimizes the free energy by counting the whole surface area underneath the droplet, Pease[73] pointed out that the liquid, solid, and air in contact is a one-dimensional system. The contact angle is determined by the contact line, rather than the contact area. Gao and McCarthy[74] supposed that wettability relates to the activation energies that need to be overcome for the contact line to move from one metastable state to another, during which the contact area is not relevant. Gao and McCarthy's experiment design[74] shown in Figure 16, demonstrates that the CA, in general, is not influenced by the area underneath the droplet.

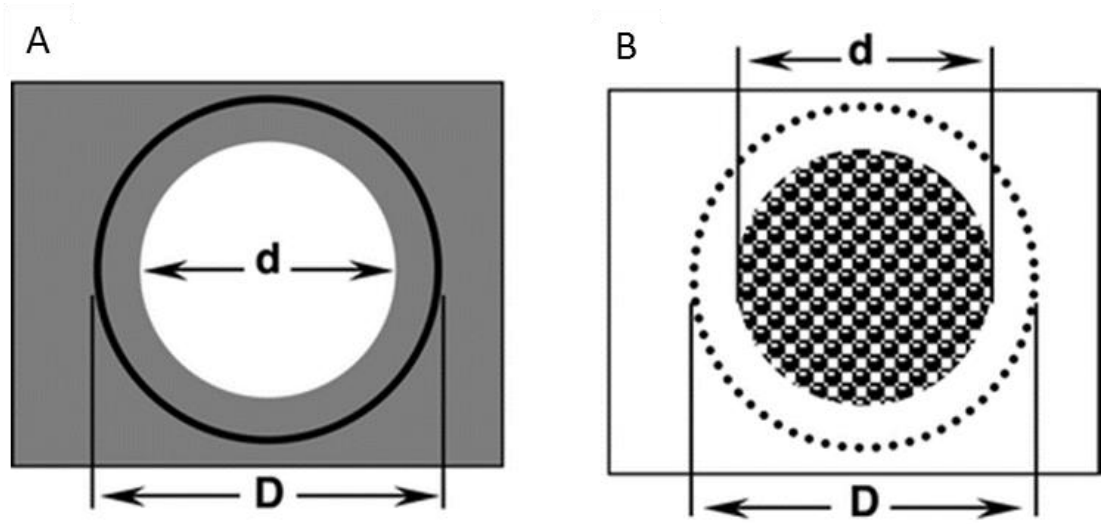

Figure 14. a) White hydrophilic spot on a gray hydrophobic silicon wafer, b) textured hydrophobic spot on a white hydrophilic wafer. d is the spot size of these "island" areas while D is the diameter of the droplet used in CA measurement. The results showed that for both case a and b, when D>d, the increasing of D within a range would not change the CA. This indicates that CA is not influenced by the area underneath the droplet.[74]

Sliding angle, also called roll-off angle, is the tilting angle of the testing stage when drops roll off the surface due to gravity. It represents the liquid resistance to mobility.[75] In tilting plate test, when a droplet starts to slide down in an asymmetric shape, the front angle driven by gravity is called the **advancing angle**, and the back contact angle opposing the driving force is

called the **receding angle**.[76] A low sliding angle is critical for self-cleaning purpose.[77] Sliding angles can be different by adopting different droplet sizes during the tilting plate test.

The difference between advancing and receding angle is called **contact angle hysteresis** (CAH = $\theta_A - \theta_R$). CAH is related to the surface roughness and heterogeneity.[68] Gao and McCarthy[78] explained it through thermodynamic analysis. Contact angle hysteresis reflects the activation energy that the droplet needs to move from one metastable state to another. The CA of a metastable droplet can be any value between the advancing and the receding contact angle.[78] This is one of the reasons why some researchers have emphasized the need to provide both advancing and receding contact angles when characterizing surface wettability.[78]

Testing methods

Needle-embedded sessile drop method

In sessile drop method, a drop is dispensed on the sample surface, and the drop profile is measured to get the static CA. In the needle-embedded sessile drop method[15] (Figure 17), the needle is buried in the liquid droplet. The droplet volume can be adjusted by adding more liquid or sucking it out while measuring the CAs. The threshold contact angles when the contact line moves by increasing and decreasing the volumes of the droplet are the advancing and receding angles, respectively.

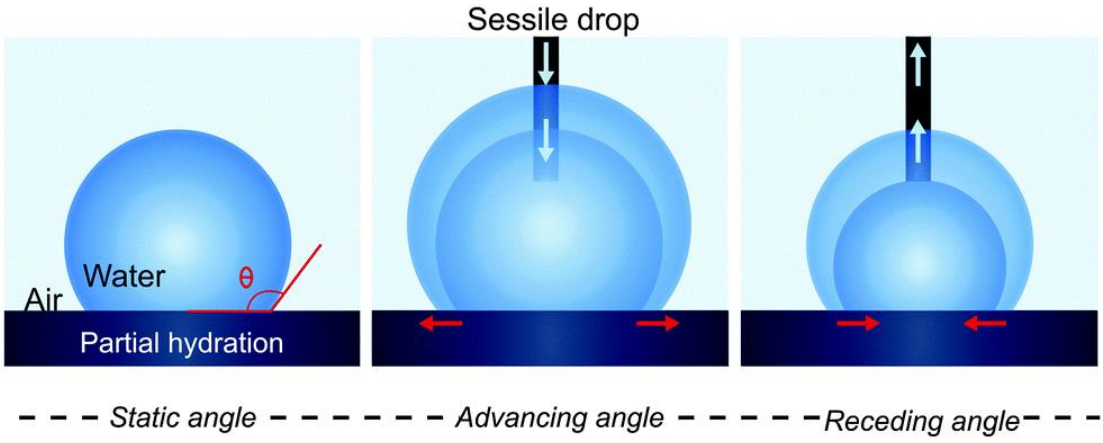

Figure 15. Sessile drop method for advancing and receding angle test. [79]

Tilting plate method

In this method, the sample surface is fixed on the testing stage, the stage is slowly tilted till the water drop rolls off the sample surface. The sliding angle corresponds to the surface tilt angle when the droplet starts to move on the tilted surface. It gives an indication of the adhesion between surface and liquid.[15] While within a given droplet volume range changing the droplet size has little effect on CA, the sliding angle is greatly influenced by the size of the droplet. Larger droplets have a smaller SA. The advancing and receding angles can also be obtained, as shown in Figure 18.

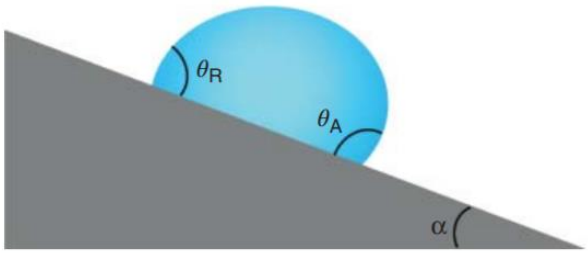

Figure 16. Tilt plate method for measuring the sliding angle, advancing and receding angles.[80]

Wilhelmy plate method

As shown in Figure 19, in the Wilhelmy plate[81] test, the testing surface is introduced vertically into the probe liquid. The CA can be measured when the plate is static in the liquid, according to Equation 8. The Wilhelmy plate method is measuring the forces exerted on the sample, which correlates with the surface tension of the liquid, and the contact angle of a liquid on this solid:

$$\mathrm{F}(h) = P\gamma\cos\theta - \rho A h g, \qquad \textit{Eq. 8}$$

where F is the measured force, P the wetted perimeter of the plate sample, γ the surface tension of the liquid, θ the contact angle, ρ is the liquid density, A the cross-sectional area of the plate sample, h the immersion depth, and g the gravitational constant. One should note that for porous and hydrophilic materials such as wood, the force from probe liquid wicking and liquid sorption will also contribute to the F (h).[82] The Wilhelmy plate method can also give advancing and receding angles through the wetting and dewetting process by judging from the contact line movement.

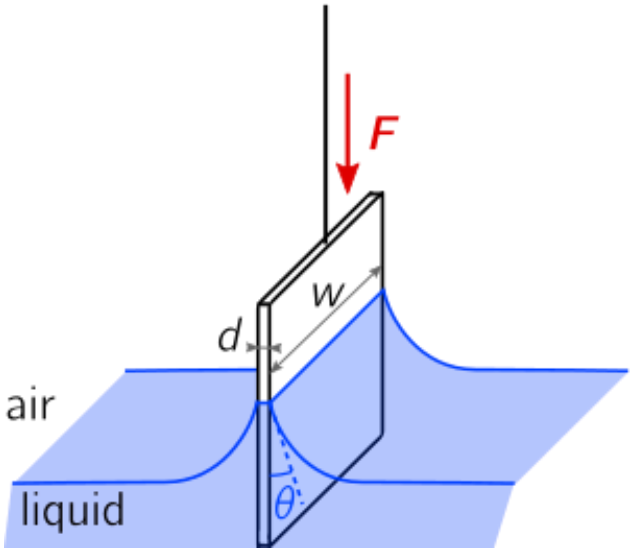

Figure 17. Wihelmy plate method. [83]

Captive bubble method

Another alternative technique for measuring wettability is the captive bubble method.[84] In this test, an air bubble of a certain volume is formed into a liquid phase on the solid surface immersed in the liquid (Figure 20). The air bubble will move up and stay under the tested surface. The CA can be measured on the bubble profile (similar to sessile drop method). With this method, the influence of needle height from the tested surface can be eliminated, and the testing temperature can be easily controlled. The disadvantage of this method is that the sample surface might be swollen by the liquid , which will influence the test result.[15]

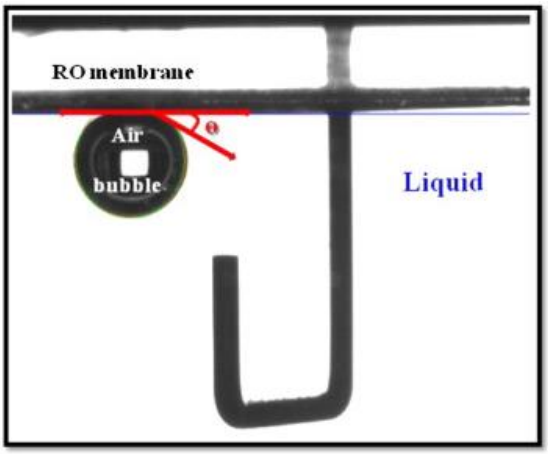

Figure 18. The setup of captive bubble method for measuring the CA of reverse osmosis (RO) membrane.[85]

1.5 Special wettabilities and their biological models

In this section, the special wettabilities and their biological role models relevant to this thesis are introduced. This includes superhydrophobicity (Subchapter 2.1 and 2.3), SLIPS (Subchapter 2.1), and anisotropic wetting (which can induce the directional flow of liquids) and wetting patterns (Subchapter 2.2). Other special wettabilities such as superomniphobicity, wetting gradients, and superhydrophilicity are also briefly discussed in this section.

1.5.1 Superhydrophobicity

Superhydrophobicity refers to the property of surfaces with a water contact angle (CA) larger than 150°. Many of these surfaces also have low sliding angles (SA), typically smaller than 10°. They are usually obtained by combining surface roughness with low surface energy chemicals, to achieve the Cassie-Baxter wetting state.[63]

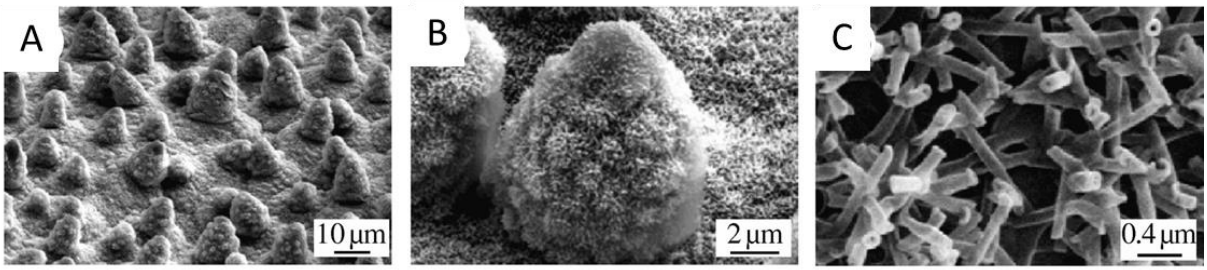

Figure 19. SEM images of a) the lotus leaf surface, b) a zoomed in papilla, and c) the epicuticular wax tubules covering the papillae.[86]

Nature gives excellent examples of superhydrophobic surfaces such as the lotus leaf, the floating fern *Salvinia*, rose petals, cicada wings, butterfly wings, fly eyes, gecko's toepads, water strider's legs.[87] Among them, lotus leaf is one of the most well-known examples of natural superhydrophobic surfaces (Figure 21a). The lotus leaf can exhibit a water contact angle larger than 150° with a sliding angle of around 2°.[14] Raindrops falling on lotus leaf surface can roll off the surface, taking away dirt and debris.[88] "Lotus effect" is used to refer to such high water contact angle combined with the low adhesion property. The surface topography of lotus leaf is made up of micro-papillae (Figure 21b) superimposed by cilium-like nanostructures (Figure 21c).[88, 89] The hierarchical surface of lotus leaf is covered by hydrophobic epicuticular wax. Inspired by the hierarchical structure of Lotus leaf, many superhydrophobic materials have been fabricated with applications in anti-icing surfaces, antifogging surfaces, anticorrosion

coatings, drag reduction in underwater applications, anti-biofouling, water resistant fabrics, and water-oil separation.[27]

Despite the numerous potential applications, superhydrophobic surfaces face many challenges such as poor durability and high fabrication costs.[27] Some (super)hydrophobization approaches are introduced in Subchapter 1.6.

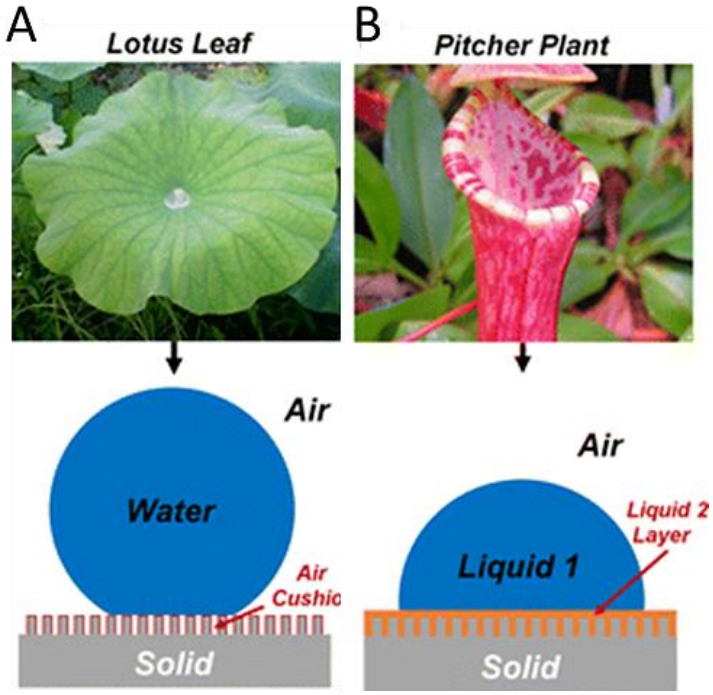

Figure 20. a) The lotus leaf wetting model and b) the pitcher plant wetting model. Pictures are adapted from Cao et al.[90]

1.5.2 SLIPS

Slippery liquid-infused porous surfaces (SLIPS) were inspired by the carnivorous pitcher plant (*Nepenthes*). By applying a proper lubricant, SLIPS can repel both water and organic solvents from the surfaces (Figure 22b). The slippery effects of the pitcher plant can be found on the peristome and the wax zone (or slippery zone) just below the peristome of the pitcher plant (Figure 23a-b). The peristome of this plant bears a very regular radial ridge microstructure (Figure 23c-d). The peristome is slippery because the microstructure is moistened by nectar secreted at the inner margin of the peristome.[19, 91] This homogeneous liquid film formed on the surface makes the peristome extremely slippery for insects. The insects walking on this rim will slide down into the digestive juices at the bottom of the pitcher.[19] The waxy zone, located below the peristome, is also the key to trap and prevent the escape of insects.[92] The waxy zone is

composed of an epidermis of flattened hexagonal cells with scattered downward-directed lunate cells (Figure 23e).[91] The entire zone is covered by wax crystals (Figure 23f).

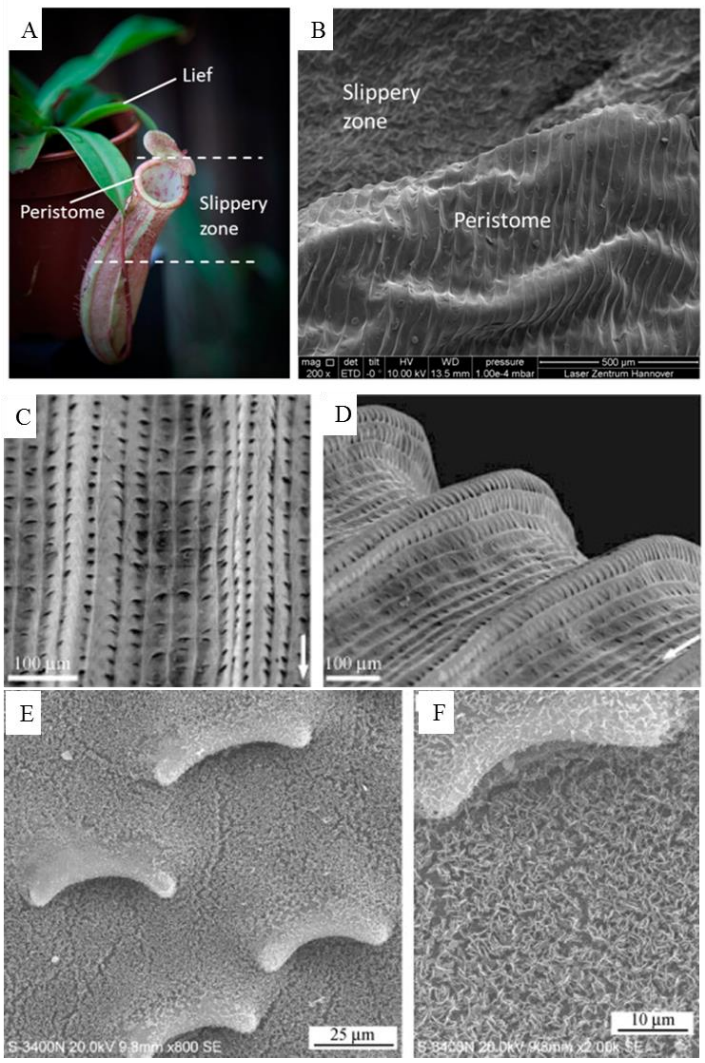

Figure 21. a-b) The peristome and slippery zone of the Nepenthes alata, c-d) The ridges on the peristome of the pitcher plant, the arrows point towards the pocket-like digestive gland, e-f) The wax zone has downward-directed lunate cells and is covered with wax crystals. Pictures are adapted from Fadeeva and Chichkov,[93] Bohn and Federle[19] and Wang et al.[91]

By mimicking this slippery effect, a SLIPS manufacturing process typically involves the structuration of the surface or the fabrication of a porous matrix followed by the infusion of a lubricant (Figure 24).The lubricating film on the solid surface can repel a wide range of liquids, when the following conditions are satisfied: the lubricants must wet and stably adhere within the substrate, the solid matrix should be preferentially wetted by the lubricants

rather than by the liquid to be repelled, and the lubricants and the repelled liquids should be immiscible.

SLIPS technology creates slick, exceptionally repellent and robust self-cleaning surfaces on metals, plastics, optical materials, textiles, and ceramics. This strategy can endow surfaces not only with exceptional liquid repellency with low hysteresis and low sliding angle but also with pressure stability, self-healing, optical transparency[20] and antibiofouling.[94]

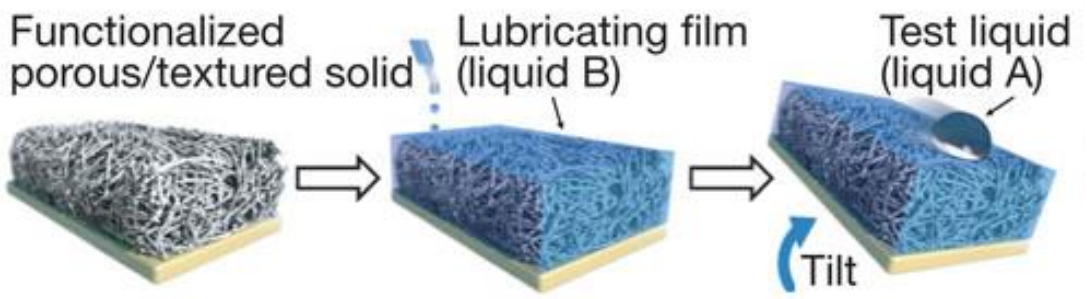

Figure 22. The fabrication process of SLIPS.[20]

1.5.3 Directional flow of liquid and anisotropic wetting

The directional flow of liquids (anisotropic flow) is promising for potential applications in micro-droplet directional transfer or microfluidic devices.[24] In nature, the phenomenon of directional flowing of water occurs on many leaves such as rice leaf [95] or crane flower leaf.[96] On a rice leaf, micropapillae are arranged with a quasi-1D ordering parallel to the leaf edge (Figure 25a),[23] This structure results in water contact angle larger than 150° with the sliding angle of several degrees.[97] One can also observe that droplets on rice leaf drip easily down in a direction parallel to the edge of the leaf rather than across it. In some reports on the wetting behaviour of rice leaf[88, 98] even anisotropic wetting properties were claimed, but this seems to be an artefact caused by damage of the leaf surface (as indicated by the white circle in Figure 25a).

On many manmade materials, the directionality of liquid flow can be generated by anisotropic wetting behavior. Anisotropic wetting refers to the inhomogeneous wetting of a surface by a liquid.[25] The surface shows different contact angles when measured from different directions. This phenomenon originates from anisotropy in chemical composition or surface topography.[25]

Usually, an anisotropic wetting surface is characterized by two CAs which are measured parallel and perpendicular to the droplet shape distortion direction as shown in Figure 25b-f. Manufacturing approaches for anisotropic wetting surfaces include lithography,[99] templating (embossing),[96] polymer wrinkling,[100] monomolecular layer transformation methods,[101] and electrospinning.[102] Anisotropic wetting can be used in microfluidic devices, lab-on-a-chip, sensors, or microreactors.[25]

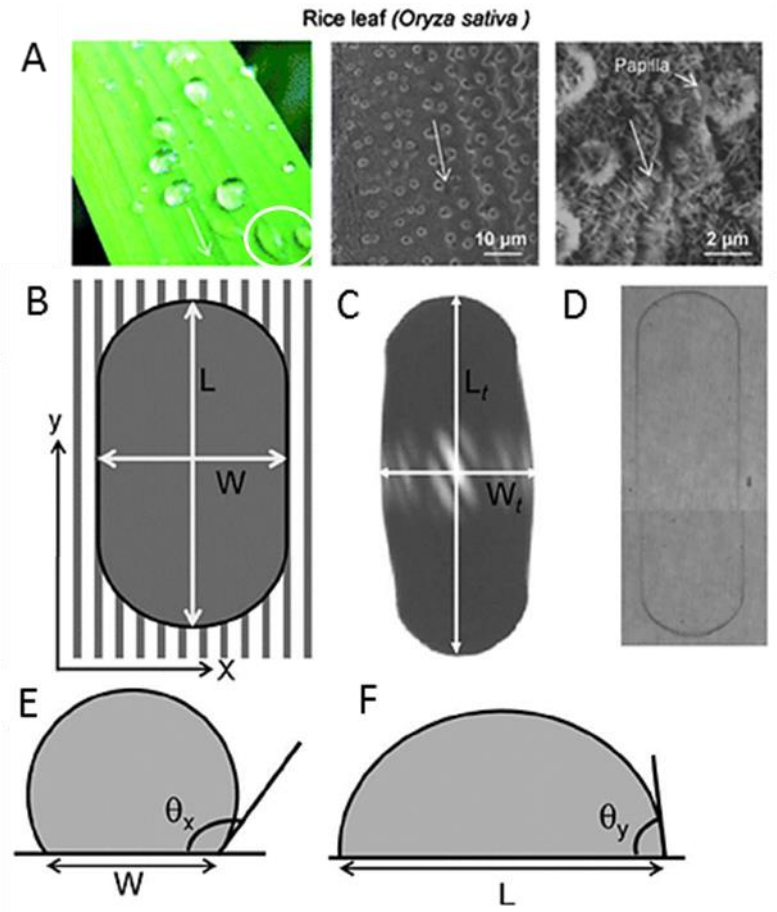

Figure 23. a) The rice leaf and the corresponding SEM images show the microstructures on rice leaf surface. The schematic drawings show b) a droplet sitting on a grooved manmade material surface c) the top view projection of the droplet on the surface, d) the contact line of this droplet on the surface, e-f) droplet profiles measured along perpendicular and parallel directions.[i] *Pictures are adapted from Bixler and Bhushan*[103] *and Xia et al.*[25]

[i] Please note the perpendicular and parallel directions in this literature are defined as parallel and perpendicular directions respectively in Subchapter 2.2.

1.5.4 Wettability patterns

A surface with wettability patterns displays both hydrophilic and hydrophobic areas. A good natural example of a surface with wettability patterns is the back of the Darkling beetles (*Stenocara sp.*) living in the Namib Desert. These insects developed a striking fog collection ability. As shown in Figure 26, the desert beetle's back is covered with randomly scattered bumps. Those bumps (0.5 mm in diameter, 0.5 - 1.5 mm apart) exhibit smooth and hydrophilic peaks, while the sloping sides and the troughs between bumps represent microstructures (hexagonal arrays made up by flattened hemispheres of 10 μm in diameter). These microstructures are coated with wax and are superhydrophobic.[22] This surface design with alternating wetting patterns combines both fog water coalescence on the hydrophilic bump tops and subsequent water drainage by the superhydrophobic area.

Inspired by the beetle's back, many processing techniques have been applied to artificial material surfaces to prepare wettability patterns, including photons catalyzed decomposition of low surface energy organic monolayer,[104] femtosecond lasering,[105] and site-selective ink patterning.[106] Surfaces with wettability patterns have applications in many fields such as microfluidics[107] (an example is shown in Figure 26d), biomedical diagnostic devices,[108] sensors,[109] cell culturing,[110] and chemical synthesis in droplets.[111]

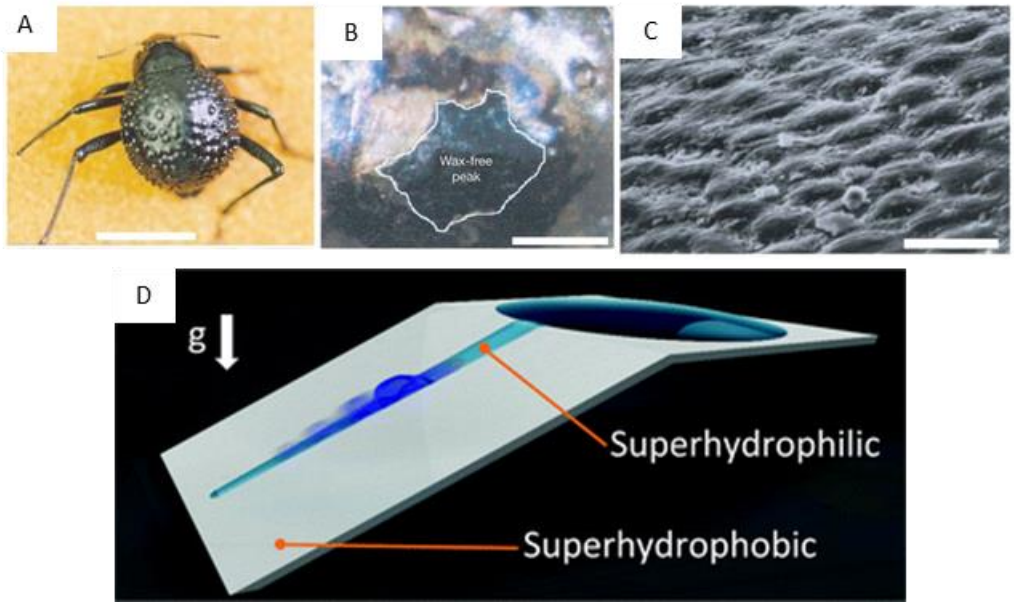

Figure 24. a) The desert beetle, b) a hydrophilic bump on the back of the beetle, c) the textured surface of beetle's back, and d) an application example: the surface with hydrophobic-hydrophilic patterns is used for pumpless fluid transport by taking advantage of hemiwicking and Laplace pressure drive.[108] Scale bars: a, 10 mm; b, 0.2 mm; c, 10 μm. The pictures are adapted from Parker and Lawrence[22] and Ghosh et al.[108]

1.5.5 Other special wettings

Omniphobicity and amphiphobicity define surfaces that can repel both water and oils. Some researchers suggest that omniphobicity has a larger repelling range (down to liquid with surface tensions smaller than 20 $mN \cdot m^{-1}$), while amphiphobic is usually used for the liquids with surface tension larger than 20 $mN \cdot m^{-1}$.[112] A well described omniphobic surface that exists in nature is the skin of springtails, which contains bristles and aligned granules.[113, 114] The omniphobicity has evolved in order to adapt to the living habitats where water is mixed with surface-active substances.[113] **Gradient wettability** refers to a surface with gradually enhanced hydrophobicity or hydrophilicity, which has potentials in microfluidic applications.[115] **Superhydrophilicity** refers to surfaces having a water CA smaller than 5°.[116] **Parahydrophobic** refers to hydrophobic surfaces having high water adhesion or high sliding angles.[117]

1.6 Manufacturing techniques to change surface wettability

In this section, we discuss the techniques for the preparation of water-repellent surfaces, with emphasis on sol-gel method, polymerization and templating method which have been used in this thesis.

1.6.1 Sol-gel

The sol-gel process can modify a solid surface with metal oxides, aiming at changing the surface roughness and/or surface chemical compositions. In the sol-gel process, a sol is first prepared from hydrolysis of the metal alkoxides (for example, $Si(OR)_4$, $Ti(OR)_4$, $R'Si(OR)_3$, $Zr(OR)_4$) in solutions. The sol (a colloidal solution) is then deposited on the substrates through dip coating or spin coating and evolves toward a gel through condensation of the hydrolyzed alkoxides. At last, the substrates together with the wet gel are heated up to remove the solvent, leading to a metal oxide layer on the surface.[118] This layer can be further grown by hydrothermal reactions to form crystals[119] or directly be used to create roughness.

In the perspective of wettability, the obtained metal oxides can be hydrophobic or hydrophilic,[120, 121] and they are usually used to increase the surface roughness. In the case of hydrophilic metal oxides, a coating of low surface energy chemicals is required to make the final surface hydrophobic.

Sol-gel is widely applied because it is cheap, easy to manipulate, does not need high temperature, and it is easy to control the porosity of the inorganic layer, the particle morphology and size.

1.6.2 Polymer grafting

Polymers can also be used to change surface wettability by grafting the surface chemicals with more hydrophobic polymers. The commonly applied polymers are fluoropolymers and alkyl polymers. The molecular weight of the grafted polymers and the grafting density will influence the water repellency performance. The alkyl has higher surface energy than fluoride, nevertheless, sufficiently long alkyl chains can achieve the same performance: very high CA with a small sliding angle.[122] A higher grafting density can lead to full coverage of the substrates and the modification homogeneity. When the polymer add-on is too abundant, the polymers will aggregate into particles, which might also increase the surface roughness. The grafting polymerization is a common process nowadays, in which grafting density and molecular weight of polymer can be controlled. Depending on the substrates, polymers can be directly grafted from the solid surface, but in many cases, a first surface functionalization step is needed to attach the polymers. In a "grafting from" approach, a substrate functionalized with initiators will be impregnated with monomer solution. The polymer chains are initiated at and grow from the surface. Atom transfer radical polymerization (ATRP)[122] or other free radical polymerization techniques are commonly used.[123] Additionally, polymers can also be attached to the solid surface through "grafting to" approaches.[124] The polymer grafting approaches are not typical for superhydrophobization of solid surfaces due to the existence of other easy alternatives such as the sol-gel method. Nevertheless, polymer grafting is common in the field of tribology and antifouling surfaces, featured by growing very hydrophilic (water solvated) polymer brushes.[125, 126]

1.6.3 Templating method

A templating process is used for surface structuration and involves the molding of a material from a master template. This method can be used to create roughness on polymer surfaces. Various techniques can be used to design templates such as polymers fabricated from breath figure arrays,[127] electrochemical etching of aluminium sheets,[128] and lithography.[129] Biological templates have also received attention due to their ingenious hierarchical natural design, low

cost, "green" nature and natural abundance. Biological materials such as lotus leaf,[89] butterfly wings,[130] springtail's skin[114] and rice leaves[131] possess highly ordered morphological architectures related to their functions.[132] The process usually involves template preparation, molding, curing of the polymers, demolding by peeling/taking off[96, 133] or destroying of the templates with strong chemicals.[134] The obtained replica surfaces from embossing natural templates can possess superhydrophobicity, antifogging property, directional flowing of liquids property, or anisotropic wettability. This easy fabrication approach does not require expensive equipment and the precise control is promising for industrial production.

1.6.4 Other techniques

Besides the abovementioned methods, there is a wide range of other manufacturing techniques available. **Photolithography**: in photolithographic approaches, light is irradiated on a surface covered by a photoresist and mask. Subsequently, the area uncovered by the mask will be irradiated and etched off by light to yield patterns/roughness. The photoresist can be removed later and an additional coating can be applied to achieve superhydrophobicity.[135] **Plasma etching**: plasma etching process involves synergistic chemical and physical etching. The plasma of reactive species bombards the matrix surface and reacts with it. The surface etched off become volatile and is removed by vacuum.[136, 137] **Colloidal assembly**: the prepared colloidal particles can be assembled on the matrix through Van der Waals interactions to create surface roughness with desired surface composition.[138] **Chemical deposition**: in the reaction process, the chemicals are deposited or assembled on the surfaces.[139] This can be achieved through chemical bath deposition or chemical vapor deposition, or electrochemical deposition.[139] **Layer by layer (LBL) technique**: the different layers of polyelectrolytes with positive or negative charges (for example, polyanions and polycations) are adsorbed on the substrate through electrostatic interactions. The surface chemistry is changed by the top adsorbed chemicals. If charged particles are applied as an alternative layer, also surface roughness can be created.

1.7 Wettability of wood materials

1.7.1 The intricateness of the wettability of native wood

Wood is a hygroscopic porous material, with a surface energy usually between 30 and 50 $mJ \cdot m^{-2}$.[140] The wettability of wood is very complex and varies depending on a number of parameters.

Besides the intrinsic differences between surface energies of different wood species,[141] roughness influences greatly the wetting process as indicated in Subchapter 1.3.2. In general, native wood is more apt to be wetted by water if the roughness is built up. Consequently, it is experimentally proven that the EW has a smaller CA than LW (when testing the CAs of formaldehyde resins on pine veneers), because the EW has a greater roughness than LW after sawing.[142] Presumably, the wettability of sawed, planed, sanded and razor-blade-cut wood surfaces would also be different due to the different surface topography/roughness. The CA tests on southern pine surfaces by polar or apolar probe liquids and by high-viscosity resins were conducted by Steher *et al.*[143] The fastest wetting for polar and apolar probe liquids happened on the sanded sample due to the high roughness, while the fastest wetting of highly viscous liquids such as polyvinyl-acetate and phenol-resorcinol-formaldehyde resins occurred on the relatively smooth surfaces such as planed wood and on the razor-blade-cut surfaces.[143] As the surface topographies/roughness can influence the CAs, the different planes of wood should also exhibit different CA values. It has been shown that the contact angle of the tangential section of wood is larger than that of the radial section or cross-section.[144, 145] On wood tangential sections, the CA of pine wood in parallel direction is smaller than that in perpendicular direction[ii].[146] Not only surface topography, but also porosity should be taken into consideration when studying wood wetting. For example, the oven-dried samples have the highest CA, and air dried has a larger CA than freeze-dried samples[144] likely due to the retained porosity.

In conclusion, the wettability of native wood is highly variable. It can be influenced by the species, the measurement locations on wood (wood planes, early- or latewood, sapwood or heartwood), measurement direction (parallel or perpendicular to grain directions), anatomical microstructures[147] (lumen and cell walls), chemical composition ratios, machining, and drying history (moisture content, porosity remaining).

1.7.2 Chemical modification to change the wood wettability

Wood modification techniques targeting changes in wood-water interactions range from surface modification to bulk modification. At the microscale, the modifying agents can be located inside the wood lumen, at the interface between cell walls and lumen, or even inside wood cell

[ii] Please note the perpendicular and parallel directions in this literature are defined as parallel and perpendicular directions respectively in Subchapter 2.2.

walls[3] (Figure 27a). According to the wood chemical composition described in section 1.2, hydroxyl groups are the most abundant chemical functionalities in wood. Therefore, chemical modifications of wood should be done with chemical species reacting with -OH groups, or compatible with them. According to the chemicals and processes involved, the modifications can be divided into the following four classes (Figure 27b):

i. Thermal treatment. In this process, there is no need for adding external chemicals for reactions. The wood samples are heated at 160 -260 °C in nitrogen, steam pressure, oil or vacuum environment to avoid combustion of wood.[148] The heating induces complex chemical/physical changes mainly including deacetylation, depolymerisation and dehydration of hemicellulose, increase in cellulose crystallinity, and lignin structure changes and crosslinking.[149] The decreased affinity to water is due to the crosslinking of lignin and the destruction of hydroxyl groups.

ii. Small molecule grafting on -OH groups or crosslinking of -OH groups can be used. This approach includes acetylation,[150] silanization,[151] isocyanation,[152] furfurylation,[153] or the Belmadur® treatment with dimethyloldihydroxyethelenurea.[154] These small molecules are used to block the hydroxyl groups and to fill up the nanopores in cell wall in order to improve the resistance of wood to water.

iii. In-situ polymerizations are another possibility. Grafting of polystyrene,[155] poly (ε-caprolactone),[156] poly-(glycidyl methacrylate),[157] or poly(methyl methacrylate)[158] have been reported on wood. In the grafting from approach, an initiator is anchored on wood biopolymers, then the monomers are added and the polymer chains grow from the immobilized initiators to large molecules. With this strategy, it is possible to target the specific regions in wood (cell wall or inside lumen) by using good or bad solvents allowing controlling the attachment of the initiator. Most of the polymer grafting techniques in bulk wood are through “grafting from” methods because a good penetration and even swelling of wood is the prerequisite for a higher degree of modification. In the “grafting to” approach, polymers might be too large in terms of molecular size and have the difficulty of penetrating into the wood scaffold as well as generate an undesired inhomogeneous grafting density.

iv. Inorganic particle deposition (TiO_2,[159] ZnO,[160] SiO_2[161]). In this approach, inorganic micro- or nano-particles are deposited on wood to construct hierarchical surface roughness and are then coated with low surface energy chemicals such as perfluorodecyltriethoxysilane (PFDTS), stearic acid (SA), or polydimethylsiloxane (PDMS). The inorganic particles can be attached on wood through sol-gel approaches,[162]

hydrothermal reactions,[163] or dip coating.[161] The particles can be located in the wood cell lumen or on the wood surface. Other functionalities can be achieved along with improved hydrophobicity, such as resistance to natural weathering and fungal attack.[147]

v. SLIPS was also transferred to wood by Guo *et al.*[21] This strategy includes growing ZnO rods on wood and infusing them with a fluorinated lubricant to generate an oil- and water-repellent wood surface (detailed strategy of SLIPS present in 1.4.2).

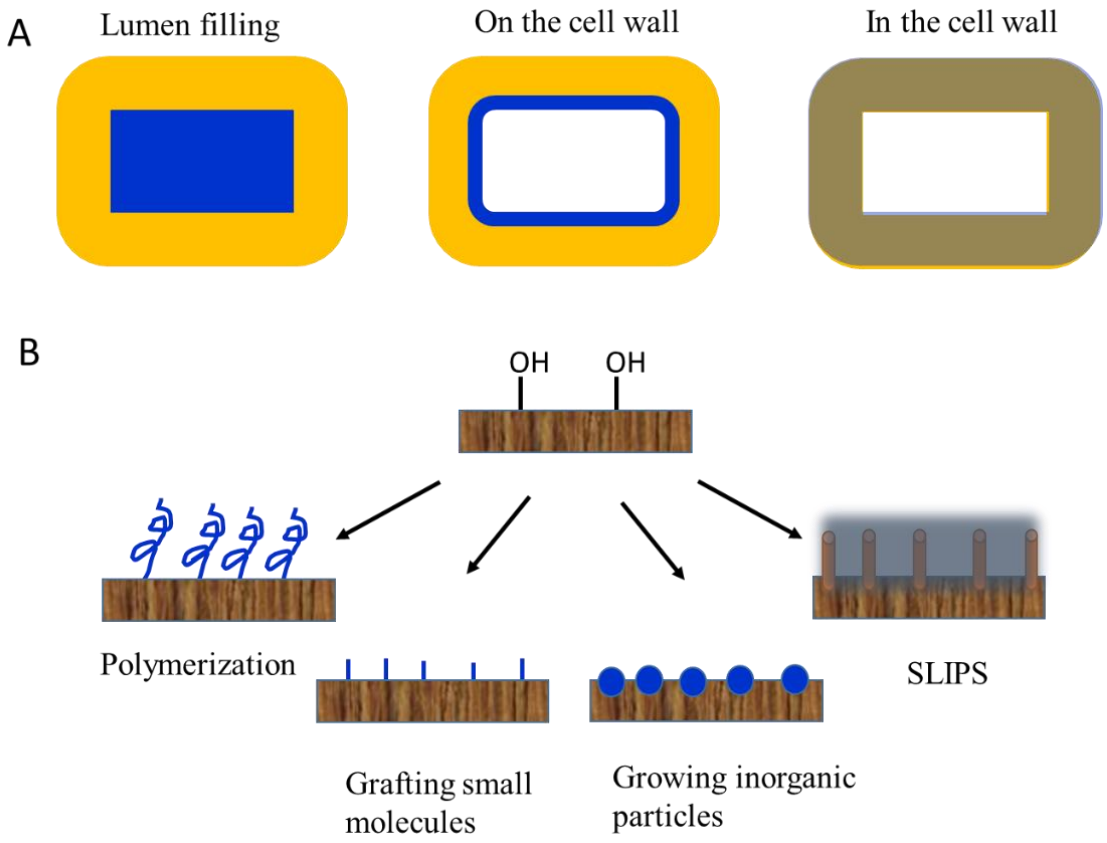

Figure 25. Wood modification for water repellency: a) targeted modification locations, b) different types of modifications.

In essence, the modification of wood for water repellency is trying to block the access to hydroxyl groups of wood cell walls or to replace them with more hydrophobic groups. Since one of the primary ideas of using wood is to reduce the environmental impact associated with the use of non-renewable resources, it is important that wood modifications take into account the environmental impact.[164]

References for Chapter 1

1. Mattsson, T.; Azhar, S.; Eriksson, S.; Helander, M.; Henriksson, G.; Jedvert, K.; Lawoko, M.; Lindström, M. E.; McKee, L. S.; Oinonen, P., The Development of a Wood-based Materials-biorefinery. *BioResources* **2017,** *12* (4), 9152-9182; Xia, D.; Brueck, S., Strongly anisotropic wetting on one-dimensional nanopatterned surfaces. *Nano Lett.* **2008,** *8* (9), 2819-2824.
2. Rowell, R. M., *Handbook of wood chemistry and wood composites*. CRC press: Florida, USA, 2012.
3. Burgert, I.; Cabane, E.; Zollfrank, C.; Berglund, L., Bio-inspired functional wood-based materials–hybrids and replicates. *Int. Mater. Rev.* **2015,** *60* (8), 431-450.
4. Rüggeberg, M.; Burgert, I., Bio-inspired wooden actuators for large scale applications. *PloS one* **2015,** *10* (4), e0120718.
5. Vidiella del Blanco, M.; Fischer, E. J.; Cabane, E., Underwater Superoleophobic Wood Cross Sections for Efficient Oil/Water Separation. *Advanced Materials Interfaces* **2017,** *4* (21), 1700584.
6. Vitas, S.; Keplinger, T.; Reichholf, N.; Figi, R.; Cabane, E., Functional lignocellulosic material for the remediation of copper (II) ions from water: Towards the design of a wood filter. *J. Hazard. Mater.* **2018,** *355*, 119-127.
7. Lv, S.; Fu, F.; Wang, S.; Huang, J.; Hu, L., Novel wood-based all-solid-state flexible supercapacitors fabricated with a natural porous wood slice and polypyrrole. *RSC Advances* **2015,** *5* (4), 2813-2818.
8. Trey, S.; Jafarzadeh, S.; Johansson, M., In situ Polymerization of Polyaniline in Wood Veneers. *ACS Appl. Mater. Interfaces* **2012,** *4* (3), 1760-1769.
9. Sun, B.; Fan, T.; Zhang, D., Porous TiC Ceramics Derived from Wood Template. *J. Porous Mater.* **2002,** *9* (4), 275-277.
10. Matovic, B.; Babic, B.; Egelja, A.; Radosavljevic-Mihajlovic, A.; Logar, V.; Saponjic, A.; Boskovic, S., Preparation of Porous Silica Ceramics Using the Wood Template. *Mater. Manuf. Processes* **2009,** *24* (10-11), 1109-1113.
11. Dong, A.; Wang, Y.; Tang, Y.; Ren, N.; Zhang, Y.; Yue, Y.; Gao, Z., Zeolitic tissue through wood cell templating. *Adv. Mater.* **2002,** *14* (12), 926-929.
12. Merk, V.; Chanana, M.; Gierlinger, N.; Hirt, A. M.; Burgert, I., Hybrid wood materials with magnetic anisotropy dictated by the hierarchical cell structure. *ACS Appl. Mater. Interfaces* **2014,** *6* (12), 9760-9767.
13. Li, Y.; Fu, Q.; Yu, S.; Yan, M.; Berglund, L., Optically Transparent Wood from a Nanoporous Cellulosic Template: Combining Functional and Structural Performance. *Biomacromolecules* **2016,** *17* (4), 1358-1364.
14. Sun, T.; Feng, L.; Gao, X.; Jiang, L., Bioinspired surfaces with special wettability. *Acc. Chem. Res.* **2005,** *38* (8), 644-652.
15. Law, K.-Y.; Zhao, H., *Surface wetting: characterization, contact angle, and fundamentals*. Springer International Publishing: 2016.
16. Boutilier, M. S.; Lee, J.; Chambers, V.; Venkatesh, V.; Karnik, R., Water filtration using plant xylem. *PloS one* **2014,** *9* (2), e89934.
17. Merk, V. Mineralization of wood cell walls for improved properties. ETH Zurich, 2016.
18. Nosonovsky, M., Materials science: Slippery when wetted. *Nature* **2011,** *477* (7365), 412.
19. Bohn, H. F.; Federle, W., Insect aquaplaning: Nepenthes pitcher plants capture prey with the peristome, a fully wettable water-lubricated anisotropic surface. *Proceedings of the National Academy of Sciences* **2004,** *101* (39), 14138-14143.
20. Wong, T.-S.; Kang, S. H.; Tang, S. K.; Smythe, E. J.; Hatton, B. D.; Grinthal, A.; Aizenberg, J., Bioinspired self-repairing slippery surfaces with pressure-stable omniphobicity. *Nature* **2011,** *477* (7365), 443-447.
21. Guo, H.; Fuchs, P.; Casdorff, K.; Michen, B.; Chanana, M.; Hagendorfer, H.; Romanyuk, Y. E.; Burgert, I., Bio‐Inspired Superhydrophobic and Omniphobic Wood Surfaces. *Advanced Materials Interfaces* **2017,** *4* (1), 1600289.

22. Parker, A. R.; Lawrence, C. R., Water capture by a desert beetle. *Nature* **2001,** *414* (6859), 33.
23. Feng, L.; Li, S.; Li, Y.; Li, H.; Zhang, L.; Zhai, J.; Song, Y.; Liu, B.; Jiang, L.; Zhu, D., Super‐hydrophobic surfaces: from natural to artificial. *Adv. Mater.* **2002,** *14* (24), 1857-1860.
24. Lu, Y.; Yu, L.; Zhang, Z.; Wu, S.; Li, G.; Wu, P.; Hu, Y.; Li, J.; Chu, J.; Wu, D., Biomimetic surfaces with anisotropic sliding wetting by energy-modulation femtosecond laser irradiation for enhanced water collection. *RSC Advances* **2017,** *7* (18), 11170-11179.
25. Xia, D.; Johnson, L. M.; López, G. P., Anisotropic Wetting Surfaces with One‐Dimesional and Directional Structures: Fabrication Approaches, Wetting Properties and Potential Applications. *Adv. Mater.* **2012,** *24* (10), 1287-1302.
26. Genzer, J.; Marmur, A., Biological and synthetic self-cleaning surfaces. *MRS Bull.* **2008,** *33* (8), 742-746.
27. Jeevahan, J.; Chandrasekaran, M.; Britto Joseph, G.; Durairaj, R. B.; Mageshwaran, G., Superhydrophobic surfaces: a review on fundamentals, applications, and challenges. *Journal of Coatings Technology and Research* **2018,** *15* (2), 231-250.
28. Wang, Y.; Yan, W.; Frey, M.; Vidiella del Blanco, M.; Schubert, M.; Adobes-Vidal, M.; Cabane, E., Liquid-like SiO_2-g-PDMS coatings on wood surfaces with underwater durability, anti-fouling, anti-smudge and self-healing properties *advanced Sustainable Systems* **2018**, 1800070.
29. Wang, Y.; Tian, T.; Cabane, E., Wood Composites with Wettability Patterns Prepared by Controlled and Selective Chemical Modification of a Three-Dimensional Wood Scaffold. *ACS Sustainable Chemistry & Engineering* **2017,** *5* (12), 11686-11694.
30. Wang, Y.; Vitas, S.; Burgert, I.; Cabane, E., Beech wood cross-sections as a natural template to fabricate superhydrophobic surfaces. *Wood Science and Technology* (submitted).
31. Anderson, A. B., The composition and structure of wood. ACS Publications: 1958.
32. Fratzl, P.; Weinkamer, R., Nature's hierarchical materials. *Prog. Mater Sci.* **2007,** *52* (8), 1263-1334.
33. Fengel, D.; Wegener, G., *Wood: chemistry, ultrastructure, reactions*. Walter de Gruyter: 1983.
34. Rafsanjani, A.; Derome, D.; Wittel, F. K.; Carmeliet, J., Computational up-scaling of anisotropic swelling and mechanical behavior of hierarchical cellular materials. *Compos. Sci. Technol.* **2012,** *72* (6), 744-751.
35. Chapter 2 Wood technology. https://www.cats-cons.dk/marette/-9711.html#refendnote_-9711_2 (accessed 23.10. 2018).
36. Higuchi, T., *Biochemistry and molecular biology of wood*. Springer Science & Business Media: 2012.
37. Microscopic structure of hardwoods. https://akela.mendelu.cz/~xcepl/inobio/nove/Wood_anatomy/WAEF-07-micro_hardwoods.pdf (accessed 18.11.2018).
38. Conners, T., Distinguishing Softwoods from Hardwoods. **2015**.
39. Bertaud, F.; Holmbom, B., Chemical composition of earlywood and latewood in Norway spruce heartwood, sapwood and transition zone wood. *Wood Science and Technology* **2004,** *38* (4), 245-256.
40. Deshpande, A. S.; Burgert, I.; Paris, O., Hierarchically Structured Ceramics by High‐Precision Nanoparticle Casting of Wood. *Small* **2006,** *2* (8‐9), 994-998.
41. Plomion, C.; Leprovost, G.; Stokes, A., Wood formation in trees. *Plant physiology* **2001,** *127* (4), 1513-1523.
42. Sjostrom, E., *Wood chemistry: fundamentals and applications*. Elsevier: 2013.
43. Pettersen, R. C., The chemical composition of wood. *The chemistry of solid wood* **1984,** *207*, 57-126.
44. Fu, L.; McCallum, S. A.; Miao, J.; Hart, C.; Tudryn, G. J.; Zhang, F.; Linhardt, R. J., Rapid and accurate determination of the lignin content of lignocellulosic biomass by solid-state NMR. *Fuel* **2015,** *141*, 39-45.
45. Ding, S.-Y.; Zhao, S.; Zeng, Y., Size, shape, and arrangement of native cellulose fibrils in maize cell walls. *Cellulose* **2014,** *21* (2), 863-871.
46. Cell wall structure. https://is.mendelu.cz/eknihovna/opory/zobraz_cast.pl?cast=19244 (accessed 25. 11. 2018).
47. Aulin, C. Novel oil resistant cellulosic materials. KTH, 2009.

48. Langan, P.; Nishiyama, Y.; Chanzy, H., X-ray Structure of Mercerized Cellulose II at 1 Å Resolution. *Biomacromolecules* **2001,** *2* (2), 410-416.
49. Cheng, J., *Biomass to renewable energy processes*. CRC press: 2017.
50. Scheller, H. V.; Ulvskov, P., Hemicelluloses. *Annual review of plant biology* **2010,** *61*.
51. Fahlén, J. The cell wall ultrastructure of wood fibres: effects of the chemical pulp fibre line. KTH, 2005.
52. Chapter 2 - Surface Tension and Its Measurement. In *Adhesives Technology Handbook (Second Edition)*, Ebnesajjad, S., Ed. William Andrew Publishing: Norwich, NY, 2009; pp 21-36.
53. Surface tension. https://en.wikipedia.org/wiki/Surface_tension (accessed 26. 11. 2018).
54. Eyland, P. B. Lecture 8 (Surface Tension and Surface Energy). http://www.insula.com.au/physics/1279/L8.html (accessed 07. 09. 2018).
55. Allan S. Hoffman, B. R. Lecture on Contact Angles. https://www.uweb.engr.washington.edu/education/pdf/ashsurfscontact%20angles05.pdf (accessed 07. 09. 2018).
56. Wikipedia-contributors Capillary action. https://en.wikipedia.org/wiki/Capillary_action (accessed 7. 09. 2018).
57. Washburn, E. W., The dynamics of capillary flow. *Physical review* **1921,** *17* (3), 273.
58. Wikipedia-contributors Wetting. https://en.wikipedia.org/w/index.php?title=Wetting&oldid=857992859 (accessed 07. 09. 2018).
59. de Gennes, P.-G.; Brochard-Wyart, F.; Quere, D., *Capillarity and Wetting Phenomena: Drops, Bubbles, Pearls, Waves*. Springer: New York, 2013.
60. Young, T., III. An essay on the cohesion of fluids. *Philosophical transactions of the royal society of London* **1805,** *95*, 65-87.
61. Seo, K.; Kim, M., Re-derivation of Young's Equation, Wenzel Equation, and Cassie-Baxter Equation Based on Energy Minimization. In *Surface Energy*, InTech: 2015.
62. Wenzel, R. N., Resistance of solid surfaces to wetting by water. *Industrial & Engineering Chemistry* **1936,** *28* (8), 988-994.
63. Cassie, A.; Baxter, S., Wettability of porous surfaces. *Transactions of the Faraday society* **1944,** *40*, 546-551.
64. Bormashenko, E. Y., *Wetting of real surfaces*. Walter de Gruyter: 2013; Vol. 19.
65. Bocquet, L.; Lauga, E., A smooth future? *Nature materials* **2011,** *10* (5), 334-337.
66. Samaha, M. A.; Vahedi Tafreshi, H.; Gad-el-Hak, M., Sustainability of superhydrophobicity under pressure. *Physics of Fluids* **2012,** *24* (11), 112103.
67. Meiron, T. S.; Marmur, A.; Saguy, I. S., Contact angle measurement on rough surfaces. *J. Colloid Interface Sci.* **2004,** *274* (2), 637-644.
68. Wang, B.; Zhang, Y.; Shi, L.; Li, J.; Guo, Z., Advances in the theory of superhydrophobic surfaces. *J. Mater. Chem.* **2012,** *22* (38), 20112-20127.
69. Michael, N.; Bhushan, B., Hierarchical roughness makes superhydrophobic states stable. *Microelectron. Eng.* **2007,** *84* (3), 382-386; Nosonovsky, M., Multiscale Roughness and Stability of Superhydrophobic Biomimetic Interfaces. *Langmuir* **2007,** *23* (6), 3157-3161.
70. Liu, G.; Fu, L.; Rode, A. V.; Craig, V. S. J., Water Droplet Motion Control on Superhydrophobic Surfaces: Exploiting the Wenzel-to-Cassie Transition. *Langmuir* **2011,** *27* (6), 2595-2600.
71. Clavijo, C. E.; Crockett, J.; Maynes, D., Wenzel to Cassie transition during droplet impingement on a superhydrophobic surface. *Physical Review Fluids* **2016,** *1* (7), 073902.
72. Sun, M.; Liang, A.; Watson, G. S.; Watson, J. A.; Zheng, Y.; Ju, J.; Jiang, L., Influence of Cuticle Nanostructuring on the Wetting Behaviour/States on Cicada Wings. *PLOS ONE* **2012,** *7* (4), e35056.
73. Pease, D. C., The Significance of the Contact Angle in Relation to the Solid Surface. *The Journal of Physical Chemistry* **1945,** *49* (2), 107-110.
74. Gao, L.; McCarthy, T. J., How Wenzel and Cassie Were Wrong. *Langmuir* **2007,** *23* (7), 3762-3765.
75. Chen, W.; Fadeev, A. Y.; Hsieh, M. C.; Öner, D.; Youngblood, J.; McCarthy, T. J., Ultrahydrophobic and ultralyophobic surfaces: some comments and examples. *Langmuir* **1999,** *15* (10), 3395-3399.

76. Eral, H.; Oh, J., Contact angle hysteresis: a review of fundamentals and applications. *Colloid. Polym. Sci.* **2013,** *291* (2), 247-260.
77. Li, S.; Huang, J.; Chen, Z.; Chen, G.; Lai, Y., A review on special wettability textiles: theoretical models, fabrication technologies and multifunctional applications. *Journal of Materials Chemistry A* **2017,** *5* (1), 31-55.
78. Gao, L.; McCarthy, T. J., Contact angle hysteresis explained. *Langmuir* **2006,** *22* (14), 6234-6237.
79. Duc, C.; Vlandas, A.; Malliaras, G.; Senez, V., Wettability of PEDOT: PSS films. *Soft matter* **2016,** *12* (23), 5146-5153.
80. Ras, R. H.; Tian, X.; Bayer, I. S., Superhydrophobic and superoleophobic nanostructured cellulose and cellulose composites. *Handbook of Nanocellulose and Cellulose Nanocomposites* **2017,** *2*, 731-760.
81. Wilhelmy, L., Ueber die Abhängigkeit der Capillaritäts‐Constanten des Alkohols von Substanz und Gestalt des benetzten festen Körpers. *Annalen der Physik* **1863,** *195* (6), 177-217.
82. Scheikl, M.; Dunky, M., Measurement of dynamic and staue contact angles on wood for the determination of its surface tension and the penetration of liquids into the wood surface. *Holzforschung-International Journal of the Biology, Chemistry, Physics and Technology of Wood* **1998,** *52* (1), 89-94.
83. Wikipedia-contributors Wilhelmy plate. https://en.wikipedia.org/w/index.php?title=Wilhelmy_plate&oldid=818410038 (accessed 07. 09. 2018).
84. Zhang, W.; Hallström, B., Membrane characterization using the contact angle technique I. Methodology of the captive bubble technique. *Desalination* **1990,** *79* (1), 1-12.
85. Baek, Y.; Kang, J.; Theato, P.; Yoon, J., Measuring hydrophilicity of RO membranes by contact angles via sessile drop and captive bubble method: A comparative study. *Desalination* **2012,** *303*, 23-28.
86. Bhushan, B.; Jung, Y. C.; Koch, K., Micro-, nano-and hierarchical structures for superhydrophobicity, self-cleaning and low adhesion. *Philosophical Transactions of the Royal Society of London A: Mathematical, Physical and Engineering Sciences* **2009,** *367* (1894), 1631-1672.
87. Darmanin, T.; Guittard, F., Superhydrophobic and superoleophobic properties in nature. *Mater. Today* **2015,** *18* (5), 273-285.
88. Liu, K.; Yao, X.; Jiang, L., Recent developments in bio-inspired special wettability. *Chem. Soc. Rev.* **2010,** *39* (8), 3240-3255.
89. Barthlott, W.; Neinhuis, C., Purity of the sacred lotus, or escape from contamination in biological surfaces. *Planta* **1997,** *202* (1), 1-8.
90. Cao, M.; Guo, D.; Yu, C.; Li, K.; Liu, M.; Jiang, L., Water-repellent properties of superhydrophobic and lubricant-infused "slippery" surfaces: A brief study on the functions and applications. *ACS Appl. Mater. Interfaces* **2015,** *8* (6), 3615-3623.
91. Wang, L.; Zhou, Q.; Zheng, Y.; Xu, S., Composite structure and properties of the pitcher surface of the carnivorous plant Nepenthes and its influence on the insect attachment system. *Progress in Natural Science* **2009,** *19* (12), 1657-1664.
92. Gaume, L.; Perret, P.; Gorb, E.; Gorb, S.; Labat, J.-J.; Rowe, N., How do plant waxes cause flies to slide? Experimental tests of wax-based trapping mechanisms in three pitfall carnivorous plants. *Arthropod structure & development* **2004,** *33* (1), 103-111.
93. Fadeeva, E.; Chichkov, B., Biomimetic Liquid-Repellent Surfaces by Ultrafast Laser Processing. *Applied Sciences* **2018,** *8* (9), 1424.
94. Xiao, L.; Li, J.; Mieszkin, S.; Di Fino, A.; Clare, A. S.; Callow, M. E.; Callow, J. A.; Grunze, M.; Rosenhahn, A.; Levkin, P. A., Slippery liquid-infused porous surfaces showing marine antibiofouling properties. *ACS Appl. Mater. Interfaces* **2013,** *5* (20), 10074-10080.
95. Lee, S. G.; Lim, H. S.; Lee, D. Y.; Kwak, D.; Cho, K., Tunable anisotropic wettability of rice leaf‐like wavy surfaces. *Adv. Funct. Mater.* **2013,** *23* (5), 547-553.
96. Mele, E.; Girardo, S.; Pisignano, D., Strelitzia reginae leaf as a natural template for anisotropic wetting and superhydrophobicity. *Langmuir* **2012,** *28* (11), 5312-5317.
97. Yao, J.; Wang, J.; Yu, Y.; Yang, H.; Xu, Y., Biomimetic fabrication and characterization of an artificial rice leaf surface with anisotropic wetting. *Chin. Sci. Bull.* **2012,** *57* (20), 2631-2634.

98. Wu, S.-Z.; Wu, D.; Yao, J.; Chen, Q.-D.; Wang, J.-N.; Niu, L.-G.; Fang, H.-H.; Sun, H.-B., One-Step Preparation of Regular Micropearl Arrays for Two-Direction Controllable Anisotropic Wetting. *Langmuir* **2010,** *26* (14), 12012-12016.
99. Zhu, J.; Tian, Y.; Liu, X.; Yang, C., Lithography-induced hydrophobic surfaces of silicon wafers with excellent anisotropic wetting properties. *Microsystem Technologies*, 1-11.
100. Chung, J. Y.; Youngblood, J. P.; Stafford, C. M., Anisotropic wetting on tunable micro-wrinkled surfaces. *Soft Matter* **2007,** *3* (9), 1163-1169.
101. Gleiche, M.; Chi, L. F.; Fuchs, H., Nanoscopic channel lattices with controlled anisotropic wetting. *Nature* **2000,** *403* (6766), 173.
102. Wu, H.; Zhang, R.; Sun, Y.; Lin, D.; Sun, Z.; Pan, W.; Downs, P., Biomimetic nanofiber patterns with controlled wettability. *Soft matter* **2008,** *4* (12), 2429-2433.
103. Bixler, G. D.; Bhushan, B., Bioinspired rice leaf and butterfly wing surface structures combining shark skin and lotus effects. *Soft matter* **2012,** *8* (44), 11271-11284.
104. Hao, B.; Lin, W.; Jie, J.; Ruize, S.; Yongmei, Z.; Lei, J., Efficient Water Collection on Integrative Bioinspired Surfaces with Star-Shaped Wettability Patterns. *Adv. Mater.* **2014,** *26* (29), 5025-5030.
105. Li, H.; Lai, Y.; Huang, J.; Tang, Y.; Yang, L.; Chen, Z.; Zhang, K.; Wang, X.; Tan, L. P., Multifunctional wettability patterns prepared by laser processing on superhydrophobic TiO 2 nanostructured surfaces. *Journal of Materials Chemistry B* **2015,** *3* (3), 342-347.
106. Lai, Y.; Pan, F.; Xu, C.; Fuchs, H.; Chi, L., In situ surface‐modification‐induced superhydrophobic patterns with reversible wettability and adhesion. *Adv. Mater.* **2013,** *25* (12), 1682-1686.
107. Seo, J.; Lee, S.; Lee, J.; Lee, T., Guided transport of water droplets on superhydrophobic–hydrophilic patterned Si nanowires. *ACS Appl. Mater. Interfaces* **2011,** *3* (12), 4722-4729.
108. Ghosh, A.; Ganguly, R.; Schutzius, T. M.; Megaridis, C. M., Wettability patterning for high-rate, pumpless fluid transport on open, non-planar microfluidic platforms. *Lab on a Chip* **2014,** *14* (9), 1538-1550.
109. Lim, H. S.; Han, J. T.; Kwak, D.; Jin, M.; Cho, K., Photoreversibly switchable superhydrophobic surface with erasable and rewritable pattern. *J. Am. Chem. Soc.* **2006,** *128* (45), 14458-14459.
110. Ishizaki, T.; Saito, N.; Takai, O., Correlation of cell adhesive behaviors on superhydrophobic, superhydrophilic, and micropatterned superhydrophobic/superhydrophilic surfaces to their surface chemistry. *Langmuir* **2010,** *26* (11), 8147-8154.
111. Ueda, E.; Levkin, P. A., Emerging applications of superhydrophilic‐superhydrophobic micropatterns. *Adv. Mater.* **2013,** *25* (9), 1234-1247.
112. Yong, J.; Chen, F.; Yang, Q.; Huo, J.; Hou, X., Superoleophobic surfaces. *Chem. Soc. Rev.* **2017,** *46* (14), 4168-4217.
113. Helbig, R.; Nickerl, J.; Neinhuis, C.; Werner, C., Smart skin patterns protect springtails. *PloS one* **2011,** *6* (9), e25105.
114. Hensel, R.; Helbig, R.; Aland, S.; Voigt, A.; Neinhuis, C.; Werner, C., Tunable nano-replication to explore the omniphobic characteristics of springtail skin. *NPG Asia Materials* **2013,** *5* (2), e37.
115. Liu, Q.; Xu, B., A unified mechanics model of wettability gradient-driven motion of water droplet on solid surfaces. *Extreme Mechanics Letters* **2016,** *9*, 304-309.
116. Drelich, J.; Chibowski, E.; Meng, D. D.; Terpilowski, K., Hydrophilic and superhydrophilic surfaces and materials. *Soft Matter* **2011,** *7* (21), 9804-9828.
117. Diouf, A.; Darmanin, T.; Dieng, S. Y.; Guittard, F., Superhydrophobic (low adhesion) and parahydrophobic (high adhesion) surfaces with micro/nanostructures or nanofilaments. *J. Colloid Interface Sci.* **2015,** *453*, 42-47.
118. Shang, H.; Wang, Y.; Limmer, S.; Chou, T.; Takahashi, K.; Cao, G., Optically transparent superhydrophobic silica-based films. *Thin Solid Films* **2005,** *472* (1-2), 37-43.
119. Gurav, A. B.; Latthe, S. S.; Vhatkar, R. S.; Lee, J.-G.; Kim, D.-Y.; Park, J.-J.; Yoon, S. S., Superhydrophobic surface decorated with vertical ZnO nanorods modified by stearic acid. *Ceram. Int.* **2014,** *40* (5), 7151-7160.

120. Yang, H.; Pi, P.; Cai, Z.-Q.; Wen, X.; Wang, X.; Cheng, J.; Yang, Z.-r., Facile preparation of super-hydrophobic and super-oleophilic silica film on stainless steel mesh via sol–gel process. *Appl. Surf. Sci.* **2010,** *256* (13), 4095-4102.
121. Schmidt, H., Chemistry of material preparation by the sol-gel process. *J. Non-Cryst. Solids* **1988,** *100* (1-3), 51-64.
122. Nystrom, D.; Lindqvist, J.; Ostmark, E.; Antoni, P.; Carlmark, A.; Hult, A.; Malmstrom, E., Superhydrophobic and self-cleaning bio-fiber surfaces via ATRP and subsequent postfunctionalization. *ACS Appl. Mater. Interfaces* **2009,** *1* (4), 816-823.
123. Yuan, S.; Pehkonen, S. O.; Liang, B.; Ting, Y. P.; Neoh, K. G.; Kang, E. T., Superhydrophobic fluoropolymer-modified copper surface via surface graft polymerisation for corrosion protection. *Corros. Sci.* **2011,** *53* (9), 2738-2747.
124. Burtovyy, O.; Klep, V.; Chen, H. C.; Hu, R. K.; Lin, C. C.; Luzinov, I., Hydrophobic modification of polymer surfaces via "grafting to" approach. *Journal of Macromolecular Science, Part B: Physics* **2007,** *46* (1), 137-154.
125. Benetti, E. M.; Spencer, N. D., Are Lubricious Polymer Brushes Antifouling? Are Antifouling Polymer Brushes Lubricious? *Polymer and Biopolymer Brushes: For Materials Science and Biotechnology* **2018**.
126. Kobayashi, M.; Terayama, Y.; Yamaguchi, H.; Terada, M.; Murakami, D.; Ishihara, K.; Takahara, A., Wettability and antifouling behavior on the surfaces of superhydrophilic polymer brushes. *Langmuir* **2012,** *28* (18), 7212-7222.
127. Zander, N. E.; Orlicki, J. A.; Karikari, A. S.; Long, T. E.; Rawlett, A. M., Super-Hydrophobic Surfaces via Micrometer-Scale Templated Pillars. *Chem. Mater.* **2007,** *19* (25), 6145-6149.
128. Lee, K.; Lyu, S.; Lee, S.; Kim, Y. S.; Hwang, W., Characteristics and self-cleaning effect of the transparent super-hydrophobic film having nanofibers array structures. *Appl. Surf. Sci.* **2010,** *256* (22), 6729-6735.
129. Roach, P.; Shirtcliffe, N. J.; Newton, M. I., Progess in superhydrophobic surface development. *Soft matter* **2008,** *4* (2), 224-240.
130. Zheng, Y.; Gao, X.; Jiang, L., Directional adhesion of superhydrophobic butterfly wings. *Soft Matter* **2007,** *3* (2), 178-182.
131. Wu, D.; Wang, J. N.; Wu, S. Z.; Chen, Q. D.; Zhao, S.; Zhang, H.; Sun, H. B.; Jiang, L., Three‐Level Biomimetic Rice‐Leaf Surfaces with Controllable Anisotropic Sliding. *Adv. Funct. Mater.* **2011,** *21* (15), 2927-2932.
132. Huang, J.; Kunitake, T., Nano-Precision Replication of Natural Cellulosic Substances by Metal Oxides. *J. Am. Chem. Soc.* **2003,** *125* (39), 11834-11835.
133. Liu, Y.; Song, Y.; Niu, S.; Zhang, Y.; Han, Z.; Ren, L., Integrated super-hydrophobic and antireflective PDMS bio-templated from nano-conical structures of cicada wings. *RSC Advances* **2016,** *6* (110), 108974-108980.
134. Fik, C. P.; Meuris, M.; Salz, U.; Bock, T.; Tiller, J. C., Ultrahigh‐Aspect Ratio Microfiber‐Furs as Plant‐Surface Mimics Derived from Teeth. *Adv. Mater.* **2011,** *23* (31), 3565-3569.
135. Lee, C. H.; Jung, P. G.; Lee, S. M.; Park, S. H.; Shin, B. S.; Kim, J.-H.; Hwang, K.-Y.; Kim, K. M.; Ko, J. S., Replication of polyethylene nano-micro hierarchical structures using ultrasonic forming. *Journal of Micromechanics and Microengineering* **2010,** *20* (3), 035018.
136. Wang, J. H., 5 - Surface preparation techniques for biomedical applications. In *Coatings for Biomedical Applications*, Driver, M., Ed. Woodhead Publishing: 2012; pp 143-175.
137. Balu, B.; Kim, J. S.; Breedveld, V.; Hess, D. W., Tunability of the adhesion of water drops on a superhydrophobic paper surface via selective plasma etching. *J. Adhes. Sci. Technol.* **2009,** *23* (2), 361-380.
138. Shiu, J.-Y.; Kuo, C.-W.; Chen, P.; Mou, C.-Y., Fabrication of Tunable Superhydrophobic Surfaces by Nanosphere Lithography. *Chem. Mater.* **2004,** *16* (4), 561-564.
139. Li, X.-M.; Reinhoudt, D.; Crego-Calama, M., What do we need for a superhydrophobic surface? A review on the recent progress in the preparation of superhydrophobic surfaces. *Chem. Soc. Rev.* **2007,** *36* (8), 1350-1368.
140. de Meijer, M.; Haemers, S.; Cobben, W.; Militz, H., Surface energy determinations of wood: comparison of methods and wood species. *Langmuir* **2000,** *16* (24), 9352-9359.
141. Mantanis, G.; Young, R., Wetting of wood. *Wood science and Technology* **1997,** *31* (5), 339.

142. Hse, C.-Y., Wettability of southern pine veneer by phenol formaldehyde wood adhesives. *Forest Products Journal, Vol. 22 (1): 51-56* **1972**.
143. Stehr, M.; Gardner, D. J.; Wålinder, M. E., Dynamic wettability of different machined wood surfaces. *The Journal of Adhesion* **2001,** *76* (3), 185-200.
144. Shupe, T. F.; Hse, C. Y.; Wang, W. H., An investigation of selected factors that influence hardwood wettability. *Holzforschung* **2001,** *55* (5), 541-548.
145. Hameed, M.; Roffael, E., Über die Benetzbarkeit von Splint-und Kernholz der Kiefer, Douglasie und Lärche. *European Journal of Wood and Wood Products* **1999,** *57* (4), 287-293.
146. Shen, Q.; Nylund, J.; Rosenholm, J. B., Estimation of the surface energy and acid-base properties of wood by means of wetting method. *Holzforschung-International Journal of the Biology, Chemistry, Physics and Technology of Wood* **1998,** *52* (5), 521-529.
147. Wang, C.; Piao, C., From hydrophilicity to hydrophobicity: A critical review—part II: Hydrophobic conversion. *Wood and Fiber Science* **2011,** *43* (1), 41-56.
148. Candelier, K.; Dumarçay, S.; Pétrissans, A.; Gérardin, P.; Pétrissans, M., Comparison of mechanical properties of heat treated beech wood cured under nitrogen or vacuum. *Polym. Degrad. Stab.* **2013,** *98* (9), 1762-1765.
149. Esteves, B.; Pereira, H., Wood modification by heat treatment: A review. *BioResources* **2008,** *4* (1), 370-404.
150. Rowell, R. M., Acetylation. *Forest products journal. Vol. 56, no. 9 (Sept. 2006): pages 4-12.* **2006**.
151. Wang, X.; Chai, Y.; Liu, J., Formation of highly hydrophobic wood surfaces using silica nanoparticles modified with long-chain alkylsilane. *Holzforschung* **2013,** *67* (6), 667-672.
152. Owen, N. L.; Banks, W. B.; West, H., FTIR studies of the "wood"-isocyanate reaction. *J. Mol. Struct.* **1988,** *175*, 389-394.
153. Thygesen, L. G.; Engelund, E. T.; Hoffmeyer, P., Water sorption in wood and modified wood at high values of relative humidity. Part I: results for untreated, acetylated, and furfurylated Norway spruce. *Holzforschung* **2010,** *64* (3), 315-323.
154. Papadopoulos, A. N.; Mantanis, G., Vapour sorption studies of Belmadur wood. *Advances in Forestry Letter* **2012,** *1* (1), 1-6.
155. Ermeydan, M. A.; Cabane, E.; Gierlinger, N.; Koetz, J.; Burgert, I., Improvement of wood material properties via in situ polymerization of styrene into tosylated cell walls. *RSC Advances* **2014,** *4* (25), 12981-12988.
156. Ermeydan, M. A.; Cabane, E.; Hass, P.; Koetz, J.; Burgert, I., Fully biodegradable modification of wood for improvement of dimensional stability and water absorption properties by poly (ε-caprolactone) grafting into the cell walls. *Green Chemistry* **2014,** *16* (6), 3313-3321.
157. Mattos, B. D.; Missio, A. L.; Cademartori, P. H. G.; Lourençon, T. V.; Gatto, D. A.; Magalhães, W. L. E., Pinewood Composite Prepared by In Situ Graft Polymerization of Epoxy Monomer. *Polym. Compos.* **2017,** *38* (3), 597-603.
158. Fu, Y.; Li, G.; Yu, H.; Liu, Y., Hydrophobic modification of wood via surface-initiated ARGET ATRP of MMA. *Appl. Surf. Sci.* **2012,** *258* (7), 2529-2533.
159. Zheng, R.; Tshabalala, M. A.; Li, Q.; Wang, H., Construction of hydrophobic wood surfaces by room temperature deposition of rutile (TiO2) nanostructures. *Appl. Surf. Sci.* **2015,** *328*, 453-458.
160. Wang, C.; Piao, C.; Lucas, C., Synthesis and characterization of superhydrophobic wood surfaces. *J. Appl. Polym. Sci.* **2011,** *119* (3), 1667-1672.
161. Chang, H.; Tu, K.; Wang, X.; Liu, J., Fabrication of mechanically durable superhydrophobic wood surfaces using polydimethylsiloxane and silica nanoparticles. *Rsc Advances* **2015,** *5* (39), 30647-30653.
162. Wang, S.; Liu, C.; Liu, G.; Zhang, M.; Li, J.; Wang, C., Fabrication of superhydrophobic wood surface by a sol–gel process. *Appl. Surf. Sci.* **2011,** *258* (2), 806-810.
163. Gan, W.; Gao, L.; Sun, Q.; Jin, C.; Lu, Y.; Li, J., Multifunctional wood materials with magnetic, superhydrophobic and anti-ultraviolet properties. *Appl. Surf. Sci.* **2015,** *332*, 565-572.
164. Hill, C. A., *Wood modification: chemical, thermal and other processes*. John Wiley & Sons: 2007; Vol. 5.

2. Publications

This cumulative thesis is mainly based on three first-authored research articles which are reprinted in Chapter 2. The authors' contributions are described.

Subchapter 2.1: Wang, Y., Yan, W., Frey, M., Vidiella del Blanco, M., Schubert, M., Adobes-Vidal, M., & Cabane, E. (2018). Liquid-Like SiO_2-g-PDMS Coatings on Wood Surfaces with Underwater Durability, Antifouling, Antismudge, and Self-Healing Properties. Advanced Sustainable Systems, 1800070.

Contribution:
Y.W. and E.C. designed the experiment. Y.W. performed the chemical modification. W.Y. conducted the antifouling test. F.M. and M.A.-V. carried out the AFM imaging and force spectroscopy. M.V. performed the ESEM imaging. M.S. performed the bacteria resistance test. Y.W. performed the rest material characterizations in the article. Y.W. and E.C. analyzed the data and co-wrote the paper. All the authors discussed results and commented on the manuscript.

Subchapter 2.2: Wang, Y., Tian, T., & Cabane, E. (2017). Wood Composites with Wettability Patterns Prepared by Controlled and Selective Chemical Modification of a Three-Dimensional Wood Scaffold. ACS Sustainable Chemistry & Engineering, 5(12), 11686-11694.

Contribution:
Y.W. and E.C. designed the experiment, analyzed the data and co-wrote the paper. T.T. measured the water contact angles of wood by the ultrasmall droplets. All the authors discussed results and commented on the manuscript.

Subchapter 2.3: Wang, Y., Vitas, S., Burgert, I. & Cabane, E. (2018) Beech Wood Cross-sections as a Natural Template to Fabricate Superhydrophobic Surfaces, ACS Applied Materials & Interfaces, submitted.

Contribution:
Y.W. and E.C. designed the experiment. S.V. analyzed wood pores counting. I.B. contributed to the analysis of wood anatomical structure. Y.W. and E.C. analyzed the rest of the data in the

article. Y.W., E.C. and I.B. co-wrote the paper. All the authors discussed results and commented on the manuscript.

2.1 Liquid-like SiO_2-g-PDMS coatings on wood surfaces with underwater durability, anti-fouling, anti-smudge and self-healing properties

Yaru Wang, Wenqing Yan, Marion Frey, Marta Vidiella del Blanco, Mark Schubert, Maria Adobes-Vidal, Etienne Cabane*

Y. Wang, M. Frey, M. Vidiella del Blanco, Dr. M. Adobes-Vidal, Dr. E. Cabane
Wood Materials Science, ETH Zürich, Stefano-Franscini-Platz 3, CH-8093 Zürich, Switzerland
Applied Wood Materials, EMPA-Swiss Federal Laboratories for Materials Science and Technology, Überlandstrasse 129, CH-8600 Dübendorf, Switzerland
E-mail: cabanee@ethz.ch

Dr. M. Schubert
Applied Wood Materials, EMPA-Swiss Federal Laboratories for Materials Science and Technology, Überlandstrasse 129, CH-8600 Dübendorf, Switzerland

W. Yan
Laboratory for Surface Science and Technology, Department of Materials, ETH Zürich, Vladimir-Prelog-Weg 1-5/10, CH-8093 Zürich, Switzerland

Wang, Y., Yan, W., Frey, M., Vidiella del Blanco, M., Schubert, M., Adobes-Vidal, M. and Cabane, E., Liquid-Like SiO_2-g-PDMS Coatings on Wood Surfaces with Underwater Durability, Antifouling, Antismudge, and Self-Healing Properties. *Advanced Sustainable Systems*, 2018, 1800070.

Keywords: wood materials, functional coatings, polydimethylsiloxane, antifouling, self-healing

Abstract

Recent research on surfaces with special wettability lead to the development of “liquid surfaces”, obtained through the immobilization of a lubricant liquid on a porous interface, or through the grafting of flexible polymer chains on smooth surfaces. We adapted the latter

method to fabricate durable protective coatings on wood surfaces. The method is based on a first modification with a silicon oxide layer, followed by the grafting of PDMS chains. The obtained surfaces are hydrophobic, and are highly durable when compared to classical superhydrophobic coatings, in particular after prolonged immersion in water. We also report on a self-healing ability, provided by the rearrangement of the PDMS chains after plasma treatment. Finally, our coatings have anti-smudge, antifouling, and antibacterial properties. With durable water repellency, quick self-healing ability, anti-smudge, antifouling, and antibacterial properties, the durability of wood is increased. Our research demonstrates the protection potential of liquid-like polymer coatings on wood, a material that will play an essential role in the transition towards more sustainable societies.

Introduction

The growing demand for sustainable products has led to a renewed interest for abundant biological materials, such as wood. Wood possesses many advantages: it is a lightweight, mechanically strong, and aesthetically appealing material with good workability and facile scale-up.[1] However, like most natural materials, wood faces durability issues in the long-term due to its interaction with water, UV-light,[2] and various living microorganisms.[3] Consequently, the development of protective treatments continues to be a very important field of research.[4]

Wood is a highly hygroscopic material, and the presence of water inevitably leads to dimensional instability – arising from the swelling and shrinking of the cell wall structure – and to slow decay caused by cell wall degradation initiated by bacteria and fungi.[5] Thus, addressing the issue of water absorption is crucial to maintain both dimensional stability and resistance to biodegradation.[1] Various wood surface modifications were proposed to increase water repellency.[6] In general, according to the treatment utilized, hydrophobizing a wood surface may not only increase water repellency, but it may also affect other surface properties: it can prevent spoilage by other substances (anti-smudge effect), or it can prevent the attachment of microorganisms (anti-fouling effect).

The development of surfaces with special wettability and associated properties (superhydrophobic, superoleophobic, anti-fouling, anti-bacterial, anti-smudge, etc…) attracts interests from both the academic and industry fields.[7-10] Reference works from Wenzel,[11] and Cassie and Baxter[12] have pointed out that superhydrophobic surfaces can be obtained through a combination of surface structuration and low energy compounds.[13-14] However, despite

decades of intensive research, practical applications of these surfaces are still limited because of various reasons: i) they usually fail under pressure and upon physical stress (low wear resistance); ii) they lack self-healing capability; iii) they usually have limited repellency towards solvents and oils; iv) they may not be transparent (light scattering due to surface microstructures); v) they are rather sophisticated (i.e. expensive to produce and structuration on large scales is still a highly challenging manufacturing process); vi) they use low surface energy chemicals such as fluorinated molecules which is problematic because they are toxic and accumulate in the environment.[15]

To circumvent part of the above-mentioned problems, a new concept inspired by the peristome of pitcher plants was proposed.[16] This technique, coined as "SLIPS" (Slippery Liquid-Infused Porous Surfaces) is based on changing a solid surface into a liquid one. A microporous material is infused by a lubricating fluid resulting in a continuous molecularly smooth liquid film, which acts as a lubricating layer. The immobilized fluid creates a slippery surface, which acts efficiently against various types of fouling, repels contaminants and liquids,[17-18] and has anti-icing and anti-frost properties.[19]

In another approach using a similar concept, Wang et al. functionalized plasma treated glass surfaces with long and flexible polydimethylsiloxane (PDMS) chains.[17] These polymer chains can be slightly hydrated, and behave like a liquid layer at the substrate surface. This lubrication effect is also used in nature, e.g. the combination of water with sugar chains on biological surfaces is the basis of biological lubrication systems.[20] The PDMS-grafted liquid-like surfaces developed by Wang et al. provide a promising alternative to SLIPS, since the utilization of a fluorinated lubricant (that can potentially leach out) and the surface structuration to obtain a porous layer are circumvented.

The development of SLIPS on wood surfaces has been reported by Guo et al.[21] They created an artificial porous layer modifying spruce wood surfaces by growing zinc oxide rods, and infusing it with a fluorinated lubricant. They demonstrated the appreciable superhydrophobic and omniphobic properties of the modified wood.

In this work, we are using the surface lubrication approach based on covalently attached flexible polymer chains to design a durable protection for spruce, which is an extensively utilized species with limited durability. The method involves the formation of a smooth SiO_2 layer at micro level on the wood surface via solvent-free base-catalyzed hydrolysis of tetraethyl orthosilicate (TEOS), followed by in-situ grafting of flexible low-molecular-weight PDMS chains by acid-catalyzed polymerization of dimethyldimethoxysilane (DMDEOS). We show

that the wood surfaces with liquid-like PDMS coating are hydrophobic, highly durable, can resist to smudge and to fouling, and have self-healing capability and a slight antibacterial effect. The process is straightforward and sustainable (none or environmentally benign solvents are used), which is favorable for up scaling. In addition, since PDMS is biocompatible,[22] the sustainability of the final wood product remains. We expect that the approach can provide wood with longer service life while preserving its prised aesthetic appearance in demanding applications for indoor as well as outdoor utilizations.

Results and discussion

Surface Modification

The coatings are prepared in a two-step process, described in Figure 1. In the first step, we build up a silica layer on the wood veneer surface. To facilitate the deposition of the polysiloxane layer, we perform a direct silanization process without pre-hydrolysis of TEOS. The obtained SiO_2 coating provides a favorable anchoring substrate to grow PDMS chains in the second step.

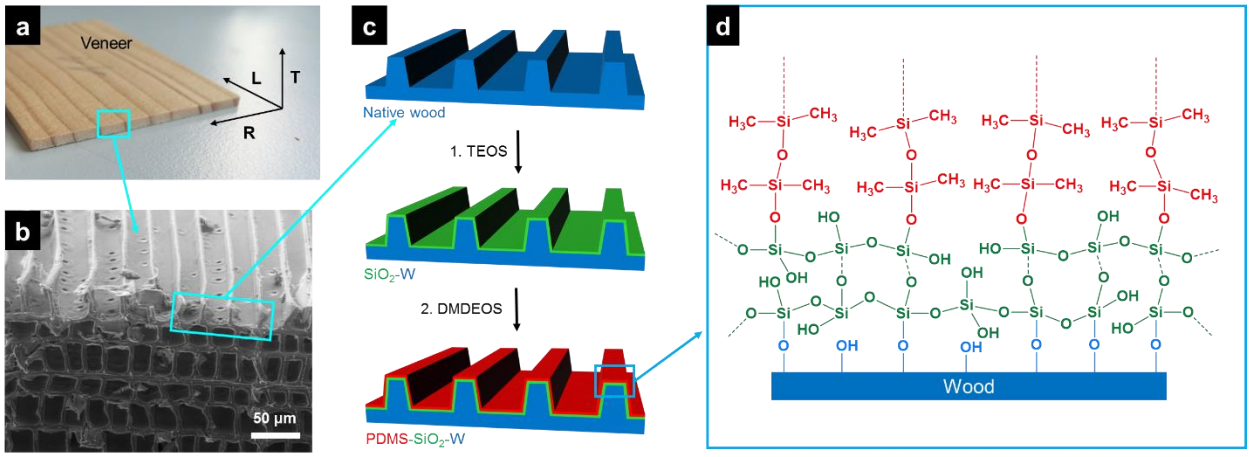

Figure 1: Scheme describing the wood surface modification approach. (a) Picture of a spruce veneer, showing the radial (R), tangential (T) and longitudinal (L) directions; (b) SEM image of the edge of a spruce veneer, showing the veneer surface and particularly its surface topography; (c) two-step modification of the wood surface; (d) scheme showing the SiO_2-PDMS coating on the wood surface.

In the second step, PDMS polymer chains are covalently attached to the silica layer through the grafting polymerization of DMDEOS monomers. The polycondensation is initiated by acid catalysis at the -OH groups from the silanols. The -O-Si-O- backbone of PDMS endows high flexibility to the linear polymers, hence the term “covalently attached liquids” was proposed by Wang et al.[17] The high mobility of the PDMS chains and its relatively low surface energy are the basis for the omniphobic properties of such surfaces.[23] For comparison purposes, a wood

sample was functionalized with fluorinated silica (from co-hydrolysis of POTS and TEOS), to design a traditional superhydrophobic wood surface (these samples are named F-SiO_2-W).[24] Fourier-transform infrared (FTIR) and X-ray diffraction (XRD) were used to characterize both the SiO_2 layer and the PDMS chains. In Figure 2a, we show the FTIR spectra of native wood (Native-W), SiO_2-W, and PDMS-SiO_2-W samples. The Native-W spectrum shows the characteristic peaks of the spruce wood polymer matrix. The broad signal between 3600 and 3100 cm^{-1} corresponds to the wood hydroxyl groups, absorbance at 1734 cm^{-1} is due to the stretching of C=O bonds from aldehydes and esters,[25] and the strong signal centered on 1060 cm^{-1} results from the C−O stretching of polysaccharides.[26] The FTIR spectrum for SiO_2-W reveals the characteristic bands associated to the silicon-based layer. The absorbance at 463 cm^{-1} is due to the bending mode of Si-O-Si, and peaks at 1087 cm^{-1} and 1200 cm^{-1} are associated with the stretching vibration of Si-O-Si.[27] For the PDMS-SiO_2-W samples, we identified various characteristic PDMS peaks. At 2961 cm^{-1}, we see the asymmetric C-H stretching in $-Si-CH_3$. The sharp peak at 1261 cm^{-1} is assigned to the symmetric C-H deformation in $-Si-CH_3$. Signal for the $Si-CH_3$ vibrations can be seen at 781 cm^{-1},[28] while the signals at 1014 and 1078 cm^{-1} correspond to the Si−O−Si vibrations.[26, 29]

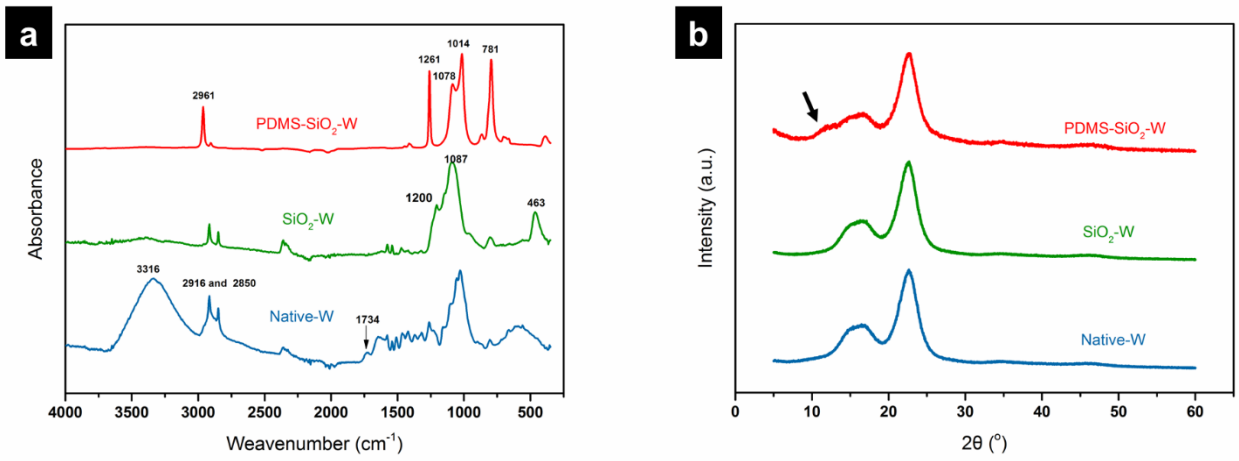

Figure 2: (a) FTIR spectra of native-W, SiO_2-W, PDMS-SiO_2-W; (b) XRD patterns of native-W, SiO_2-W, PDMS-SiO_2-W (the arrow shows the shoulder at 11.6°, characteristic for the PDMS).

The XRD patterns are shown in Figure 2b (the XRD pattern for F-SiO_2-W is given in Figure S1). In all samples, we observed the two characteristic diffraction peaks at 16.0° and 22.3°, which result from the crystalline regions of cellulose in the wood matrix.[30] The synthesized silica layer is amorphous, therefore no additional diffraction peaks are observed in the SiO_2-W pattern. PDMS on the other hand is known to display a characteristic peak at 11.6°.[28] This

signal can be identified in the PDMS-SiO_2-W pattern as a clear shoulder preceding the cellulose peak at 16°.

Surface morphology and surface roughness

Surface roughness and the homogeneity of the surface treatment can strongly influence surface wettability. We therefore characterized the surface morphology and roughness of our wood surfaces before and after each step of the modification process. We analyzed the surfaces at micro- and nano-scale. At the microscale, we can observe the natural structuration of the spruce wood surface, resulting from the cut open tracheids (see Figure 3).

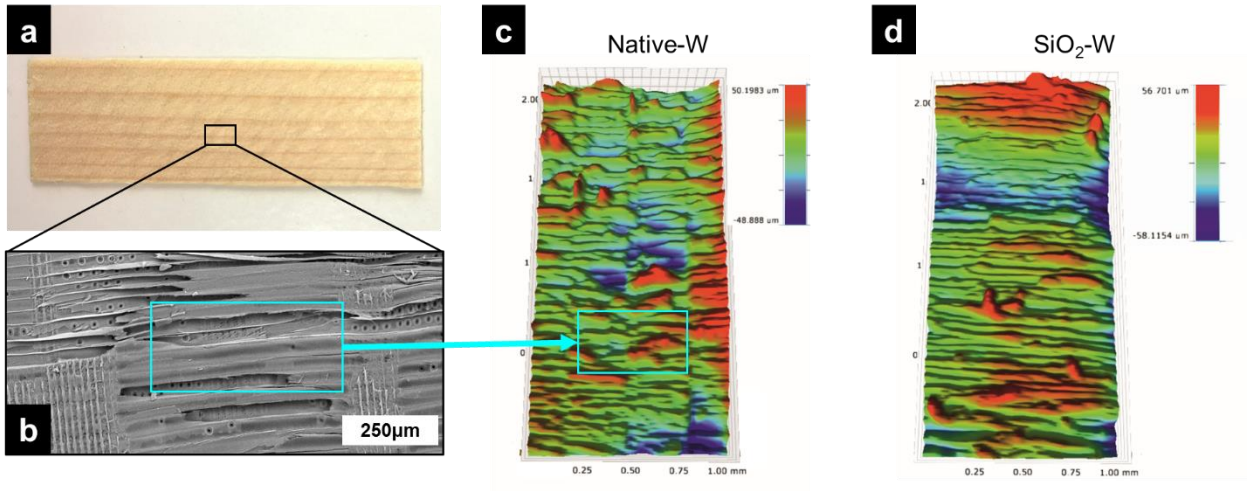

Figure 3: (a) picture of the unmodified spruce veneer; (b) SEM image of the native spruce wood surface showing the cut-open tracheids; (c) and (d) 3D surface profiles of native-W and SiO_2-W obtained by stylus surface profilometry.

At the microscale, the 3D profiles obtained with stylus profilometry do not show large differences in roughness between native wood and wood coated with the SiO_2 layer (roughness values are given Table S1). This confirms that the silica layer deposited in the first step is conformal to the wood natural structure at micro-scale.

The homogeneous coverage of the surface with the two-step process can be revealed by scanning electron microscopy. SEM images of the cell wall surface (S3 layer) from a native spruce wood sample are shown in Figure 4a-d. In the first step, we optimized the reaction conditions to obtain a homogeneous SiO_2 layer covering the wood surface. The process involves base-catalyzed hydrolysis and condensation of TEOS,[31] without any solvent. We found out that when low concentrations of NH_4OH are used, the silica layer is plagued with many defects

(Figure S2). We therefore opted for a high base concentration (~16.7% NH_4OH in water). Sol-gel reactions with high base concentrations are known to increase the reaction rates,[32] and the polymer network obtained is larger and more crosslinked.[31] This helps form a dense SiO_2 layer on the wood surface. The "craters" seen in Figure 4f, g may be generated from the evaporation of unreacted TEOS. With these optimal conditions, the SiO_2 layer obtained consists of a network of coalesced nanoparticles (Figure 4h, and a TEM image of the nanoparticles is provided in Figure S3), providing a rather homogeneous coverage of the wood structure. Most of the native wood features are still clearly visible after this first treatment step, confirming the conformal deposition of SiO_2.

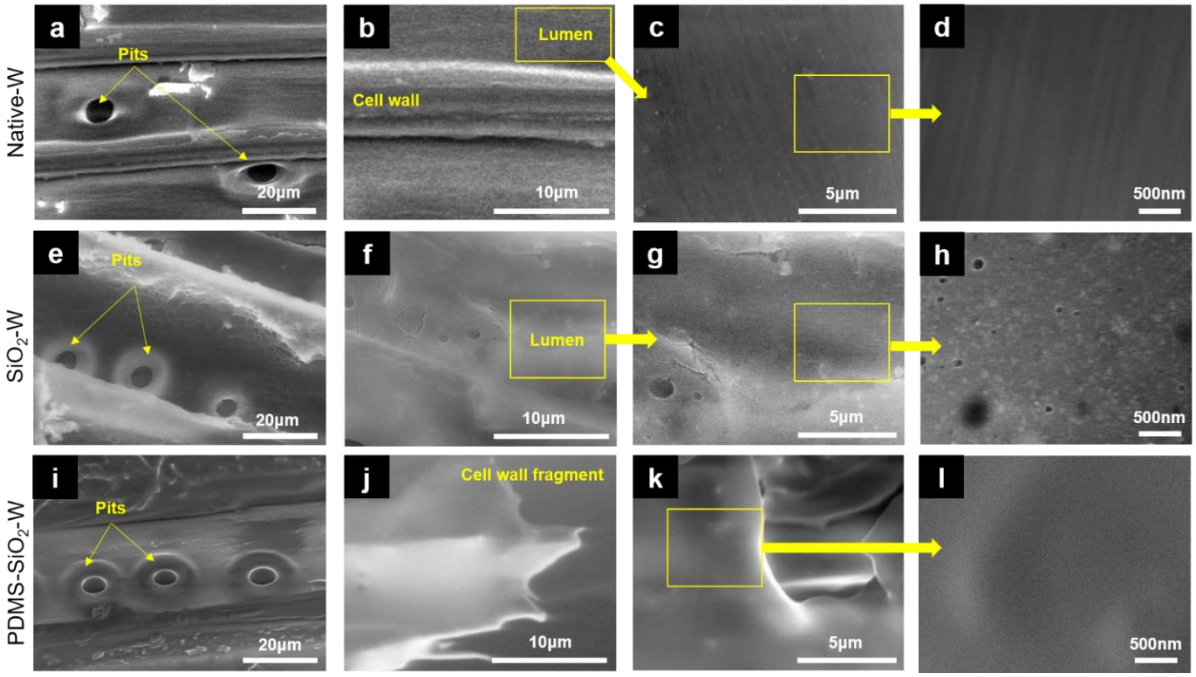

Figure 4: (a) to (d) SEM images of Native-W; (e) to (h), SEM images of SiO_2-W; (i), (k), and (l) SEM images of PDMS-SiO_2-W, and (h) is an ESEM image of PDMS-SiO_2-W.

As shown in Figure 4i, the grafting of PDMS chains on the SiO_2 layer does not affect the micro-structured wood surface (natural features remain), and a rather "liquid like" layer seems to form on the wood surface (see Figure 4j-l). In comparison to the smooth PDMS-SiO_2-W surfaces, fluorinated silica particles are clearly seen on the surface of wood treated with POTS (F-SiO_2-W, see Figure S4), thereby increasing the roughness of the native spruce wood surface.

The effect of the two treatment steps on surface morphology was further characterized at the nano-scale with AFM in QI-mode. In this imaging mode, force-distance curves are acquired in every pixel allowing obtaining topographical and physicochemical information of the surface

simultaneously, since the appearance of the force-distance curve provides insights into the nature of the tip-sample interaction. In Figure 5a,b the optical and AFM height images of the native wood lumen surface shows the fibrilar texture that is typically observed for an untreated spruce cell wall S3 layer.[33] After the first modification step, the wood surface is covered with the silica layer. While the fibrilar structure cannot be seen anymore, a distinct granular structure at nanoscale can be observed (see Figure 5c). This confirms the SEM observations, and supports the hypothesis of a silica layer constituted by the dense packing of nano-sized SiO_2 particles. The AFM height image of the surface taken after the grafting of PDMS chains (Figure 5d) shows very little difference with the SiO_2-W sample (the roughness values given in Table S2 are similar). This indicates that the tip penetrates the PDMS layer and profiles the underneath SiO_2 layer.

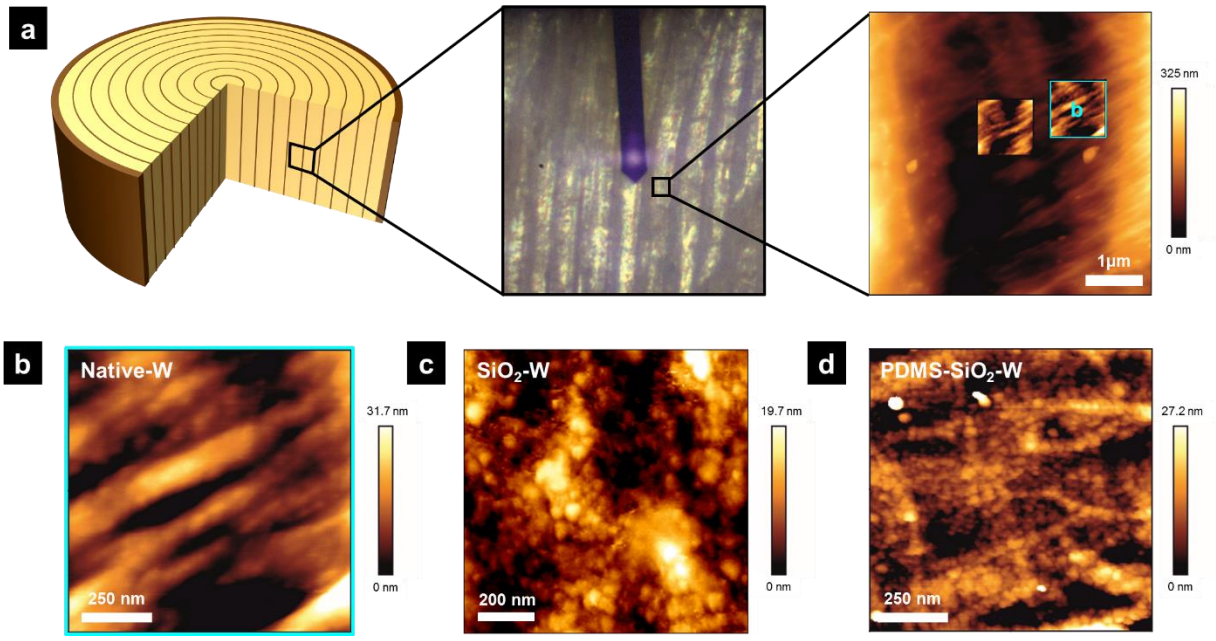

Figure 5: (a) Description of the location of the AFM measurements, with the optical image showing the position of the AFM tip on the wood surface, and a large AFM scan on native wood. The 1 µm² areas shown in (b) to (d) correspond to scans from the cell wall surfaces. (b) AFM height image of the S3 layer of native-W; (c) AFM image of the SiO_2 layer on SiO_2-W; (d) AFM height image of PDMS-SiO_2-W.

Although the surface topography is comparable, the force-distance curves obtained on both surfaces are very different, revealing the distinctive nature of the modified wood surfaces. In the case of SiO_2-W, a classic force-distance curve on a hard and incompressible surface is observed (Figure 6a). As the cantilever approaches the surface there is no deflection of the

cantilever (Figure 6a, point 1) until attractive forces (Van der Waals and capillary forces) overcome the cantilever spring constant and the tip jumps into contact with the sample, bending the cantilever towards the surface (Figure 6a, point 2). The tip remains in contact with the surface until the tip-sample separation is further decreased, causing an increase in repulsive contact force and cantilever deflection in the opposite direction (Figure 6a, segment 3). Once the cantilever deflection reaches a predetermined value, the tip is retracted (Figure 6a, point 4). The tip often remains in contact with the surface due to attractive interactions and the cantilever is deflected again towards the surface (Figure 6a, point 5) until the attractive forces are overcome and the tip breaks free (Figure 6a, point 6).

On the other hand, the force-distance curves obtained on PDMS-SiO_2-W are those typically observed for lubricant thin films on a solid surface[34] (Figure 6b), demonstrating the presence of a "liquid-like" layer. The cantilever approaches the PDMS-SiO_2-W surface and there is no deflection of the cantilever (Figure 6b, point 7) until the tip is attracted by the liquid film by capillary forces and jumps into contact with the PDMS liquid layer, bending the cantilever towards the surface (Figure 6b, point 8). As the cantilever advances further towards the surface, the tip goes through the liquid film causing the cantilever to continue bending monotonically towards the surface until the tip touches the stiff SiO_2 layer (Figure 6b, point 9). The tip remains in contact with the solid surface until the tip-sample separation is further decreased, causing an increase in repulsive contact force and a steep cantilever deflection in the opposite direction (Figure 6b, segment 10). Once the cantilever deflection reaches a desired value, the tip is retracted (Figure 6b, point 11). Hence, it is evident that the AFM height images of SiO_2-W and PDMS-SiO_2-W are very similar, since the morphology of the solid SiO_2-W layer is imaged in both samples.

Upon retraction of the cantilever from the SiO_2 layer, the tip goes back through the liquid PDMS layer (Figure 6b, from point 12 to 13). The distance is longer than the one between the same stages during the approach motion (Figure 6b, from point 8 to 9) due to the formation of a liquid neck around the tip. With increasing distance from the PDMS-SiO_2-W surface, the attractive capillary forces decrease until the force becomes smaller than the spring constant of the cantilever and the tip disengages from the surface, such that the cantilever is no longer bent (Figure 6b, point 14). The force between the tip and the surface (F) can be calculated according to Hooke's law $F = -kd$, where k is the spring constant of the cantilever and d is the measured deflection.

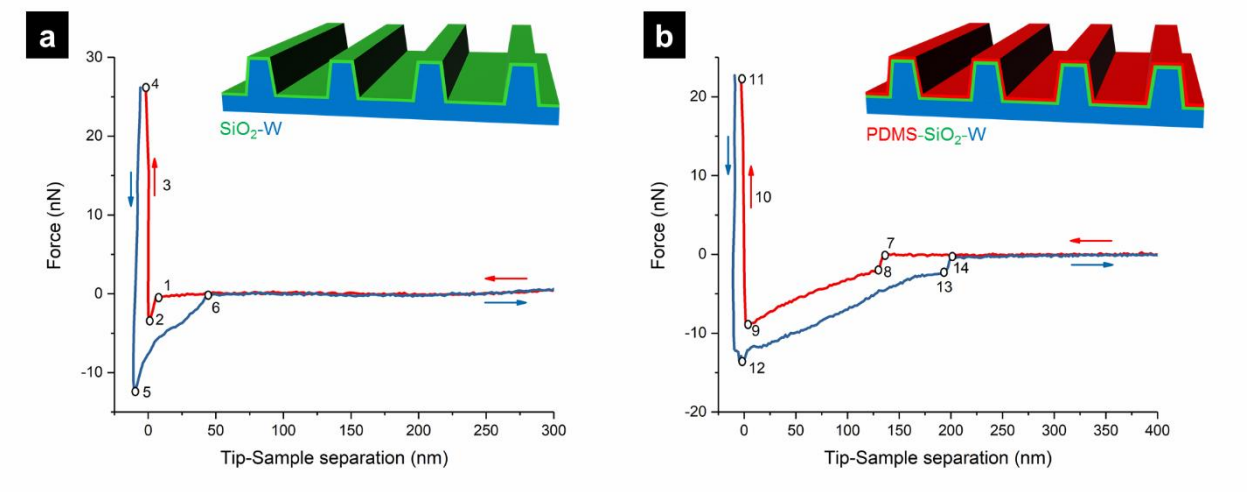

Figure 6: Force-distance curves on (a) SiO_2-W and (b) PDMS-SiO_2-W acquired during AFM imaging in QI mode. Approach and retract segments are depicted in red and blue color respectively. Force-distance curve on SiO_2-W resembles a classic force-distance curve on a hard and incompressible solid where the different points depict: 1-2 jump-to-contact, 3 cantilever deflection due to repulsive forces, 4 maximum desired force and 5-6 jump-off-contact. Force distance curve on PDMS-SiO_2-W shows the presence of a liquid film on a solid surface where the points depict: 7-8 jump-to-contact to the liquid, 8-9 tip goes through the PDMS liquid layer and touches the solid SiO_2-W surface, 10 cantilever deflection due to repulsive forces, 11 maximum desired force, 12-13 tip detaches from solid SiO_2-W surface and goes though the liquid PDMS layer and 13-14 jump-off-contact.

Surface wettability

Despite various attempts to modify wood with a wide range of hydrophobization methods, long-term underwater sustainability is rarely achieved. This is due to the difficulties of fully blocking hydroxyl groups on the wood surface, and to the limited resistance of classical superhydrophobic modifications. The latter are usually obtained with a combination of surface structuration and low energy compounds, to minimize the contact of water with the material through the creation of air pockets. However, these composite surfaces are known to undergo a transition from the Cassie-Baxter state to the Wenzel state under pressure.[35] Therefore, the Cassie state is not stable. In the case of wood (a naturally hygroscopic material), if such a surface treatment is used, water can be absorbed by capillary forces and spread inside the wood porous structure. Finally, a water film will cover the surface and the hydrophobic protection loses its effect.

The durability of a superhydrophobic surface can be characterized by the time during which the surface keeps its hydrophobic feature.[36] We compared the surface wettability of Native-W, PDMS-SiO_2-W, and F-SiO_2-W before and after long-term exposure to water by drop shape

analyzer. Static contact angle measurements in air show the effect of the treatments on the surface wetting with water (Figure 7a, b).

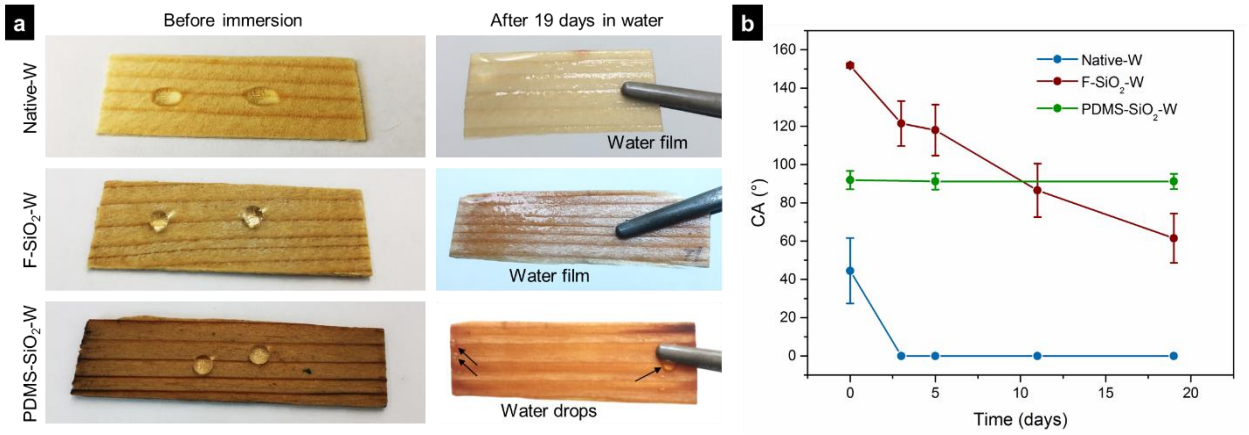

Figure 7: (a) pictures showing the behavior of water at the surface of native-W, F-SiO_2-W, and PDMS-SiO_2-W before and after immersion in water for 19 days. (b) Evolution of contact angles on native-W, F-SiO_2-W, and PDMS-SiO_2-W surfaces during immersion.

A comparison of the initial contact angles indicated that native wood is rather hygroscopic (CA of 44.5°) and that PDMS-SiO_2-W is hydrophobic (CA = 91.9°). Unsurprisingly, F-SiO_2-W exhibits superior hydrophobic properties with a CA above 150°.

We then compared the wettability of the three samples after prolonged immersion in water, and we observed a drastic decrease in CA for both native wood and F-SiO_2-W (Figure 7b). After three days, a water drop deposited on the native wood surface immediately spreads and forms a water film (Figure 7a), indicating that wood is fully soaked with water. For the F-SiO_2-W specimens, the CA slowly decreased from 151.8° to 61.5° after 19 days in water, and a water film covers the surface (Figure 7a, b). This indicates that the fluorinated particle treatment can hardly maintain its performance after a long exposition to water. It is well known that superhydrophobic surfaces obtained through micro-structuration face the danger of a transition from a Cassie-Baxter state to a Wenzel sate under pressure.[37] This results in a decrease in the apparent contact angle. In most severe cases, the hydrophobic effect is lost, and the material is no longer protected against water sorption. Remarkably, in comparison to native wood and F-SiO_2-W, the CA for PDMS-SiO_2-W is stable around 91° over 19 days immersion in water (Figure 7b). This shows that the PDMS treatment is robust, and as shown in Figure 7a, the hydrophobicity is retained (additional images showing the dewetting property of PDMS-SiO_2-W surfaces after 19 days immersion are given in Figure S5). The sliding angle (SA) and contact angle hysteresis (CAH) were also measured (see Table 1).

Table 1: Contact angles, sliding angles, and contact angle hysteresis for different wood surfaces before and after immersion in water.

Sample	Immersion time (days)	CA (°)	TA (°)	CAH (°)
Native-W	0	44.5 ± 17.1	--	--
	5	0	--	--
	19	0	--	--
F-SiO_2-W	0	151.8 ± 1.2	20.1 ± 7.0	18.4 ± 1.2
	5	118.0 ± 13.3	--	--
	19	61.5 ± 12.9	--	--
PDMS-SiO_2-W	0	91.9 ± 4.8	24.0 ± 8.1	16.7 ± 4.9
	5	91.2 ± 4.3	58.8 ± 14.2	39.7 ± 8.8
	19	91.2 ± 4.0	51.0 ± 12.7	29.4 ± 13.8

Before immersion in water, both F-SiO_2-W and PDMS-SiO_2-W are capable of repelling water away, with comparable TAs (respectively 20.1 ° and 24.0 °), while water droplets cannot roll off native wood surfaces. After 5 days exposure to water, F-SiO_2-W surface failed to shed water droplets (TA not measurable), while PDMS-SiO_2-W shows an increase in TA (from 24 ° to 58.8 °), with the CAH increasing from 16.7° to 39.7°. This indicates that F-SiO_2-W completely loses the water repellence ability. In contrast, even after 19 days, the low adhesion of water droplets to the PDMS-SiO_2-W surface persists, with a final CAH of around 30°. Although the nature of CAH is not fully explained yet, it is generally thought to be related to surface roughness and/or chemical heterogeneity. The critical contribution of the contact line structure to hysteresis phenomenon has been discussed in literature.[38] In their study, Gao and McCarthy clearly demonstrate that a smooth surface (at molecular and higher levels) exhibits a much lower CAH than a rough surface (at micro-level) made of the same material.[39] The higher CAH observed for the structured surface results from the liquid receding contact line pinning to micro-size posts.[39] As shown before, our modification barely affects the topography: the modified wood surface retains the microscopic wood anatomic features. Therefore, while smooth surfaces (such as clean glass) coated with PDMS brushes have low CAH,[17] the micro-size topography defects of our PDMS-coated wood surfaces leads to higher CAH values.

The water repellency mechanism of the liquid-like grafted PDMS surface is different from the structured superhydrophobic surfaces. As mentioned previously, and as observed for the F-SiO_2-W samples, water may penetrate the microstructures, destroying the superhydrophobic effect. In the case of the liquid-like grafted PDMS surfaces, although PDMS is hydrophobic, traces of water may wick into the flexible PDMS chains,[17] which will enhance the mobility of

the polymer chains. When the PDMS is swollen by traces of water, hydrophobic chains may rearrange and "burry" −OH groups inside the PDMS chains, presenting only hydrophobic $-CH_3$ groups to the surface. Decreasing the [−OH]/[$-CH_3$] ratio at the surface consequently leads to a reduction of surface energy, and in turn the interaction of water drops and PDMS surface is weakened.[40] This explains the low adhesion of water on the PDMS-SiO_2-W surface.

As discussed before, hydrostatic pressure might break the metastable state of superhydrophobic composite interfaces upon prolonged immersion. In the case of the SLIPS technology, the lubricant provides a liquid surface, which is homogeneous, defect-free, molecularly smooth, and resistant to pressure-induced water penetration.[38] However, the lubricant might finally be depleted and the effect is lost. In our work, the flexible grafted PDMS chains assume the function of the lubricants used in SLIPS. PDMS layer behaves as a liquid: the surface is smooth and presents much less defects than a classical structured surface. Like the SLIPS technology, problems related to the destruction of the solid-air-liquid interface are irrelevant. Besides, as opposed to SLIPS, since the PDMS chains are covalently attached to the substrate, there is no issue regarding depletion of the lubricant.

To conclude, the durability of the hydrophobicity from the PDMS-SiO_2 coating reported in Figure 7 results from the smooth and stable interface allowing to minimize the presence of defects leading to water intrusion and to eliminate problems related to pressure-induced penetration of water, and the covalent attachment ensures stability of the treatment.

Anti-smudge, antifouling, and antibacterial properties

Anti-smudge and antifouling properties are highly desirable for wood surfaces. They would allow for clean surfaces in various applications where the wood aesthetics are emphasized, such as wood veneers for the automotive industry, wood panels for interior decoration, or wood furniture.[41]

We tested the anti-smudge property of our modified wood surfaces by applying two acrylic paints. The pink solvent-based paint was sprayed on native-W and PDMS-SiO_2-W. We then removed the wet paint with a paper tissue. As shown in Figure 8a, the native wood sample is permanently stained with fluorescent pink color. In contrast, the paint can be easily removed from the treated wood surface, and we observe only traces of color on the wood surface. In the second test, the green lacquer was applied on the two wood surfaces and allowed to dry. After complete drying, we tried to peel the dried coating off the surfaces. As shown in Figure 8b, it was not possible to remove the varnish without damaging the surface of native wood, indicating

that the lacquer adheres strongly to the surface. Contrarily, we could easily detach the coating from the PDMS-SiO_2-W, without pulling of wood fibers, and without leaving traces of the green color. The anti-smudge property was also demonstrated by the easy cleaning with ethanol (experiment described in Figure S6).

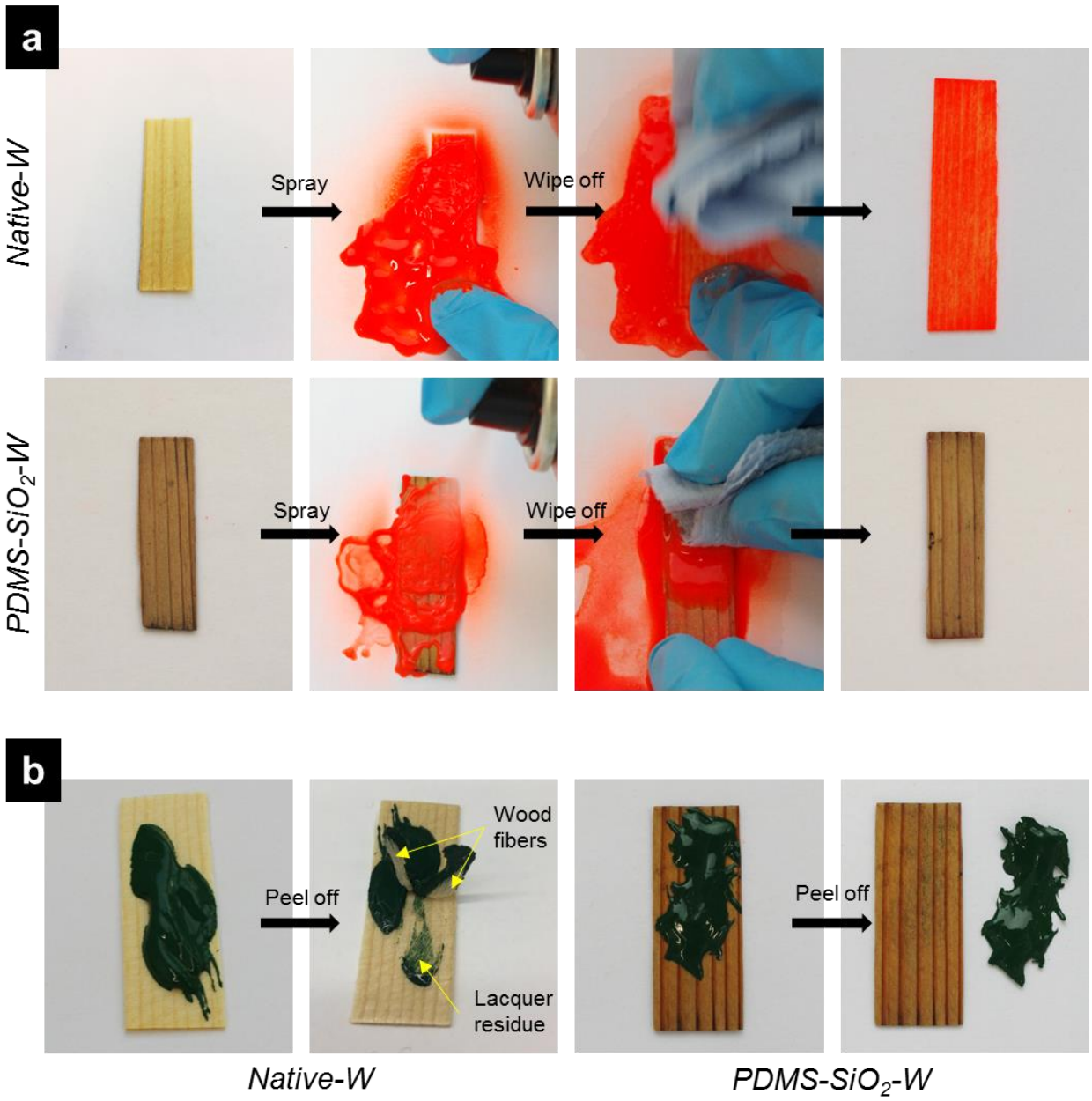

Figure 8: Images of the anti-smudge tests on native wood (Native-W) and surface treated wood (PDMS-SiO_2-W). (a) Test with a solvent-borne paint sprayed on wood surfaces, wiping with a dry tissue. Images of the cleaned surfaces clearly show the anti-smudge effect of the treated wood when compared to native wood. (b) Anti-smudge test with lacquer. This test shows that the lacquer adheres to untreated wood, but fails to attach to the treated wood. This result demonstrates that our modified wood has good resistance to smudge.

The oleophobic and hydrophobic properties of flexible PDMS chains has been discussed already by the Hozumi group.[42-43] Based on these reports, Rabnawaz et al.[44] developed anti-smudge coatings with block copolymers bearing flexible linear PDMS chains. Their surfaces repelled water due to the hydrophobic properties of PDMS, and repelled certain low surface tension liquids as well due to the conversion of the liquid/solid interface to a liquid/liquid interface: upon contact with a low surface tension liquid, the PDMS chains swell. Since a liquid flows faster in contact with another liquid, all tested liquids slip on the swollen grafted PDMS chains. Our PDMS-SiO_2-W surfaces most likely behave in the same way. Whether a solvent-based paint or lacquer is used, both substances cannot adhere on our PDMS grafted surface.

The growth of marine organisms on wooden boats can increase energy consumption, contribute to disseminate invasive species,[45] and increase maintaining costs. Controlling fouling is of both technical and economic interest.[18, 46-47] The design of antifouling coatings is associated with various surface characteristics, including surface energy, elastic modulus, electrostatic interactions, steric repulsion, hydration and topography.[48] Firstly, low surface free energy and low elastic modulus are two important characteristics in inducting the failure of adhesion between the organisms and the matrix surface.[49] As an example, fluorosilicones have a low surface tension and low elastic modulus, and thus excellent foul-releasing performances.[50]

Secondly, polymer brushes are known to induce a “steric barrier” effect prohibiting protein adsorption.[51] In our case, the dense PDMS layer may act as a steric barrier. In addition, our PDMS coating can be considered as a defect free liquid-like layer. Such smooth surfaces have been shown to improve antifouling capability, while foulants can be easily trapped on a rough or porous surface.[49]

Based on the above analysis, we evaluated the foulants adsorption through a model compound, albumin. FITC labeled albumin (albumin fluorescein isothiocyanate conjugate) was used, therefore, the presence of the protein at the surface was observed quantitatively with fluorescence spectroscopy. As shown in Figure 9, both modified wood samples displayed reductions in protein adsorption with respect to the native wood. This may result from hydrophobic groups on surface which inhibit the aqueous protein solution to permeate into the wood.[52] However, the protein was able to adsorb on the F-SiO_2-W surface, but to a lesser extent (28% reduction of fluorescence intensity when compared to Native-W). The PDMS-SiO_2-W surfaces showed the lowest adsorption, demonstrating the biopassivation of the covalently grafted PDMS layer capable of shielding aqueous protein solutions. This is an interesting result, since no biocides are involved, avoiding issues of water pollution and toxicity.[53]

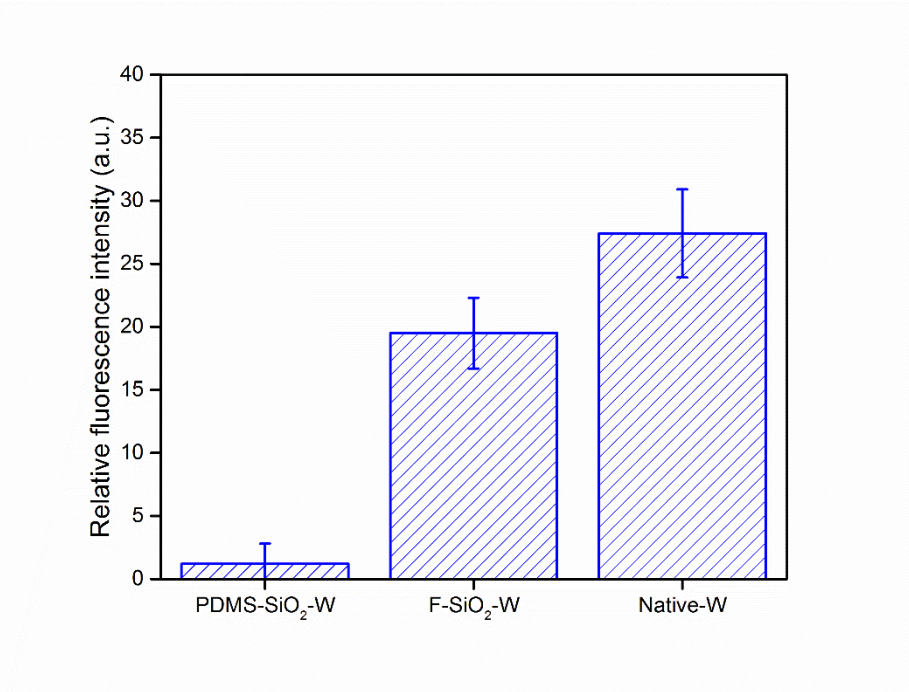

Figure 9: Protein adsorption on Native-W, F-SiO_2-W and PDMS-SiO_2-W expressed as the increase of fluorescence intensity. The error bars indicate the standard deviation of three independent experiments. Statistically significant differences between each two are analyzed by ANOVA test. All the p-values are smaller than 10^{-5}.

The biodegradation of wood elements is also an important drawback for both indoor and outdoor installations. We performed a basic qualitative experiment to estimate the resistance of the surface treated wood to bacterial growth. The results given in Table 2 show a significant reduction of bacterial growth beneath the PDMS-SiO_2-W wood sample when compared to the control (Native-W) and to F-SiO_2-W. The properties of our PDMS coating are likely to hinder the settlement of bacteria on the surface (confirmed by the inhibitory effect), but it does not have a lethal effect against the *S. aureus* and *E. coli*.

Table 2: Bacterial growth beneath the wood sample.

Bacteria strain	Native-W	F-SiO_2-W	PDMS-SiO_2-W
S. aureus	4.0 ± 0.0	3.7 ± 0.3$^{n.s.}$	2.0 ± 0.5*
E. coli	4.0 ± 0.0	3.8 ± 0.3$^{n.s.}$	3.2 ± 0.3*

Kruskal-Wallis-test and Mann-Whitney U-test for pairwise comparison. * = significant ($p < 0.05$); n.s. = not significant ($p \geq 0.05$). Growth was determined as follow: 0: no growth, 1: weak growth, 2: intermediate growth, 3: strong growth and 4: contact area completely grown.

Self-healing

As discussed previously, we hypothesized that the robustness of the PDMS treatment results from the mobility of the PDMS chains. The reorganization of polymer chains through molecular movement at interfaces is also the basis for physical self-healing processes.[54] We therefore studied the ability of our PDMS surface treatment to self-heal after exposing it to plasma. Oxygen plasma treatment of PDMS renders the surface more hydrophilic, through the creation of silanol groups.[55] As shown in Figure 10a, b, this phenomenon was observed with our PDMS-SiO_2-W samples: the contact angle after plasma treatment went down to a minimum of 10°. The creation of silanol groups was confirmed by FTIR measurements (Figure S7). However, after hours of storage at room temperature, we observed a hydrophobic recovery, shown by the CA measurements in Figure 10a. The hydrophobic recovery phenomenon on PDMS surfaces has been widely investigated.[56-58] Changes in PDMS surface hydrophilicity are essentially related to the amount of hydroxyl vs. methyl groups present at the outmost surface. The ratio between hydroxyl and methyl groups decreases due to the reorientation of silanols towards the bulk, and to the migration of low molecular weight PDMS chains from the bulk to the surface.[58] These surface rearrangements minimizing the surface energy are particularly clear with PDMS chains, which have a very low glass transition temperature,[59] due to their very flexible backbone (an explicative scheme is provided in Figure S8).[60] Figure 10c shows that the self-healing ability of our PDMS layers are still effective after five cycles of plasma treatment.

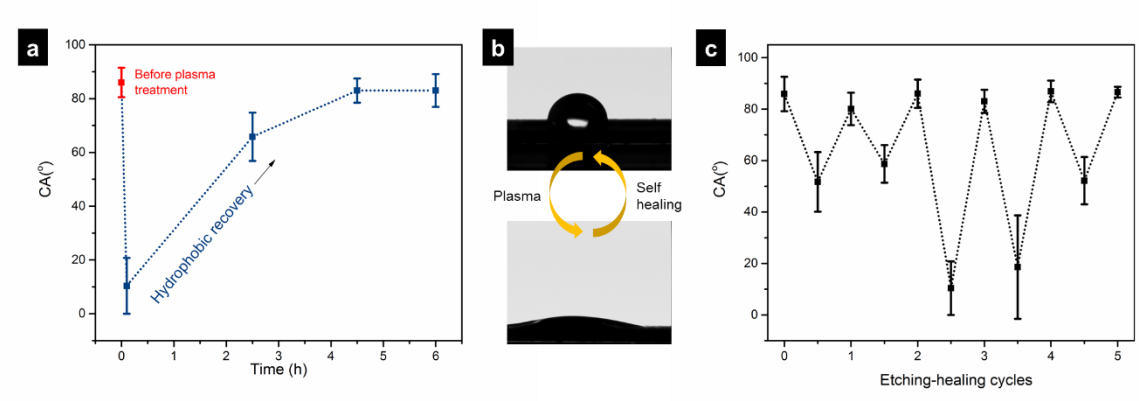

Figure 10: (a) contact angle measurements showing the hydrophobic recovery after plasma treatment; (b) profiles of water drops on PDMS-SiO_2-W surface before and after plasma treatment; (c) contact angle measurement for the plasma etching/self-healing cycles.

Applicability to other wood species

We performed our study on a single wood species. *Picea abies* was chosen due to its low durability,[61] which requires specific treatments to protect it against decay. While many wood species possess their own unique anatomic microstructure, the chemical composition of the cell wall from different species are similar: lignin accounts for 18 to 35%, carbohydrates (essentially cellulose and hemicelluloses) account for 65 to 75%, the rest consists in extractives and inorganic materials (4 to 10%).[62] Therefore, hydroxyl groups are the predominant functional group available for chemical modification in all wood species, and the two-step treatment could be applied to other wood species. According to the surface topology generated by the wood microstructure upon cutting, some wood species might have slight differences in wettability and/or open porosity. Therefore, some minor process adjustments might be needed to ensure that the surface is homogeneously coated, but the treatment should be applicable to all wood species.

Conclusion

In this work, we presented a simple method for the development of protective coatings on wood surfaces. The treatment was inspired by lubrication systems found in nature. The native wood surface was modified with silica and PDMS polymer chains were attached to the silica layer in a second step, creating a liquid-like surface with special wettability. We showed that the treatment hydrophobized the wood surface and led to anti-smudge and antifouling properties, and to an improved resistance to bacterial growth. We also demonstrated the robustness and the self-healing ability of our surface treatment, which will improve the service life of the protected wood. The chemical modification utilized were performed with environmentally friendly solvents, the wood structure was preserved. Such a facile method will possibly open new venues in the field of wood protection and wood functionalization.

Experimental section

Materials

Tetraethyl orthosilicate (TEOS), sulfuric acid (H_2SO_4), Ammonia solution (NH_4OH, 25%), dimethoxydimethylsilane (DMDEOS), ethanol, phosphate buffered saline (PBS) and albumin fluorescein isothiocyanate conjugate (FITC-albumin) were purchased from Sigma-Aldrich, 1H,1H,2H,2H-Perfluorooctyltriethoxysilane (POTS) was purchased from J&k Scientific. All

chemicals were used as received. Wood samples were prepared from Norway spruce (*Picea abies*) veneers.

Modification of Wood

Step 1: wood silanization with TEOS. To impregnate wood with pure TEOS, wood veneers were positioned vertically in a beaker containing TEOS (1 cm, for 10 min), allowing for liquid penetration into wood structure through capillary sorption. Impregnated wood samples were transferred to a NH_4OH solution (~ 16.7% NH_4OH in water). After 30 minutes, veneers were washed with water and then condensed at 65 °C. This procedure was repeated three times. Hydrolysis of TEOS with ~ 5% and ~ 0.6% NH_4OH solution were also preformed to investigate the influence of ammonia concentration on the morphology of the SiO_2 layer (characterization given in Figure S2). These samples are labeled SiO_2-W.

Step 2: growth of PDMS chains. The preparation was adapted from the method proposed by Wang et al.[17] 10 ml of ethanol, 5 ml of dimethyldimethoxysilane and 0.5 ml of hydrochloric acid were mixed and stirred together, then left for 30 min at room temperature before use. The PDMS grafting on SiO_2-W was done as follows: wood veneers were dip-coated and subsequently dried at 75 °C, and the process was repeated for eight times. After the last cycle, wood veneers were dried at 75 °C overnight. These samples are labeled PDMS-SiO_2-W.

Preparation of superhydrophobic wood: The fluoro-silica particles were synthesized according to a previous report.[24] 5 ml of TEOS and 0.86 ml of POTS were dissolved in 25 ml of ethanol. The solution was mixed with an ammonium hydroxide/ethanol solution (6 ml, 25% NH_4OH in 25 ml ethanol), and stirred for 12h. The F-SiO_2 sol was ultra-sonicated for 15 min before use. Wood veneers were then dipped in the F- SiO_2 sol and stirred for another 5h. Samples were finally dried at 65 °C overnight.

Characterization

FTIR: an attenuated total reflectance Fourier-transform infrared (ATR-FTIR) spectrometer (Bruker Tensor 27, Bruker, Ettlingen, Germany) was used to characterize the surface chemistry of the different wood samples.

XRD: the crystal phases of the unmodified wood, SiO_2-W, PDMS-SiO_2-W and F-SiO_2-W were analyzed by X-ray diffraction (XRD) (PANalytical Empyrean diffractometer, Almelo, Netherlands) in θ-2θ geometry with Cu-K radiation.

SEM and ESEM: surface morphology of the different wood samples were studied by scanning electron microscope (SEM, FEI Quanta 200F, Hillsboro, USA) and FEI Quanta 600 FEG ESEM equipped with a Peltier cooling stage set at 2 °C.

Surface profilometry: Surfaces were profiled with a Bruker Dektak XT Stylus profilometer (Bruker Corporation, Billerica, Massachusetts) equipped with a 2 µm radius tip.

AFM: The surface morphology and surface roughness of unmodified wood, SiO_2-W and PDMS-SiO_2-W were characterized with Atomic Force Microscopy (Nano Wizard 4, JPK Instruments AG, Berlin, Germany) in the Quantitative Imaging (QI) mode at 20 °C and 65% relative humidity. A force modulation cantilever (Multi75-G, BudgetSensors, resonance frequency 75 kHz) with a silicon probe was used and a setpoint of 10 nN was used. The sensitivity (45.77 nm/V) and the spring constant (1.96 N/m) of the cantilever were determined by the thermal noise method for a beam-shaped cantilever taking into account the environmental conditions and cantilever dimensions. Force-distance curves were acquired with a setpoint of 10nN, z-length of 800 nm and a pixel time of 12 ms, resulting in an extend speed of 167µm/s. The scan size was set to 1 × 1 µm and a resolution of 256 × 256 pixels. Another image of 5 × 5 µm for native wood was also profiled. Image processing was done in the JPK image processing software (JPK Instruments AG). PDMS-SiO_2-W were intensively washed before measurement to avoid tip contamination from any loosely bonded PDMS chains.

Performance testing

Surface wettability measurement: Contact angle (CA), tilt angle (TA) and contact angle hysteresis (CAH) were measured by the sessile drop method and analyzed with a Krüss drop shape analyzer (DSA 100); 10 µl water drops were used. For unmodified wood, the contact angle was taken after 30 s. The wettability measurements on the different wood samples were also conducted after prolonged immersion in water in order to evaluate the durability of the treatment. Excess water was wiped off the wood surfaces with a tissue before testing. We assume that water evaporation on wood surfaces is negligible for all the measurement. It should be noted that the natural fiber alignment in wood creates a structural anisotropy resulting in anisotropic wetting properties. Therefore, the CA values might largely differ according to the orientation of the camera, either parallel or perpendicular to fiber direction. The measurement conditions will be clarified in the text.

Anti-smudge tests: to show the anti-smudge properties, a solvent-based commercial paint (Neon Fluorescent Paint, DUPLI-COLOR, Switzerland) and a wood lacquer (2 in 1 Buntlack,

COLODUR, Switzerland) were used. According to the manufacturers, these two substances are highly suitable for wood surfaces. The paint and lacquer were respectively sprayed and manually applied to stain Native-W and PDMS-SiO_2-W samples. Attempts to remove the substances from the wood surface were done either immediately after painting or after drying, wiping the wood surfaces with dry paper or with ethanol. Pictures taken at each step provide clear insights into the ability of the different wood surfaces to repel the paint and lacquer.

Anti-fouling test: Phosphate buffered saline solutions (PBS, pH=7.484) were prepared as media for the protein adsorption studies. A 1mg/ml FITC-albumin solution in PBS was prepared. Three different sets of samples were studied: Native-W, F-SiO_2-W and PDMS-SiO_2-W. The samples were put in the FITC-albumin PBS solution for 1 day, then dried at 100 °C for 20 min. Then 50 µL of the FITC-albumin solution was placed over the samples surface and stored in the dark for 20 min. This process was repeated three times, until the wood samples were rinsed with MilliQ water for 10 s, and dried with N_2 gas. The surfaces of the treated samples were subsequently imaged with an optical microscope (Zeiss Axioskop 2 Plus, Carl Zeiss Microscopy GmbH, Germany) to evaluate the protein adsorption. Images of each sample before and after the protein adsorption test were taken under fluorescence microscopy, by using 488 nm light with a 20x objective magnification, reflective light shutter, brightness -0.50, intensity 1.00, 1300x1030 pixels, 250 s exposure time and linear fitting. ImageJ 1.42q was used to measure the intensity changes in the fluorescence pictures before and after protein adsorption.

Bacterial growth: For the detection of the anti-bacterial effect of the different treatments, agar diffusion test were conducted. Inoculums of either a gram positive or negative bacterial suspension with an optical density of 0.2 (OD600) were prepared. After inoculating the agar plates, the wood samples were placed on the plates. Afterwards, the plates were incubated at 37 °C for 24 h. The bacterial growth beneath the wood samples was visually determined by a stereomicroscope, giving the following growth values: 0: no growth, 1: weak growth, 2: intermediate growth, 3: strong growth and 4: contact area completely grown.

Plasma treatment: Oxygen plasma (diener ATTO) was used to activate the surface of PDMS-SiO_2-W at 12 W for 6 min. The chamber pressure was set to 0.8 mbar. The CAs of the samples were measured by the drop shape analyzer (DSA 100) before and after plasma treatment and after storage at RT for around 4 h. For CA measurements, the wood samples were placed with the year ring grain perpendicular to the camera.

Acknowledgements

The authors would like to thank the China Scholarship Council (CSC) for funding, the Surface Science and Technology group from ETHZ for kindly providing access to the drop shape analyzer. The authors are grateful to Prof. Dr. Nicholas Spencer from the Surface Science and Technology group at ETH Zürich for his helpful discussion and suggestions and to Pavel Iliev from the Computational Physics for Engineering Materials group at ETH Zürich for helpful discussions. The authors thank Dr. Karsten Kunze from ScopeM at ETH Zürich, and Dr. Kirstin Casdorff from Wood Materials Science group at ETH Zürich for their help during SEM sessions and for support during AFM measurements respectively.

References

[1] R. M. Rowell, W. B. Banks, *Water repellency and dimensional stability of wood*, Forest Products Laboratory, Department of Agriculture, Forest Service, Forest Products **1985**.
[2] H. Guo, D. Klose, Y. Hou, G. Jeschke, I. Burgert, *ACS Appl. Mater. Interfaces* **2017**, *9*, 39040.
[3] K. Eriksson, R. Blanchette, P. Ander, *Microbial and enzymatic degradation of wood and wood components*, Springer Verlag, Berlin, Germany **1990**.
[4] P. Evans, *Forest Products Journal* **2003**, *53*, 14.
[5] R. M. Rowell, *Handbook of wood chemistry and wood composites*, CRC press, Florida, USA **2012**.
[6] I. Burgert, T. Keplinger, E. Cabane, V. Merk, M. Rüggeberg, in *Secondary Xylem Biology*, Elsevier, Amsterdam **2016**, 259.
[7] C.-H. Xue, J. Chen, W. Yin, S.-T. Jia, J.-Z. Ma, *Appl. Surf. Sci.* **2012**, *258*, 2468.
[8] S. Peng, B. Bhushan, *J. Colloid Interface Sci.* **2016**, *461*, 273.
[9] A. Tuteja, W. Choi, M. Ma, J. M. Mabry, S. A. Mazzella, G. C. Rutledge, G. H. McKinley, R. E. Cohen, *Science* **2007**, *318*, 1618.
[10] L. Zhao, Q. Liu, R. Gao, J. Wang, W. Yang, L. Liu, *Corros. Sci.* **2014**, *80*, 177.
[11] R. N. Wenzel, *Industrial & Engineering Chemistry* **1936**, *28*, 988.
[12] A. Cassie, S. Baxter, *Transactions of the Faraday society* **1944**, *40*, 546.
[13] L. Bocquet, E. Lauga, *Nature materials* **2011**, *10*, 334.
[14] F. M. Fowkes, *Contact angle, wettability, and adhesion*, ACS Publications, Washington **1964**.
[15] X. Yao, L. Zhong, *Mutation Research/Genetic Toxicology and Environmental Mutagenesis* **2005**, *587*, 38.
[16] T.-S. Wong, S. H. Kang, S. K. Tang, E. J. Smythe, B. D. Hatton, A. Grinthal, J. Aizenberg, *Nature* **2011**, *477*, 443.
[17] L. Wang, T. J. McCarthy, *Angew. Chem.* **2016**, *128*, 252.
[18] D. Edwards, T. Nevell, B. Plunkett, B. Ochiltree, *International biodeterioration & biodegradation* **1994**, *34*, 349.
[19] P. Kim, T.-S. Wong, J. Alvarenga, M. J. Kreder, W. E. Adorno-Martinez, J. Aizenberg, *ACS nano* **2012**, *6*, 6569.
[20] S. Lee, N. D. Spencer, *Science* **2008**, *319*, 575
[21] H. Guo, P. Fuchs, K. Casdorff, B. Michen, M. Chanana, H. Hagendorfer, Y. E. Romanyuk, I. Burgert, *Advanced Materials Interfaces* **2017**, *4*, 1600289.
[22] A. Colas, *Silicones: Preparation, properties and performance*, Dow Corning, Life Sciences, **2005**.
[23] S. Wooh, D. Vollmer, *Angew. Chem. Int. Ed.* **2016**, *55*, 6822.
[24] H. Wang, J. Fang, T. Cheng, J. Ding, L. Qu, L. Dai, X. Wang, T. Lin, *Chem. Commun.* **2008**, 877.

[25] G. Li, W. Lao, T. Qin, L. Huang, *Holzforschung* **2015**, *69*, 399.
[26] L. M. Johnson, L. Gao, C. W. Shields IV, M. Smith, K. Efimenko, K. Cushing, J. Genzer, G. P. López, *Journal of nanobiotechnology* **2013**, *11*, 22.
[27] A. Bertoluzza, C. Fagnano, M. A. Morelli, V. Gottardi, M. Guglielmi, *J. Non-Cryst. Solids* **1982**, *48*, 117.
[28] F. Ataollahi, S. Pramanik, A. Moradi, A. Dalilottojari, B. Pingguan-Murphy, W. Abas, W. A. Bakar, A. Osman, N. Azuan, *Journal of biomedical materials research Part A* **2015**, *103*, 2203.
[29] A. Lozhechnikova, D. Dax, J. Vartiainen, S. Willför, C. Xu, M. Österberg, *Carbohydr. Polym.* **2014**, *110*, 163.
[30] H. Wang, Q. Yao, C. Wang, B. Fan, Q. Sun, C. Jin, Y. Xiong, Y. Chen, *Scientific reports* **2016**, *6*, 35549.
[31] A. Buckley, M. Greenblatt, *J. Chem. Educ* **1994**, *71*, 599.
[32] E. Pope, J. Mackenzie, *J. Non-Cryst. Solids* **1986**, *87*, 185.
[33] H. Bellanger, K. Casdorff, L. F. Muff, R. Ammann, I. Burgert, B. Michen, *Journal of Colloid and Interface Science* **2017**, *500*, 133.
[34] B. Cappella, *Micron* **2017**, *93*, 20.
[35] W. Fang, H.-Y. Guo, B. Li, Q. Li, X.-Q. Feng, *Langmuir* **2018**, *34*, 3838.
[36] M. A. Samaha, H. Vahedi Tafreshi, M. Gad-el-Hak, *Physics of Fluids* **2012**, *24*, 112103.
[37] B. Wang, Y. Zhang, L. Shi, J. Li, Z. Guo, *J. Mater. Chem.* **2012**, *22*, 20112.
[38] P.-G. de Gennes, F. Brochard-Wyart, D. Quere, *Capillarity and Wetting Phenomena: Drops, Bubbles, Pearls, Waves*, Springer, New York **2013**.
[39] L. Gao, T. J. McCarthy, *Langmuir* **2006**, *22*, 6234.
[40] C. Urata, B. Masheder, D. F. Cheng, D. F. Miranda, G. J. Dunderdale, T. Miyamae, A. Hozumi, *Langmuir* **2014**, *30*, 4049.
[41] G. Janin, J. C. Gonçalez, R. A. Ananías, B. Charrier, G. F. d. Silva, A. Dilem, *Aesthetics appreciation of wood colour and patterns by colorimetry. Part 1. Colorimetry theory for the CIELab system*, Departamento de Engenharia da Madeira, da Universidade de Bío-Bío em Concepción, Chile **2001**.
[42] D. F. Cheng, C. Urata, B. Masheder, A. Hozumi, *J. Am. Chem. Soc.* **2012**, *134*, 10191.
[43] D. F. Cheng, C. Urata, M. Yagihashi, A. Hozumi, *Angew. Chem. Int. Ed.* **2012**, *51*, 2956.
[44] M. Rabnawaz, G. Liu, H. Hu, *Angew. Chem. Int. Ed.* **2015**, *54*, 12722.
[45] J. B. McClintock, B. J. Baker, *Marine chemical ecology*, CRC press, US **2001**.
[46] H. Zhang, R. Lamb, J. Lewis, *Science and Technology of Advanced Materials* **2005**, *6*, 236.
[47] M. Cowling, T. Hodgkiess, A. Parr, M. Smith, S. Marrs, *Sci. Total Environ.* **2000**, *258*, 129.
[48] M. A.-A. AlMa'adeed, I. Krupa, *Polyolefin Compounds and Materials*, Springer, **2016**.
[49] R. F. Brady Jr, I. L. Singer, *Biofouling* **2000**, *15*, 73.
[50] R. F. Brady, *Prog. Org. Coat.* **1999**, *35*, 31.
[51] P. Hamilton-Brown, T. Gengenbach, H. J. Griesser, L. Meagher, *Langmuir* **2009**, *25*, 9149.
[52] Z. Wang, H. Zuilhof, *Langmuir* **2016**, *32*, 6310.
[53] L. D. Chambers, K. R. Stokes, F. C. Walsh, R. J. Wood, *Surf. Coat. Technol.* **2006**, *201*, 3642.
[54] D. Bodas, C. Khan-Malek, *Sensors and Actuators B: Chemical* **2007**, *123*, 368.
[55] S. Bhattacharya, A. Datta, J. M. Berg, S. Gangopadhyay, *Journal of microelectromechanical systems* **2005**, *14*, 590.
[56] V. Jokinen, P. Suvanto, S. Franssila, *Biomicrofluidics* **2012**, *6*, 016501.
[57] B. T. Ginn, O. Steinbock, *Langmuir* **2003**, *19*, 8117.
[58] H. Hillborg, J. Ankner, U. W. Gedde, G. Smith, H. Yasuda, K. Wikström, *Polymer* **2000**, *41*, 6851.
[59] J. Andrade, D. Gregonis, L. Smith, *Surface and interfacial aspects of biomedical polymers*, Vol. Volume 1 Surface Chemistry and Physics, PLENUM PRESS, New York and London **1985**.
[60] H. Hillborg, U. Gedde, *Polymer* **1998**, *39*, 1991.
[61] T. C. Scheffer, J. J. Morrell, *Natural durability of wood: A worldwide checklist of species*, Vol. 22, College of Forestry, Forest Research Laboratory, Oregon State University, **1998**.
[62] R. C. Pettersen, *The chemistry of solid wood*, American Chemical Society, Washington, USA **1984**.

2.1.1 Supplementary information

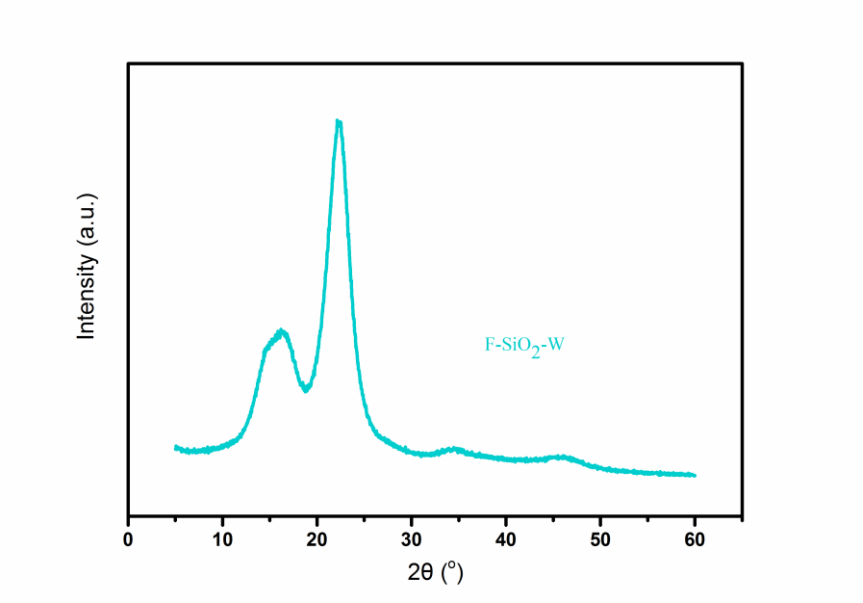

Figure S1: XRD pattern of the F-SiO_2-W sample.

Table S1: The surface roughness parameters for native-W and SiO_2-W by Stylus Profilometry.

Parameters	Native-W (µm)	SiO_2-W(µm)
Sz	99.1	84.2
Sa	9.6	4.3
Sq	12.6	6.0

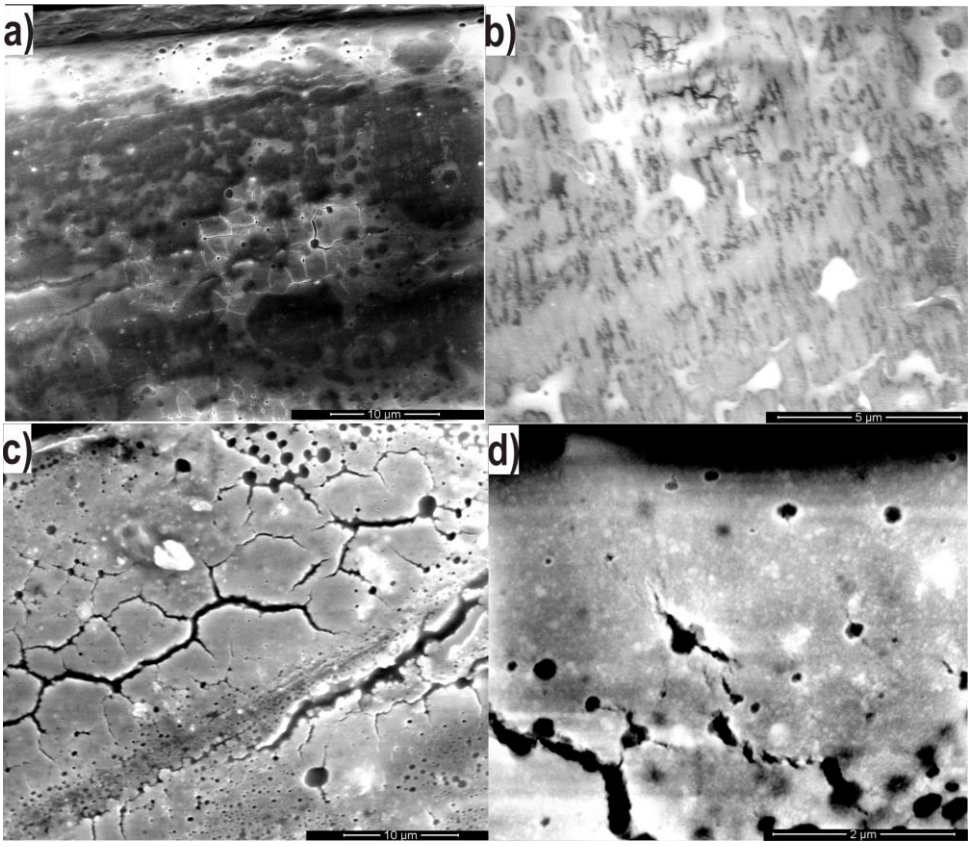

Figure S2: SEM images of SiO_2-W samples, obtained from TEOS hydrolysis with various amount of NH_4OH to investigate the influence of base concentration on the morphology of the SiO_2 layer on wood: (a) to (b) 0.6% and (c) to (d) 5% solution.

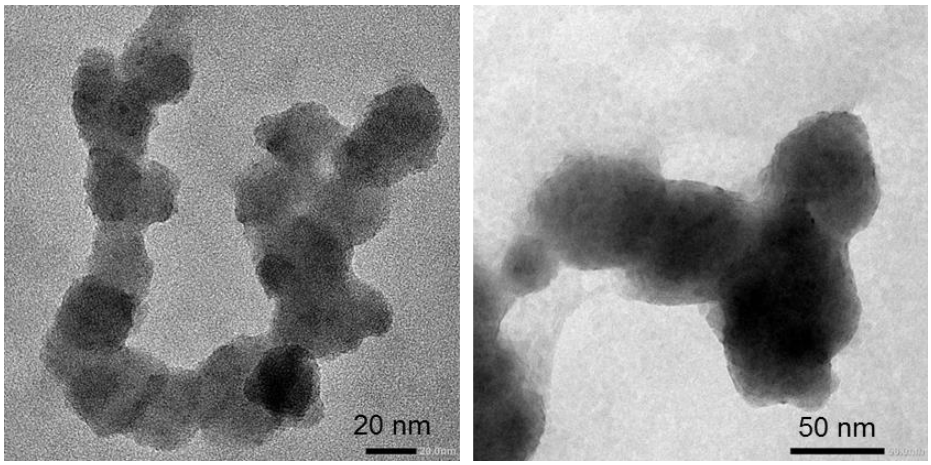

Figure S3: TEM images of the silica particles synthesized by reducing TEOS with ~16.7% NH_4OH in water as described in the experimental part.

Transmission electron microscopy (TEM, JEOL JEM-2010, Japan) was employed to take high resolution images of the silica particle. One dilute drop of silica particles suspension was deposited onto the carbon film on copper grids, and dried before measurement.

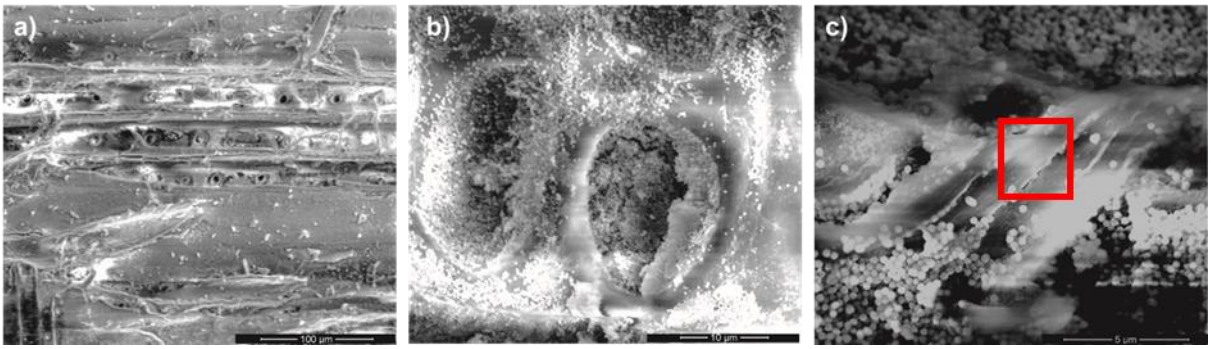

Figure S4: SEM images of F-SiO_2-W, showing the fluorinated silica particles on the wood surface.

Table S2: The surface roughness parameters for Native-W, SiO_2-W, and PDMS-SiO_2-W by AFM, corresponding to the images shown in Figure 5.

Parameters	Native-W	SiO_2-W	PDMS-SiO_2-W
Sa (nm)	5.5	3.5	4.5
Sq (nm)	7.2	4.5	6.2

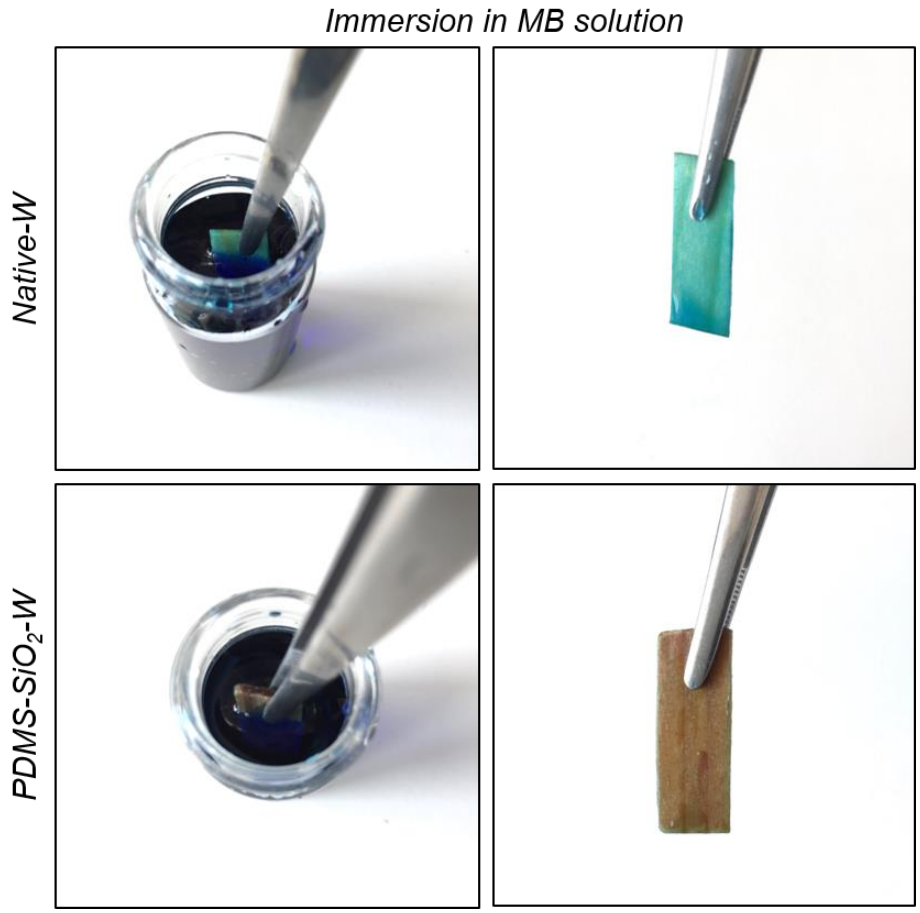

Figure S5: Images showing the wetting of native wood PDMS-SiO_2-W surfaces with a Methylene Blue (MB) aqueous solution directly after a 19 days immersion in pure water.

In this experiment, a native wood sample and a PDMS-SiO_2-W sample were immersed in pure water for 19 days. They were then taken out, transferred to a vial containing methylene blue dyed water, and immediately withdrawn. Once removed from the MB solution, we took the images shown in Figure S5.

The top image clearly shows that native wood immediately turns blue because it is fully wetted by the MB aqueous solution. When exposed to the same solution, the PDMS-SiO_2-W sample retains its original color, which proves that the MB solution did not wet its surface. This confirms that the treatment continues to perform, even after 19 days immersion in water.

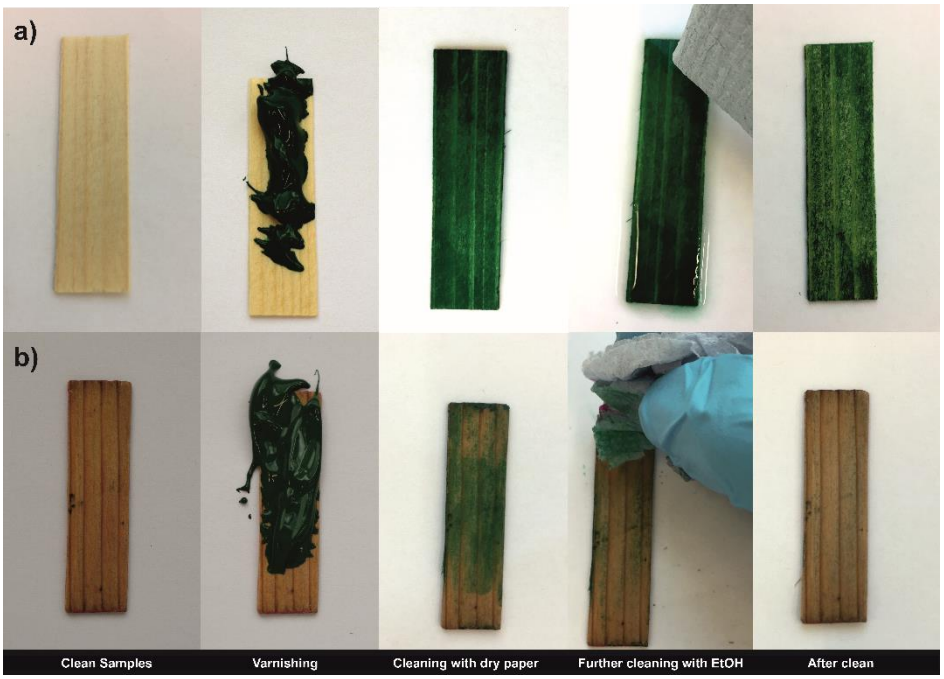

Figure S6: (a) Native-W before application of the wood lacquer, after direct application of the lacquer, after wiping with dry paper, wiping with ethanol, after EtOH cleansing; (b) same sequence for the PDMS-SiO_2-W samples.

When a wet lacquer is applied on native wood and modified wood, it cannot be fully removed with a simple dry paper cleaning; both samples remain stained (although the PDMS-SiO_2-W samples is less colored). Upon further cleaning with ethanol, the green color is completely remove from the modified sample, but the native wood is permanently stained. This experiment shows that the wet varnish may penetrate the PDMS layer (and it is then easily washed with ethanol), but it does not penetrate below to stain wood irreversibly.

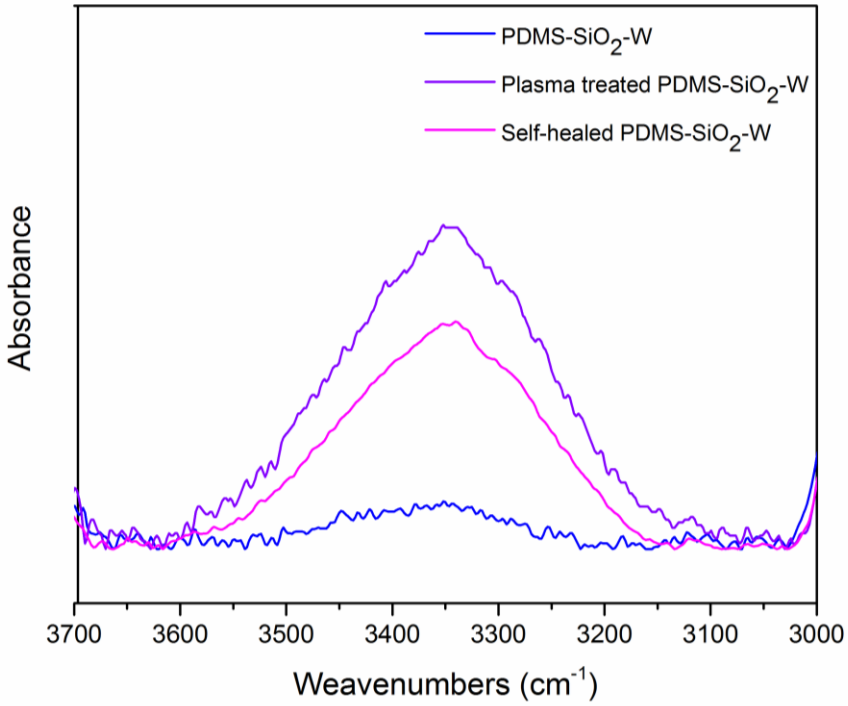

Figure S7: FTIR spectra of PDMS-SiO_2-W before and after plasma treatment, and after healing.

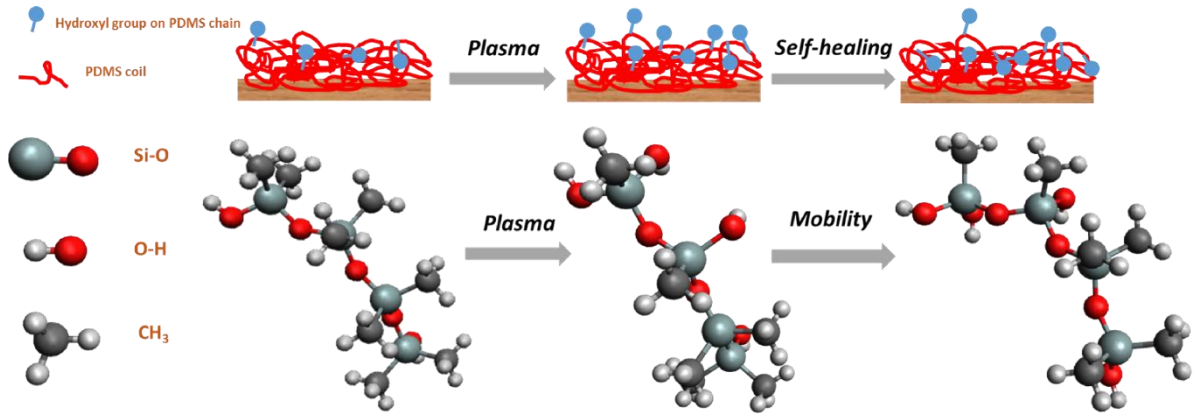

Figure S8: scheme describing the surface rearrangement of the flexible PDMS chains, at the origin of the self-healing property.

2.2 Wood composites with wettability patterns prepared by controlled and selective chemical modification of a 3D wood scaffold

Yaru Wang[a,b], Tian Tian[c], and Etienne Cabane*[a,b]

[a]Wood Materials Science, ETH Zürich, Stefano-Franscini-Platz 3, CH-8093 Zürich, Switzerland

[b]Applied Wood Materials, EMPA – Swiss Federal Laboratories for Materials Science and Technology, Überlandstrasse 129, CH-8600 Dübendorf, Switzerland

[c]Lab for Interface and Surface Engineering of Nanomaterials, ETH Zürich, Vladimir-Prelog-Weg 1-5/10, CH-8093 Zürich, Switzerland

Corresponding author email: cabanee@ethz.ch or etienne.cabane@empa.ch

Reprinted (adapted) with permission from Wang, Y., Tian, T. and Cabane, E., Wood Composites with Wettability Patterns Prepared by Controlled and Selective Chemical Modification of a Three-Dimensional Wood Scaffold. *ACS Sustainable Chemistry & Engineering*, 2017 *5* (12), 11686-11694.

KEYWORDS

Hierarchical porous structure, lignocellulose, wettability pattern, anisotropic wetting, wood composites, sol-gel process

ABSTRACT

Wood-composite materials with patterned wetting properties were synthesized by applying hydrothermal growth of ZnO rods into a wood scaffold. We exploited the natural morphological features of wood, to selectively modify the wood material via a self-directed deposition of ZnO in the biological scaffold. Characterizations using scanning electron microscopy, energy-dispersive X-ray spectroscopy and X-ray powder diffraction confirmed the successful surface modification and revealed the predominant growth of ZnO rods on earlywood (EW) regions. The wetting properties of these new wood-composite materials have been extensively investigated to study the influence of the grooved wood surface structure and its chemical heterogeneity on the wettability. We demonstrate that the ZnO-Wood samples have alternating hydrophilic and hydrophobic “strips”, corresponding to the EW and latewood grains from the

native wood, and that the surfaces are endowed with an interesting anisotropic wetting property. Using these special wetting properties, we further modified ZnO-Wood samples with inorganic and organic compounds and we report on basic experiments to show potential applications, in the design of biphasic materials and the control of water droplet movement on surfaces.

INTRODUCTION

Historically, wood is a very important material used by humankind in diverse applications, where sustainability, lightweight, excellent mechanical properties, large scale, and aesthetic properties are needed. After wood is felled and used as a construction material, it is known to face several problems affecting its long-term use: this prompted chemists to develop the field of chemical wood modification, addressing reliability issues related to dimensional instability, UV degradation, and biodegradation.[1-3] Wood is also an important source of energy and raw materials, and researchers have been proposing chemical processes for the fractionation of lignocellulosic materials, in order to recover pure cellulose, lignin, and other wood compounds for various industries.[4-6]

Recently, our group and others started to look at the native wood structure from an entirely new perspective, with a common goal: making a direct use of the biological scaffold to develop new advanced materials, using a top-down manufacturing approach.[7-19] In all these studies, particular attention was given to maintain and to best exploit the interesting native wood scaffold and its structural features. The obtained biohybrid materials (i.e. wood/inorganic or wood/synthetic polymer) were endowed with new functionalities, including conductivity, magnetism, or stimuli-responsiveness. To expand the applications of wood in the materials science field, we propose a novel approach to synthesize wood composites with special wettability properties.

Surfaces with wettability patterns – i.e. integrating (super)hydrophilicity and (super)hydrophobicity on the same surface in two-dimensions – provide a unique opportunity to control the wetting behavior at interfaces in a wide range of applications, including microfluidics,[20] water droplet splitting,[21] fog collection,[22] cell culturing,[23] biomedical diagnostic devices,[24] sensors,[25] and chemical synthesis in droplets.[26] Manipulation of liquids on a surface may be obtained through surface structuration with the implementation of physical barriers: microwells and microchannels have been constructed using various techniques such as lithography, laser ablation, or chemical etching among others. Alternatively, the droplet movement can be guided on surfaces patterned with areas showing extreme surface energies. In this case, a water droplet preferentially adheres to a hydrophilic patch and is repelled by

neighboring more hydrophobic areas. Such patterned surfaces are usually produced by bottom-up techniques, including lithography and chemical modifications. Most of these approaches require multistep sophisticated techniques, and are faced with issues related to difficulties of up-scaling, high costs, and usually do not make use of environmentally friendly materials.[27] One way to circumvent processing issues would be to use a top-down approach, with a substrate already having an intrinsic anisotropic surface or structure, and to use these attributes to functionalize the material selectively.

In nature, many biological materials have 2D and 3D anisotropic or patterned structures.[28-29] Surface anisotropy or patterning may be found on the back of beetles to collect fog,[30] the wing scales of butterflies to generate structural colors,[31] or the legs of water striders to walk on water.[32] Three-dimensional porous materials such as wood and bone are composite materials with a hierarchical and anisotropic – structure, which gives them superior mechanical properties.[33] At the nanoscale, the fiber cell walls are constituted by a composite material made from cellulose fibrils embedded within a lignin and hemicelluloses matrix.[34] At the microscale, wood shows a highly anisotropic arrangement of hollow cells (wood fibers), varying in size and shape depending on the wood species.[35] At the macroscale, wood from many tree species have a regular and circular alternation of earlywood (EW) and latewood (LW) known as tree year rings or growth rings. EW and LW differ in morphology, density, color, and other characteristics.

In this work, our goal is to exploit the structural anisotropy of a 3D wood scaffold to manufacture a wood-based composite material with well-defined wettability patterns. One of the challenges associated with a top-down manufacturing technique lies in the imposed chemistry and structure. In bulk 3D matrices, the control over the chemistry modification process is not trivial. In particular, selectivity to target specific regions may prove to be highly challenging. However, well-ordered porous materials such as wood, present anisotropic properties due to their intrinsic structure that could be advantageously used to dictate the introduction – and subsequently the distribution – of a new material.

Here, we report on the growth of ZnO rods in spruce wood cubes using a sol-gel approach, and we demonstrate their predominant growth in the EW region of the wood samples, resulting in an inorganic-wood hybrid material with a clear patterned ZnO distribution. The surface wettability properties after modification were investigated. Results confirm the targeted patterned functionality, and the wood surfaces show patterned wetting properties with anisotropic wettability. Further experiments exploiting these new properties were also

performed to show the potential of our approach in the design of biphasic materials and the control of water droplet movement on surfaces.

EXPERIMENTAL SECTION

Materials. Wood cross-sections (10 × 10 × 5 mm^3, Radial × Tangential × Longitudinal) from Norway spruce (*Picea abies*) were cut using a regular circular saw. Several samples were subsequently microtomed using a Leica rotary microtome to smoothen the cross-sections. The surface morphologies generated by rotary microtome cut, circular saw cut, sanding, and band saw cut were investigated. The most suitable surface showing roughness contrast was obtained with circular sawn samples. Microtome cut samples were used to visualize the wood anatomy. SEM images of sanded and band-sawn cut samples are given in Figure S1.

All reagents, zinc acetate dehydrate (Sigma-Aldrich), monoethanolamine (MEA; Sigma-Aldrich), ethanol (Sigma-Aldrich), zinc nitrate hexahydrate (Sigma Aldrich), hexamethylenetetramine (Sigma-Aldrich), dopamine hydrochloride (Alfa Aesar), poly(ethyleneimine) solution in water (Sigma-Aldrich), Silica nanoparticle dispersion in water (< 50 nm, Sigma-Aldrich): all reagents were used without further purification.

ZnO rods synthesis. ZnO rods were grown on wood surface through a sol-gel process adapted from a previous report.[36] In the first step, the seed layer was deposited on wood: 0.3 M Zinc acetate dehydrate and equivalent molar monoethanolamine were dissolved in ethanol and then stirred at 60 °C for 2 h to yield a homogeneous colloidal solution. The ZnO colloids were deposited onto wood by applying vacuum to enhance penetration of the seeds inside the wood tracheids. Note that a simple impregnation (i.e. without vacuum) may be used to deposit the colloids on the surface only. Subsequently, the gel films were annealed at 100°C for 90 min. The vacuum-heating cycle were repeated three times to form dense ZnO seed layers. EDX mappings showing the Zn distribution on surface and inside the wood cube are given in Supporting Information (Figure S2 and S3).

In the second step, we performed the hydrothermal growth of ZnO rods. A 50 mM zinc nitrate hexahydrate and 50 mM hexamethylenetetramine solution was added to the autoclave containing the wood samples, and heated at 90 °C for 4 hours. The obtained ZnO-wood samples were rinsed with deionized water to remove any residual salt, and dried at 100 °C under vacuum.

Characterization. The crystal phases of the unmodified wood and ZnO modified wood (ZnO-W) were acquired by powder X-ray diffraction (XRD) (PANalytical Empyrean diffractometer, Almelo, Netherlands) with Cu-Kα radiation. Surface morphology and ZnO distribution were studied by with a scanning electron microscope (SEM, FEI Quanta 200F, Hillsboro, USA)

equipped with energy dispersive X-ray spectroscopy (EDX, Ametek-EDAX). Static contact angles were conducted with the sessile drop method and analyzed on a Krüss drop shape analyzer (DSA100). Water drops of 2 μL volume were placed on the samples and measured in both parallel (∥) and perpendicular (⊥) directions, while the top views of shape and size of a droplet were observed by the camera or under optical microscope (Olympus BX 51). To examine the wetting properties of LW only, ultrasmall drops were deposited on surfaces by microscopic Contact Angle Meter (MCA-3, Kyowa Hakko Kirin Co., Ltd.) allowing for measurement of contact angle on 100 μm wide areas. Water droplets with controlled diameters were dispensed through glass capillaries with 5 μm opening at a gas pressure of 180-220 kPa. The outer walls of the capillaries were treated to be hydrophobic by octadecyltrichlorosilane before use. The droplet sizes were corrected by image J. In the microdroplet tracking test, ZnO-W was first treated with a polydopamine-polyethyleneimine (PDA/PEI) solution. The PDA/PEI solution was prepared according to a method reported in the literature.[37] After the treatment, water drops (~10 μL) were placed above the LW on sample surface, tilted at ~ 44°. Droplet moving path were recorded with a high-speed camera (Nikon 1j1).

RESULTS AND DISCUSSIONS

Wood Surface Morphology. Wood from trees grown in regions with distinct seasons (such as Norway spruce felled in Switzerland) display a well-defined pattern known as growth rings.[38] In the early season, rapid growth yields wood fibers with thin cell walls and large luminal areas. In the wood formed later in the season, the cell walls are thicker, and the lumina are smaller. These two wood regions are respectively called earlywood (EW) and latewood (LW), and can be seen in Figure 1a.

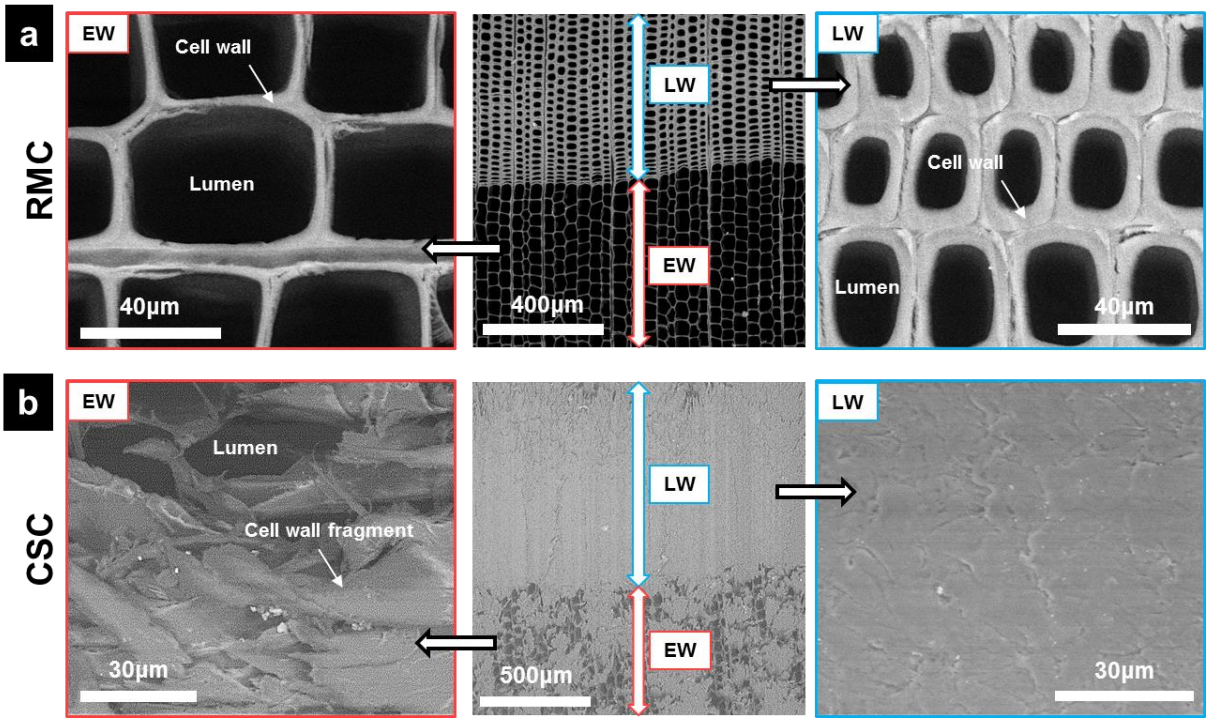

Figure 1: SEM images of native spruce wood cross-sections obtained from rotary microtome cutting (RMC), and circular saw cutting (CSC). (a) After the RMC process, the typical spruce wood anatomy details – cell wall, lumen, EW and LW regions – are easily observed. (b) After the CSC process, the wood anatomy is hardly recognizable.

These morphological patterns are already known to influence the diffusion of chemicals and the homogeneity of bulk chemical wood modifications. [12, 39-40]

The EW and LW regions are also known to have rather different mechanical properties.[41-42] The effect of woodworking operations on the wood surface roughness have been studied,[43-45] and reveal that the roughness generated by the cutting process is not homogeneous on the wood cross-section. Among various cross–section cutting processes, circular saw cutting was shown to generate important roughness contrasts between the EW and LW regions that were less pronounced with other cutting techniques.[46] As shown in Figure 1, the smooth cut obtained from the microtome preparation reveals the wood anatomy, with well-defined cell cross-sections: the cell wall and lumen area are clearly identified (Figure 1a). When using a circular saw, wood surfaces are damaged: it results in wood cell wall deformation and fiber shredding. As seen in Figure 1b, the EW structure is irregularly destroyed: EW tracheids have torn edges, and in some cases, torn cell walls fragments are folded, either overlapping each other or partially covering the luminal area. In contrast, the thick LW tracheid walls are folded and compressed into a dense flat sheet with a rather closed or sealed structure when compared to EW. The SEM

observations were confirmed by surface topology measurements with stylus profilometry that clearly revealed the grooved structure resulting from the CSC process (see Figure S4).

Selective Growth of ZnO Rods. Native wood can absorb large quantities of liquids, especially through capillary absorption on a cross-section face, where the lumina are open. The morphology patterns generated by the cutting process will therefore be critical to wet chemistry modifications: according to the structural and morphological features described above for the CSC wood samples, we hypothesized that the wettability of LW and EW should be rather different. As a result, the different penetration rate and penetration depths of a reactive solution inside the wood fibers should lead to a selective wood modification.

We applied a two-step modification to our CSC wood samples to grow ZnO rods. The growth of ZnO rods in wood scaffolds and surfaces has received a lot of attention recently, due to its various potential applications, and the mild reaction conditions employed. It has been shown to provide flame retardancy,[47-48] UV resistance,[48-50] resistance against biodegradation,[51-52] but also interesting wettability properties, such as superhydrophobicity[48, 53] and superamphiphobicity.[49] Among these properties, the (super)hydrophobic behavior is of particular interest to us. Figure 2 illustrates the fabrication steps of the patterned wood surfaces. In the first step, the wood is seeded with the zinc colloid, binding to wood throught hydrogen bonding.[54] In the second step, the seed layer enables the hydrothermal growth of the Zinc oxide rods on the wood interfaces.

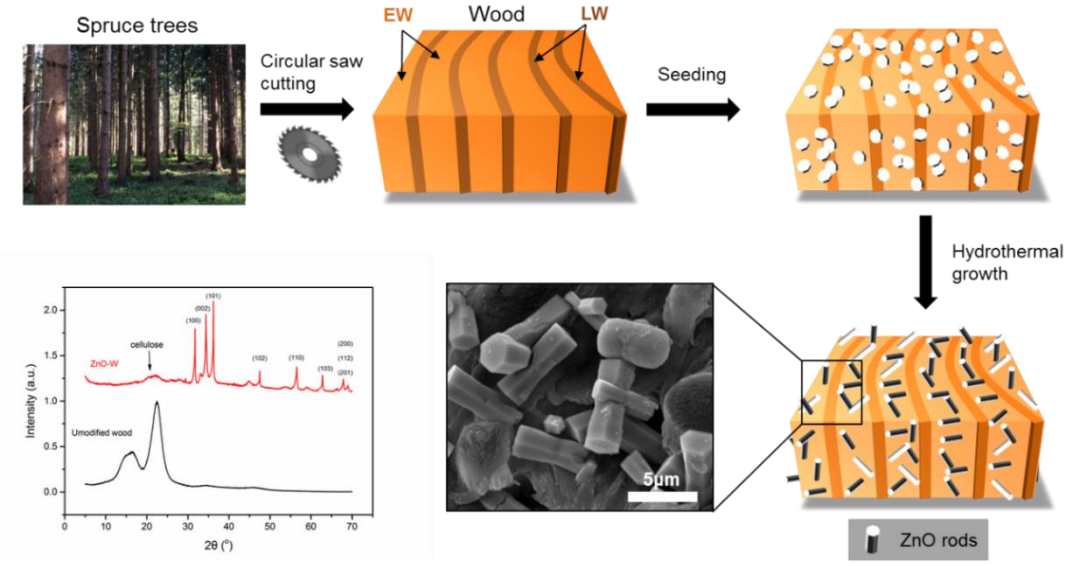

Figure 2: Preparation method of the ZnO modified wood samples (ZnO-W) and XRD patterns for native wood and ZnO-Wood.

The XRD pattern for native spruce wood shows the typical diffraction peaks related to the cellulose crystallinity (2θ = 16° and 22°, Figure 2). After the growth of the ZnO rods, the sharp

diffraction peaks attributed to hexagonal ZnO (Wurtzite-type JCPDS 75-0576) appear, and a weak cellulose signal from the wood substrate can still be seen.

The distribution of the ZnO rods was characterized with SEM/EDX. As shown in Figure 3a, the SEM images reveal the inhomogeneous distribution of the ZnO rods in the wood template. In EW, most of the wood scaffold is covered with rods (the empty dark zones correspond to open lumina). In contrast, the ZnO rods are less densely distributed over the LW region. EDX mapping of the relevant atoms are shown in Figure 3b. The carbon and oxygen distributions correlate well with the wood anatomy and the wood cutting process: both oxygen and carbon signals are more intense in the LW region where the lumina are mostly covered with cell wall fragments.

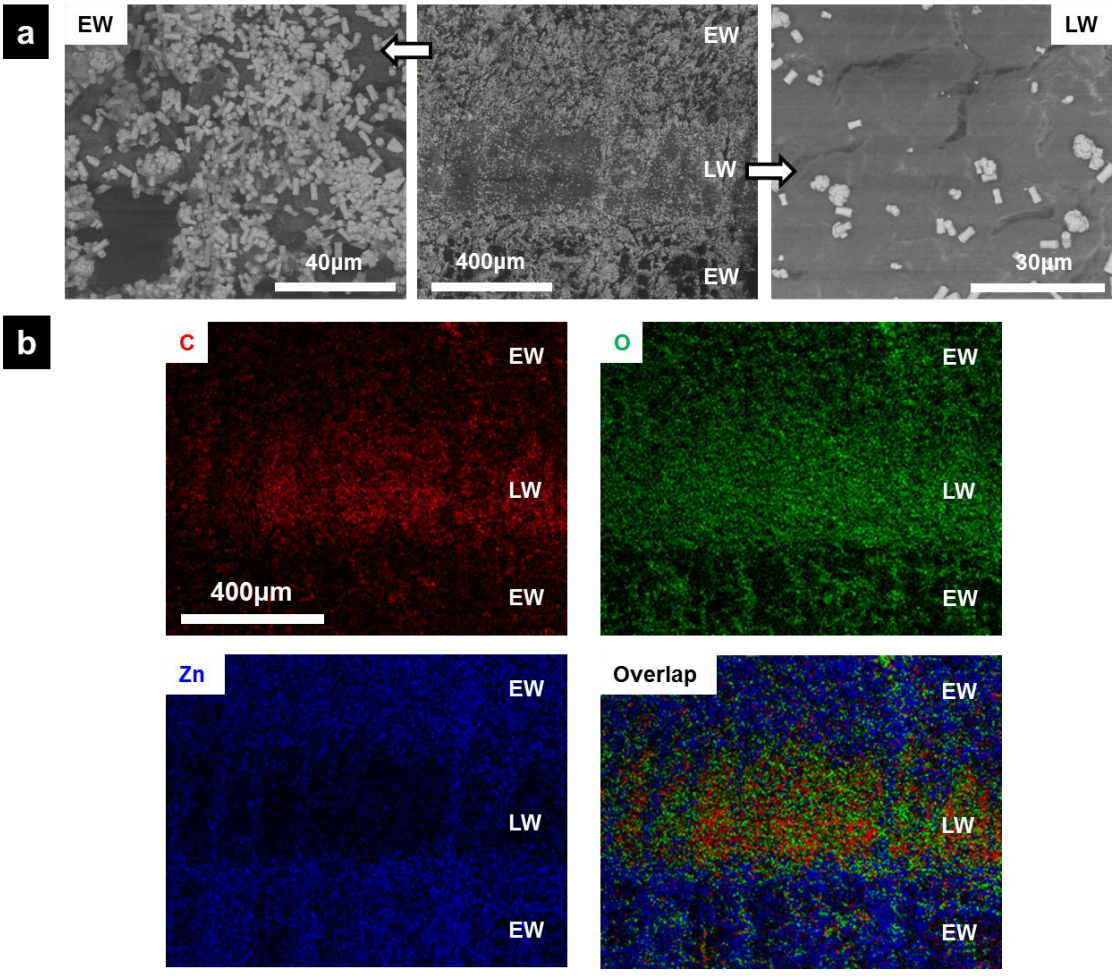

Figure 3: SEM images and the corresponding EDX mapping of ZnO-W cross-sections revealing the preferential distribution of ZnO rods in the EW regions. a) SEM images of W-ZnO cross-sections, with zoom in on EW and LW regions. (b) EDX mapping of the area shown in (a), for carbon, oxygen, and zinc atoms, and the overlapping map.

According to the Zn mapping, the growth of ZnO rods was more efficient in the EW regions. The overlapping EDX signals confirm that we obtained a clearly patterned material, dictated by the morphology of the wood template, i.e. the alternating EW and LW regions.

We applied the same modification process to RMC wood samples which present a fully open porous structure on the cross-section (see Figure 1a). As shown in the SEM images (Supporting Information, Figure S5), in contrast to the CSC samples, the growth of ZnO rods on a RMC sample is more homogeneous: in both EW and LW, we observe a high density of ZnO rods.

Results confirm that the inhomogeneous surface morphology generated by the CSC process leads to variable impregnation efficiencies. After the CSC process, the EW regions have an open morphology: liquids can easily penetrate into the empty lumina and wet the wood fibers efficiently. Therefore, the reagents in solution are well-impregnated in the EW regions and yield a dense modification. In the LW regions, the "sealed" surface is less permeable to liquids, and leads to a poor impregnation of reactive species, hence a sparse distribution of ZnO rods.

Surface Wettability Contrast. As shown in Figure 4a, a water droplet resting on the ZnO-W surface is exclusively pinned to the LW grain, while for native wood, a typical wetting behavior is observed (immediate water spreading and absorption inside the wood scaffold, see Figure 4b). The optical microscopy image (Figure 4c) also shows that when a water drop is deposited on the EW region, it adopts a spherical shape, with a contact angle of 128.1 ± 5.1° that is typical for a homogeneous hydrophobic surface. The wettability contrast observed here correlates well with the distribution of the ZnO rods: because there are fewer rods on the LW region, it is still a rather hydrophilic surface when compared to EW regions.

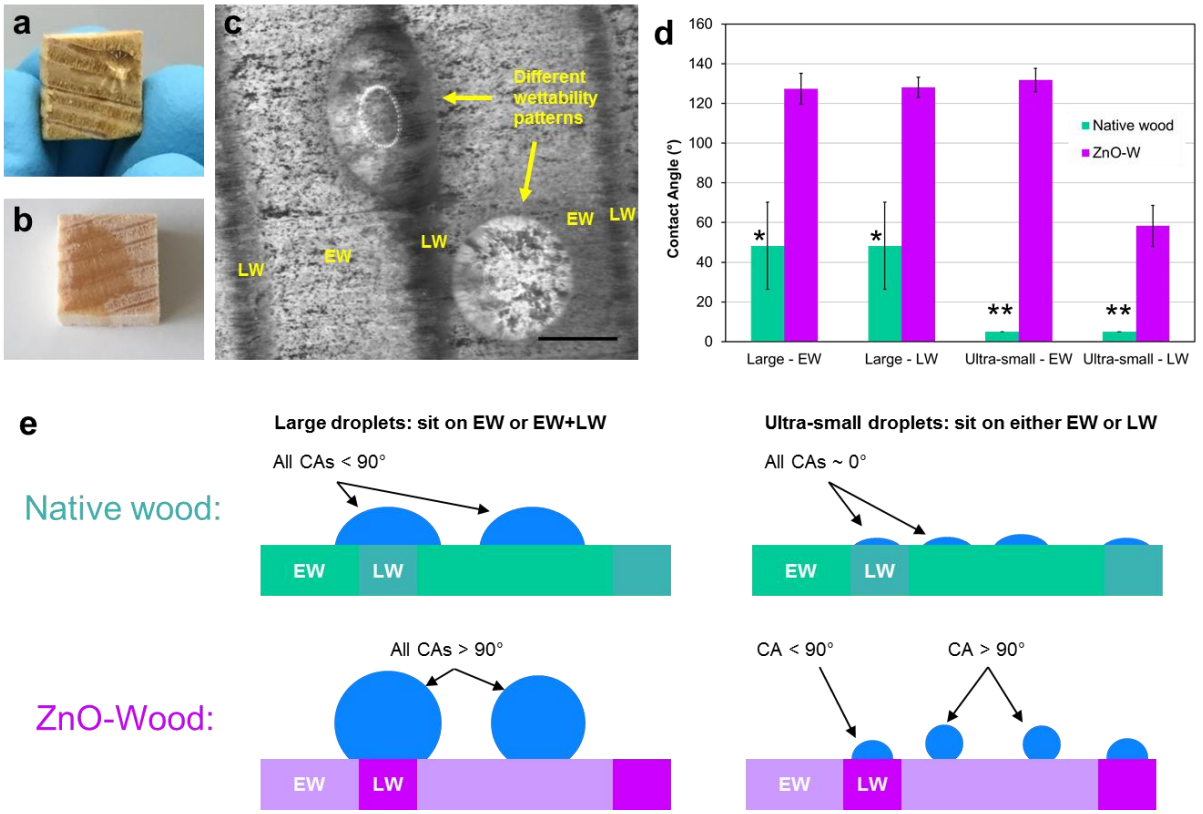

*Figure 4: images of a large water droplet on a ZnO modified spruce wood cube (a), and a native wood cube (b). (c) Optical microscopy image of large water droplets deposited on the EW and LW regions of a ZnO-W sample (scale bar: 1mm). (d) Contact angle values measured on native and modified wood, for different droplet sizes. CA values are all taken at 1000 milliseconds. In the case of large droplets, the CA for the native wood (labeled with *) is the same for both EW and LW (water drop rapidly spreads over both EW and LW). In the case of very small droplets, the contact angles for the native wood (labeled with **) are assumed to be zero due to the extremely fast absorption of water by the hygroscopic native wood. For LW, the CA data are obtained from the parallel direction. (e) Scheme explaining the water droplet behavior on the wood cross-sections, according to droplet size: large droplets sit on EW or EW + LW, while ultrasmall droplets are deposited on either EW or LW.*

To confirm our visual observations, we peformed CA measurement on two drop shape anaylizer devices in order to achieve different drop sizes: large (2 µl, Ø =1563 µm) and ultrasmall water droplets (Volume ≤ 0.008 µl, Ø ≤ 250 µm). With large droplets, results show that native wood is hydrophilic with a contact angle of 48.3 ± 22.0° (the large deviation is caused by the inhomogeneous wood surface comprising both EW and LW and the strong capillary effect on the Radial x Tangential face of the wood cubes). With contact angles of 127.4 ± 7.8° and 128.1 ± 5.1° for LW and EW respectively, the ZnO-W samples are clearly hydrophobic. However, large droplets have diameters exceeding the width of a LW region. Therefore the droplet is either sitting on EW only, or it sits on an area comprising both EW and LW (see Figure 4c and

4e). As a result, the CA value for the ZnO-W LW obtained with a large droplet is most likely erroneous.

To probe the LW and EW regions independently, we used ultrasmall droplets (Ø ≤ 250 μm) to ensure that they can be deposited on either EW or LW (see Figure 4e). In the case of native spruce wood, the contact angle is hardly measurable, because the small droplets are immediately absorbed within the wood structure via capillary effect. For the ZnO-W samples, the experiment reveals a significant wettability difference between the LW and EW regions: LW regions display a rather hydrophilic behavior with a contact angle of 58.3 ± 10.4° (value taken at t = 1000 ms, the droplet is then slowly adsorb by wood, see optical microscopy images in Figure S6), while the EW regions show the largest contact angles (131.8 ± 5.9°). With this experiment, we further demonstrate that the wettability of the wood cube is patterned according to its EW/LW morphology. With our approach, we achieved a high wettability contrast between LW and EW of ca. 74°.

Anisotropic Wetting. Accompanying the special wettability described in the previous paragraphs, we also observed a clear anisotropic wetting phenomenon. In Figure 5a, the optical image shows a water droplet pinning to LW and adopting a clear elliptic shape, which indicates an anisotropic wetting behavior. In other words, the droplet exhibits different contact angles depending on the direction of measurement (see Figure 5b). The parallel and perpendicular contact angles $\theta_{/\!/}$ and $\theta_{\perp}$ measured over time are shown in Figure 5c. $\theta_{\perp}$ slowly decreases with time, due to the progressive wetting of the droplet in the LW (see Movie S1, and averaged data showing $\Delta\theta = \theta_{\parallel} - \theta_{\perp}$ in Figure S7).

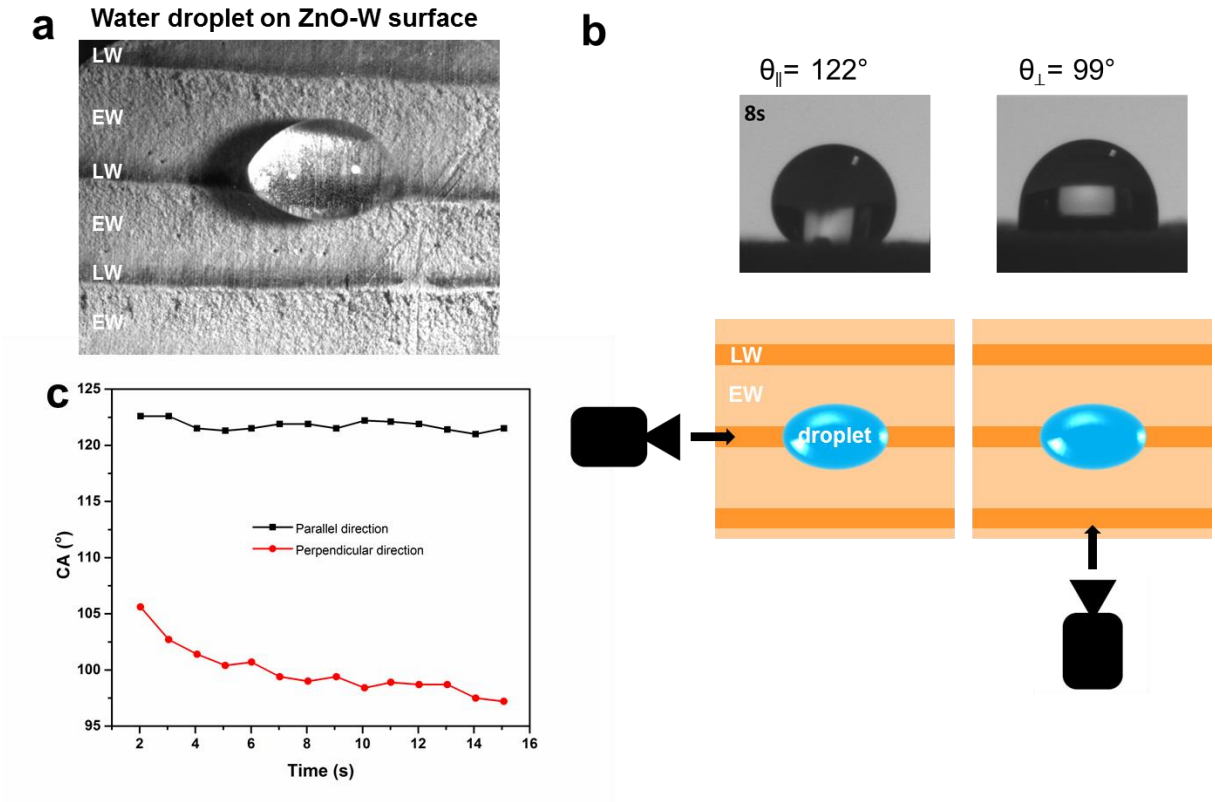

Figure 5: Anisotropic wetting on ZnO-W surfaces. (a) Optical microscopy image of a water droplet sitting on a ZnO-W surface. (b) Contact angles for a 2 μL water droplet measured from parallel (∥) and perpendicular (⊥) directions (data point at 8 seconds). (c) Evolution of the parallel and perpendicular CAs ($\theta_{\parallel}$ and $\theta_{\perp}$) with time.

The anisotropic wetting arises from the grooved surface generated by the cutting process (alternating rough EW and smooth LW, see profilometry in Figure S4), in combination with the chemical heterogeneity provided by the ZnO rods preferentially grown on the EW: the water droplet spontaneously spreads over the hydrophilic LW area while avoiding the hydrophobic EW areas.

For ultrasmall droplets deposited on LW, the CAs are similar from both directions (~ 75° for parallel and ~74° for perpendicular directions), since the drop does not contact with the hydrophobic EW region.

Further Patterning Exploiting Special Wetting Properties. In this part, we demonstrate the potential utilization of the special wettability of our ZnO-W samples. After modification, the EW is highly hydrophobic, and water does not wet these regions but it wets the LW areas. We took advantage of this property to selectively impregnate chemicals within the LW scaffold, and develop biotemplated materials with a simple approach. Here we give two simple examples covering further inorganic patterning and organic patterning.

In a first experiment, we studied the interactions of a silica solution with the ZnO-W samples. ZnO-W samples were simply dipped into the solution (cross section facing the liquid surface). EDX mapping was used to characterize the distribution of the various elements in the SiO_2-ZnO-W samples. As shown in Figure 6, selective deposition of SiO_2 took place mostly in LW regions. This demonstrates the possibility to use the contrasting wetting properties of EW and LW to control the impregnation of new materials in the wood scaffold, and to create new composite materials.

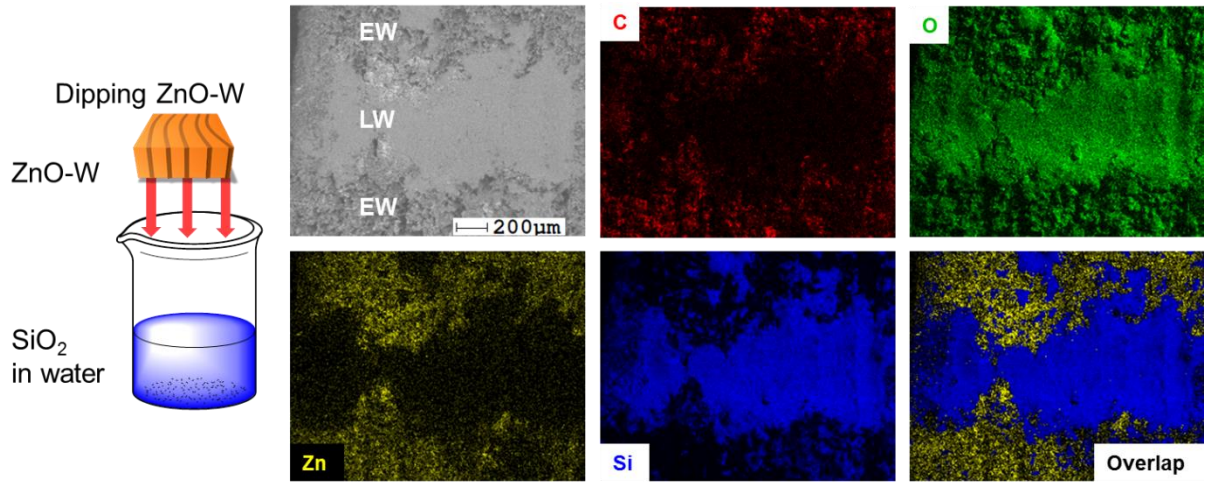

Figure 6: SEM-EDX analysis of SiO_2-ZnO-wood.

This simple experiment shows that the ZnO-W scaffold could be functionalized with various chemicals in a selective way. The obtained modified wood could be converted into ceramics via a sintering process,[55-56] affording biphasic ceramics that could have interesting mechanical properties.

Manipulating the surface tension and topography on a surface may also be interesting to control droplet motion for microfluidic applications, to control attachment of cells for biomedical applications, or to manufacture surfaces with antifouling or antifogging purposes.[57] Here, an example of the manipulation of the motion of a water droplet placed on the LW region on a tilted ZnO-W surface is demonstrated. The hydrophilic LW is supposed to act as a guiding track for the water droplet. We selected a wood sample with slightly curved annual rings, in order to better visualize the drop movement. As shown in Figure 7, when a water droplet is placed on the ZnO-W surface, it initially follows the LW track but fails to follow the curvature at some point. This indicates that at large curvature, the capillary forces exerted by the LW track cannot balance gravity forces and are unable to guide the water droplet along the LW track. One possible solution to force the trajectory of water in the LW guiding track is to enhance the

hydrophilicity of LW surface, resulting in an increase of the wettability contrast between hydrophilic and hydrophobic regions.

To do so, we used again the special wettability of the ZnO-W. By dipping the wood into a PDA/PEI water solution, we created a ZnO-W sample with PDA/PEI deposited preferentially in the LW regions.

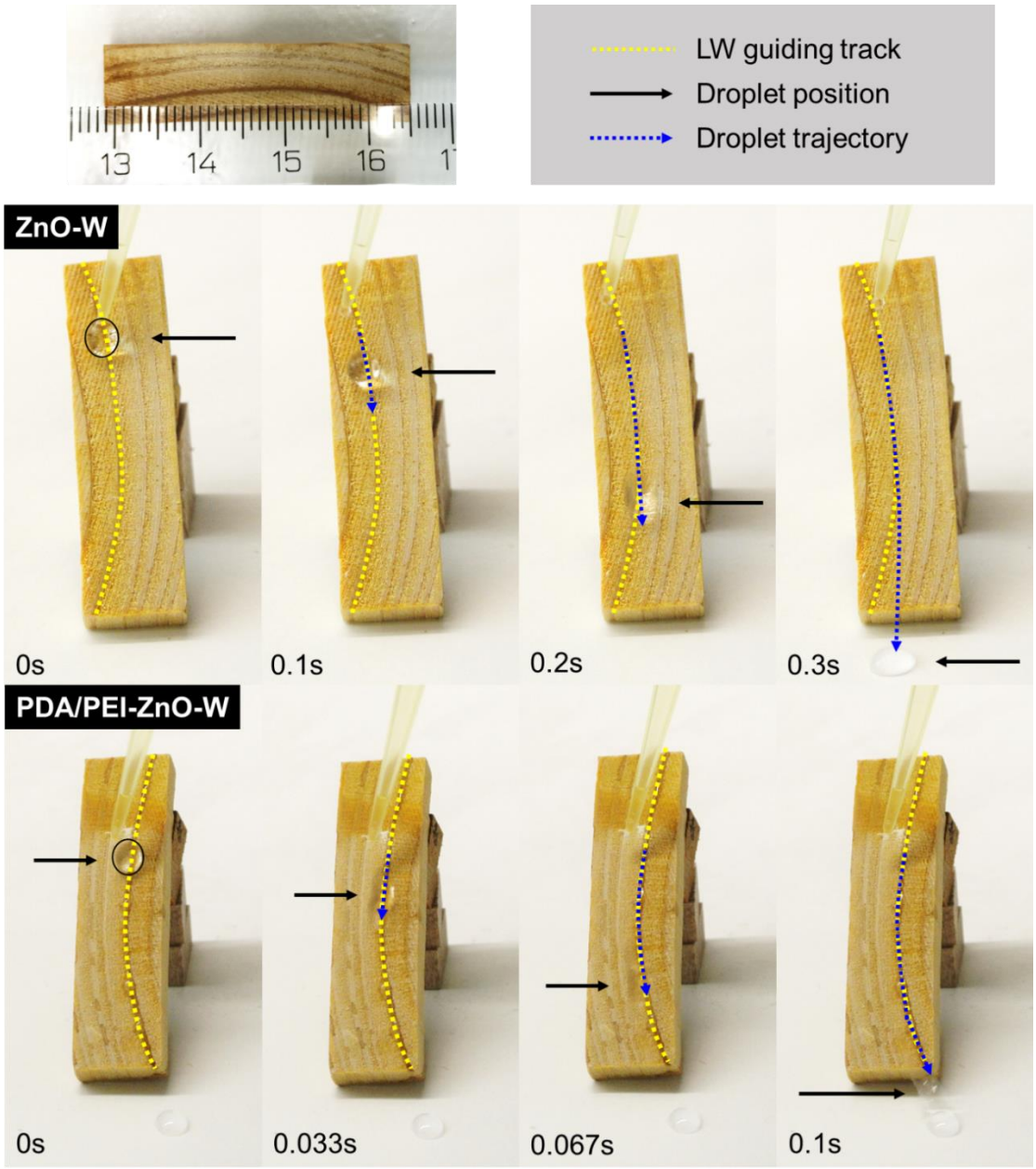

Figure 7: Movement of 10 µL droplets deposited on the LW grain of ZnO-W and PDA/PEI-ZnO-W. The wood sample is tilted (40°).

A new test of the water tracking experiment showed that with PDA/PEI patterned LW, the ZnO-PDA/PEI-W surface redirected the water drop at the point where ZnO-W failed. This time, as

shown in Figure 7, the water guiding experiment showed that with PDA/PEI patterned LW, the water droplet is successfully guided along the LW track.

CONCLUSIONS

In this work, we demonstrated the selective modification of a wood scaffold by using its natural morphology patterns, i.e. the alternating EW and LW grain. We have shown that the open structure of the EW region favors impregnation of aqueous solutions, and subsequently the growth of a dense array of ZnO rods, while the "sealed" LW surface leads to a more scattered distribution. The ZnO-modified surfaces have special wetting properties: the EW regions are highly hydrophobic due to the presence of the ZnO rods, and the LW regions remain hydrophilic. In addition, we observed a convincing anisotropic wetting effect on these surfaces, resulting from the chemical and topographical heterogeneity. Taking advantage of these functional patterns, we further modified the ZnO-W surfaces with a simple dipping approach, and reported on basic experiments to show the potential of these new wood-composite materials.

We have developed a new route to manufacture 2D patterned surfaces using a biological material. Some of the advantages to use wood as a template to develop new materials are obvious: i) the utilization of a bioresource is more sustainable than oil-based synthetic materials, ii) it provides a direct access to a complex anisotropic structure, iii) large scales are more easily accessible as opposed to many sophisticated techniques used to generate synthetic materials with well-defined anisotropic properties.

The facile and low-cost method to generate wettability pattern on spruce wood cross-section is an interesting pioneering work contributing to the development of advanced materials made from wood, and it could be used as a basis for the design of anisotropic wetting properties on other porous materials. In the future, we intend to study more sophisticated wood modifications to introduce for instance chemical gradients that could generate interesting anisotropic wetting properties.

ASSOCIATED CONTENT

Supporting Information. A PDF file containing additional characterization including EDX mapping, CA measurements, and profilometry measurements is available. A supplementary movie is also provided.

AUTHOR INFORMATION

Corresponding Author:

*Email: cabanee@ethz.ch or etienne.cabane@empa.ch

ACKNOWLEDGMENT

The authors would like to thank the China Scholarship Council (CSC) scholarship for funding, and the Surface Science and Technology group from ETHZ for kindly providing access to the drop shape analyzer. The authors are grateful to Marta Vidiella del Blanco from the Wood Materials Science group at ETH Zürich, for her support on the SEM measurements.

REFERENCES

1. Rowell, R. M., Chemical modification of wood: A short review. *Wood Material Science and Engineering* **2006,** *1* (1), 29-33, doi:10.1080/17480270600670923.
2. Rowell, R. M., *Handbook of Wood Chemistry and Wood Composites*. 2nd ed.; CRC Press: Boca Raton, 2012.
3. Hill, C. A. S., *Wood Modification: Chemical, Thermal and Other Processes* Wiley: New York, 2006.
4. Peleteiro, S.; Rivas, S.; Alonso, J. L.; Santos, V.; Parajó, J. C., Utilization of Ionic Liquids in Lignocellulose Biorefineries as Agents for Separation, Derivatization, Fractionation, or Pretreatment. *Journal of Agricultural and Food Chemistry* **2015,** *63* (37), 8093-8102, doi:10.1021/acs.jafc.5b03461.
5. Zhang, Z.; Song, J.; Han, B., Catalytic Transformation of Lignocellulose into Chemicals and Fuel Products in Ionic Liquids. *Chemical Reviews* **2017,** *117* (10), 6834-6880, doi:10.1021/acs.chemrev.6b00457.
6. Mussatto, S. I.; Dragone, G. M., Chapter 1 - Biomass Pretreatment, Biorefineries, and Potential Products for a Bioeconomy Development. In *Biomass Fractionation Technologies for a Lignocellulosic Feedstock Based Biorefinery*, Elsevier: Amsterdam, 2016; pp 1-22.
7. Zhu, M.; Song, J.; Li, T.; Gong, A.; Wang, Y.; Dai, J.; Yao, Y.; Luo, W.; Henderson, D.; Hu, L., Highly Anisotropic, Highly Transparent Wood Composites. *Advanced Materials* **2016,** *28* (26), 5181-5187, doi:10.1002/adma.201600427.
8. Li, Y.; Fu, Q.; Yu, S.; Yan, M.; Berglund, L., Optically Transparent Wood from a Nanoporous Cellulosic Template: Combining Functional and Structural Performance. *Biomacromolecules* **2016,** *17* (4), 1358-1364, doi:10.1021/acs.biomac.6b00145.
9. Trey, S.; Olsson, R. T.; Strom, V.; Berglund, L.; Johansson, M., Controlled deposition of magnetic particles within the 3-D template of wood: making use of the natural hierarchical structure of wood. *RSC Advances* **2014,** *4* (67), 35678-35685, doi:10.1039/C4RA04715J.
10. Cabane, E.; Keplinger, T.; Merk, V.; Hass, P.; Burgert, I., Renewable and functional wood materials by grafting polymerization within cell walls. *ChemSusChem* **2014,** *7* (4), 1020-1025, doi:10.1002/cssc.201301107.
11. Merk, V.; Chanana, M.; Gierlinger, N.; Hirt, A. M.; Burgert, I., Hybrid Wood Materials with Magnetic Anisotropy Dictated by the Hierarchical Cell Structure. *ACS Applied Materials & Interfaces* **2014,** *6* (12), 9760-9767, doi:10.1021/am5021793.
12. Cabane, E.; Keplinger, T.; Künniger, T.; Merk, V.; Burgert, I., Functional lignocellulosic materials prepared by ATRP from a wood scaffold. *Scientific Reports* **2016,** *6*, 31287, doi:10.1038/srep31287
13. Keplinger, T.; Cabane, E.; Berg, J. K.; Segmehl, J. S.; Bock, P.; Burgert, I., Smart Hierarchical Bio-Based Materials by Formation of Stimuli-Responsive Hydrogels inside the Microporous Structure of Wood. *Advanced Materials Interfaces* **2016,** *3* (16), 1600233-n/a, doi:10.1002/admi.201600233.

14. Liu, K.-K.; Jiang, Q.; Tadepalli, S.; Raliya, R.; Biswas, P.; Naik, R. R.; Singamaneni, S., Wood–Graphene Oxide Composite for Highly Efficient Solar Steam Generation and Desalination. *ACS Applied Materials & Interfaces* **2017,** *9* (8), 7675-7681, doi:10.1021/acsami.7b01307.
15. Xue, G.; Liu, K.; Chen, Q.; Yang, P.; Li, J.; Ding, T.; Duan, J.; Qi, B.; Zhou, J., Robust and Low-Cost Flame-Treated Wood for High-Performance Solar Steam Generation. *ACS Applied Materials & Interfaces* **2017,** *9* (17), 15052-15057, doi:10.1021/acsami.7b01992.
16. Lv, S.; Fu, F.; Wang, S.; Huang, J.; Hu, L., Novel wood-based all-solid-state flexible supercapacitors fabricated with a natural porous wood slice and polypyrrole. *RSC Advances* **2015,** *5* (4), 2813-2818, doi:10.1039/C4RA13456G.
17. Trey, S.; Jafarzadeh, S.; Johansson, M., In situ polymerization of polyaniline in wood veneers. *ACS applied materials & interfaces* **2012,** *4* (3), 1760-1769, doi:10.1021/am300010s.
18. Chen, F.; Gong, A. S.; Zhu, M.; Chen, G.; Lacey, S. D.; Jiang, F.; Li, Y.; Wang, Y.; Dai, J.; Yao, Y.; Song, J.; Liu, B.; Fu, K.; Das, S.; Hu, L., Mesoporous, Three-Dimensional Wood Membrane Decorated with Nanoparticles for Highly Efficient Water Treatment. *ACS Nano* **2017,** *11* (4), 4275-4282, doi:10.1021/acsnano.7b01350.
19. Sedighi Gilani, M.; Zhao, S.; Gaan, S.; Koebel, M. M.; Zimmermann, T., Design of a hierarchically structured hybrid material via in situ assembly of a silica aerogel into a wood cellular structure. *RSC Advances* **2016,** *6* (67), 62825-62832, doi:10.1039/C6RA12480A.
20. Seo, J.; Lee, S.; Lee, J.; Lee, T., Guided Transport of Water Droplets on Superhydrophobic–Hydrophilic Patterned Si Nanowires. *ACS Applied Materials & Interfaces* **2011,** *3* (12), 4722-4729, doi:10.1021/am2011756.
21. Song, D.; Song, B.; Hu, H.; Du, X.; Zhou, F., Selectively splitting a droplet using superhydrophobic stripes on hydrophilic surfaces. *Physical Chemistry Chemical Physics* **2015,** *17* (21), 13800-13803, doi:10.1039/C5CP01530H.
22. Zhang, L.; Wu, J.; Hedhili, M. N.; Yang, X.; Wang, P., Inkjet printing for direct micropatterning of a superhydrophobic surface: toward biomimetic fog harvesting surfaces. *Journal of Materials Chemistry A* **2015,** *3* (6), 2844-2852, doi:10.1039/C4TA05862C.
23. Ishizaki, T.; Saito, N.; Takai, O., Correlation of Cell Adhesive Behaviors on Superhydrophobic, Superhydrophilic, and Micropatterned Superhydrophobic/Superhydrophilic Surfaces to Their Surface Chemistry. *Langmuir* **2010,** *26* (11), 8147-8154, doi:10.1021/la904447c.
24. Ghosh, A.; Ganguly, R.; Schutzius, T. M.; Megaridis, C. M., Wettability patterning for high-rate, pumpless fluid transport on open, non-planar microfluidic platforms. *Lab on a Chip* **2014,** *14* (9), 1538-1550, doi:10.1039/C3LC51406D.
25. Lim, H. S.; Han, J. T.; Kwak, D.; Jin, M.; Cho, K., Photoreversibly Switchable Superhydrophobic Surface with Erasable and Rewritable Pattern. *Journal of the American Chemical Society* **2006,** *128* (45), 14458-14459, doi:10.1021/ja0655901.
26. Ueda, E.; Levkin, P. A., Emerging Applications of Superhydrophilic-Superhydrophobic Micropatterns. *Advanced Materials* **2013,** *25* (9), 1234-1247, doi:10.1002/adma.201204120.
27. Liu, K.; Zeng, X.; Jiang, S.; Ji, D.; Song, H.; Zhang, N.; Gan, Q., A large-scale lithography-free metasurface with spectrally tunable super absorption. *Nanoscale* **2014,** *6* (11), 5599-5605, doi:10.1039/C4NR00747F.
28. Chen, P.-Y.; McKittrick, J.; Meyers, M. A., Biological materials: Functional adaptations and bioinspired designs. *Progress in Materials Science* **2012,** *57* (8), 1492-1704, doi:http://dx.doi.org/10.1016/j.pmatsci.2012.03.001.
29. Darmanin, T.; Guittard, F., Superhydrophobic and superoleophobic properties in nature. *Materials Today* **2015,** *18* (5), 273-285, doi:http://dx.doi.org/10.1016/j.mattod.2015.01.001.
30. Parker, A. R.; Lawrence, C. R., Water capture by a desert beetle. *Nature* **2001,** *414* (6859), 33-34, doi:10.1038/35102108.
31. Yoshioka, S.; Kinoshita, S., Wavelength–selective and anisotropic light–diffusing scale on the wing of the Morpho butterfly. *Proceedings of the Royal Society of London. Series B: Biological Sciences* **2004,** *271* (1539), 581-587, doi:10.1098/rspb.2003.2618.
32. Feng, X.-Q.; Gao, X.; Wu, Z.; Jiang, L.; Zheng, Q.-S., Superior Water Repellency of Water Strider Legs with Hierarchical Structures: Experiments and Analysis. *Langmuir* **2007,** *23* (9), 4892-4896, doi:10.1021/la063039b.

33. Fratzl, P.; Weinkamer, R., Nature's hierarchical materials. *Progress in Materials Science* **2007,** *52* (8), 1263-1334, doi:http://dx.doi.org/10.1016/j.pmatsci.2007.06.001.
34. Salmén, L.; Burgert, I., Cell wall features with regard to mechanical performance. A review COST Action E35 2004–2008: Wood machining – micromechanics and fracture. *Holzforschung* **2009,** *63* (2), 121, doi:10.1515/hf.2009.011.
35. Fengel, D.; Wegener, G., *Wood : chemistry, ultrastructure, reactions*. W. de Gruyter: Berlin ; New York, 1984; p xiii, 613 p.
36. Huang, J.-S.; Lin, C.-F., Influences of ZnO sol-gel thin film characteristics on ZnO nanowire arrays prepared at low temperature using all solution-based processing. *Journal of Applied Physics* **2008,** *103* (1), 014304, doi:10.1063/1.2828172.
37. Yang, H.-C.; Liao, K.-J.; Huang, H.; Wu, Q.-Y.; Wan, L.-S.; Xu, Z.-K., Mussel-inspired modification of a polymer membrane for ultra-high water permeability and oil-in-water emulsion separation. *Journal of Materials Chemistry A* **2014,** *2* (26), 10225-10230, doi:10.1039/C4TA00143E.
38. Uggla, C.; Magel, E.; Moritz, T.; Sundberg, B., Function and Dynamics of Auxin and Carbohydrates during Earlywood/Latewood Transition in Scots Pine. *Plant Physiology* **2001,** *125* (4), 2029-2039, doi.
39. Keplinger, T.; Cabane, E.; Chanana, M.; Hass, P.; Merk, V.; Gierlinger, N.; Burgert, I., A versatile strategy for grafting polymers to wood cell walls. *Acta Biomaterialia* **2015,** *11* (0), 256-263, doi:http://dx.doi.org/10.1016/j.actbio.2014.09.016.
40. Ermeydan, M. A.; Cabane, E.; Hass, P.; Koetz, J.; Burgert, I., Fully biodegradable modification of wood for improvement of dimensional stability and water absorption properties by poly(ε-caprolactone) grafting into the cell walls. *Green Chemistry* **2014,** *16*, 3313-3321, doi:10.1039/C4GC00194J.
41. Wimmer, R.; Lucas, B. N.; Oliver, W. C.; Tsui, T. Y., Longitudinal hardness and Young's modulus of spruce tracheid secondary walls using nanoindentation technique. *Wood Science and Technology* **1997,** *31* (2), 131-141, doi:10.1007/bf00705928.
42. Mott, L.; Groom, L.; Shaler, S., Mechanical Properties of Individual Southern Pine Fibers. Part II. Comparison of Earlywood and Latewood Fibers with Respect to Tree Height and Juvenility. *Wood and Fiber Science* **2002,** *34* (2), 221-237.
43. Donaldson, L.; Bardage, S.; Daniel, G., Three-dimensional imaging of a sawn surface: a comparison of confocal microscopy, scanning electron microscopy, and light microscopy combined with serial sectioning. *Wood Science and Technology* **2007,** *41*, 551-564, doi: 10.1007/s00226-007-0132-y.
44. Magoss, E., General Regularities of Wood Surface Roughness. *Acta Silvatica & Lignaria Hungarica* **2008,** *4*, 81-93.
45. Gurau, L.; Mansfield-Williams, H.; Irle, M., Processing roughness of sanded wood surfaces. *Holz als Roh- und Werkstoff* **2005,** *63* (1), 43-52, doi:10.1007/s00107-004-0524-8.
46. Follrich, J.; Vay, O.; Veigel, S.; Müller, U., Bond strength of end-grain joints and its dependence on surface roughness and adhesive spread. *Journal of Wood Science* **2010,** *56* (5), 429-434, doi:10.1007/s10086-010-1118-1.
47. Zhang, H.; Zhang, W.; Jin, C.; Li, S., Inorganic Antiflaming Wood Caused by a -Decorated ZnO Nanorod Arrays Coating Prepared by a Facile Hydrothermal Method. *Journal of Nanomaterials* **2016,** *2016*, 9 pages, doi:10.1155/2016/2358276.
48. Kong, L.; Tu, K.; Guan, H.; Wang, X., Growth of high-density ZnO nanorods on wood with enhanced photostability, flame retardancy and water repellency. *Applied Surface Science* **2017,** *407*, 479-484, doi:https://doi.org/10.1016/j.apsusc.2017.02.252.
49. Yao, Q.; Wang, C.; Fan, B.; Wang, H.; Sun, Q.; Jin, C.; Zhang, H., One-step solvothermal deposition of ZnO nanorod arrays on a wood surface for robust superamphiphobic performance and superior ultraviolet resistance. *Scientific Reports* **2016,** *6*, 35505, doi:10.1038/srep35505.
50. Guo, H.; Fuchs, P.; Cabane, E.; Michen, B.; Hagendorfer, H.; Romanyuk Yaroslav, E.; Burgert, I., UV-protection of wood surfaces by controlled morphology fine-tuning of ZnO nanostructures. *Holzforschung* **2016**, *70* (8), 699-708, doi:https://doi.org/10.1515/hf-2015-0185.
51. Shupe, T.; Piao, C.; Lucas, C., The termiticidal properties of superhydrophobic wood surfaces treated with ZnO nanorods. *European Journal of Wood and Wood Products* **2012,** *70* (4), 531-535, doi:10.1007/s00107-011-0563-x.

52. Zhang, J.; Zhang, B.; Chen, X.; Mi, B.; Wei, P.; Fei, B.; Mu, X., Antimicrobial Bamboo Materials Functionalized with ZnO and Graphene Oxide Nanocomposites. *Materials* **2017,** *10* (3), 239, doi:10.3390/ma10030239.
53. Fu, Y.; Yu, H.; Sun, Q.; Li, G.; Liu, Y., Testing of the superhydrophobicity of a zinc oxide nanorod array coating on wood surface prepared by hydrothermal treatment. *Holzforschung* **2012,** *66* (6), 739-744, doi:10.1515/hf-2011-0261.
54. Liu, Y.; Fu, Y.; Yu, H.; Liu, Y., Process of in situ forming well-aligned Zinc Oxide nanorod arrays on wood substrate using a two-step bottom-up method. *Journal of Colloid and Interface Science* **2013,** *407* (Supplement C), 116-121, doi:https://doi.org/10.1016/j.jcis.2013.06.043.
55. Zhou, M.; Zang, D.; Zhai, X.; Gao, Z.; Zhang, W.; Wang, C., Preparation of biomorphic porous zinc oxide by wood template method. *Ceramics International* **2016,** *42* (9), 10704-10710, doi:https://doi.org/10.1016/j.ceramint.2016.03.188.
56. Van Opdenbosch, D.; Fritz-Popovski, G.; Paris, O.; Zollfrank, C., Silica replication of the hierarchical structure of wood with nanometer precision. *Journal of Materials Research* **2011,** *26* (10), 1193-1202, doi:10.1557/jmr.2011.98.
57. Xia, D.; Johnson, L. M.; López, G. P., Anisotropic Wetting Surfaces with One-Dimesional and Directional Structures: Fabrication Approaches, Wetting Properties and Potential Applications. *Advanced Materials* **2012,** *24* (10), 1287-1302, doi:10.1002/adma.201104618.

2.2.1 Supplementary information

Cutting process

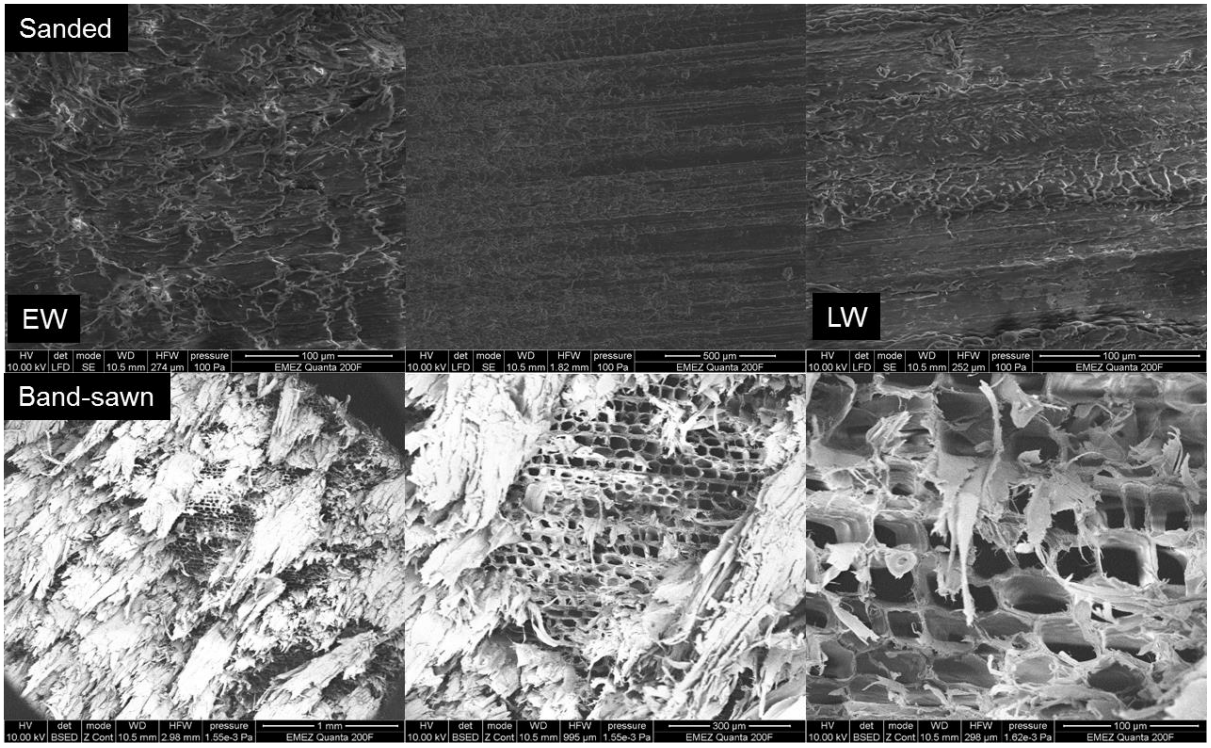

Figure S1: SEM images of spruce wood surfaces obtained after sanding and band saw cutting.

Sanding of wood surfaces results in surface roughness homogenization at the microscale. We can clearly see that the surface is homogeneously "closed", and would therefore not be suitable for our process exploiting the contrast between "open" EW and "closed" LW regions.

Band saw cutting yielded extremely rough surfaces, with highly damaged fibers. The EW and LW regions were barely recognizable, and such surfaces are not well defined for our applications.

ZnO seeds distribution

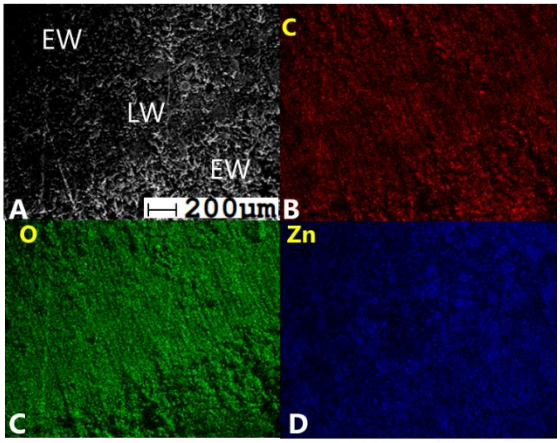

Figure S2: ZnO colloid deposited on the wood surface under vacuum showed a relatively homogeneous distribution over EW and LW. (a) SEM image of seeded wood cross-section. (b) to (d): EDX mapping of carbon, oxygen, and zinc.

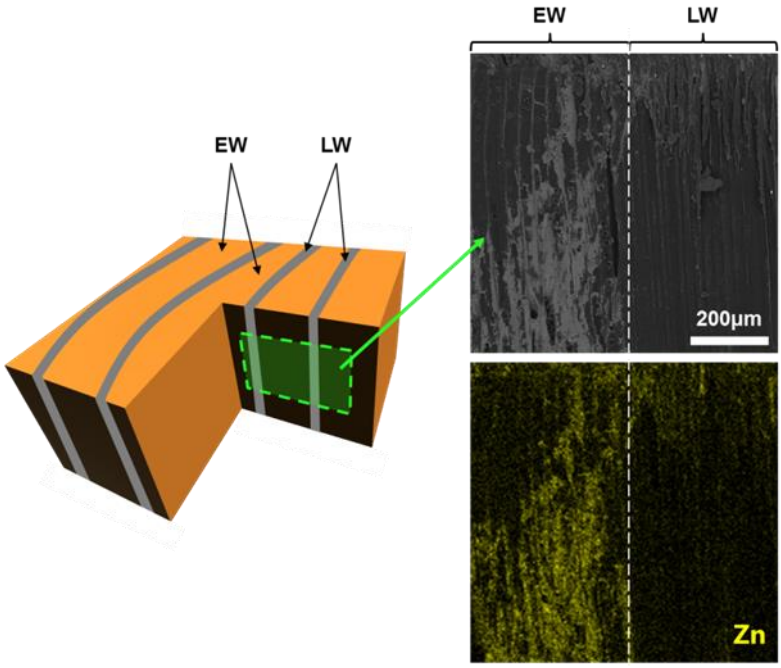

Figure S3: Tangential section of seeded wood, showing the ZnO seed distribution inside the wood cube. The ZnO seed clearly penetrates deeper in the EW regions.

The seed layer is impregnated under vacuum for three times, and the distribution on wood surface appears relatively homogeneous (Figure S2). SEM-EDX images in Figure S3 show that ZnO seeds are present deep inside the wood scaffold in the EW fiber region, while it is barely penetrating inside the LW region. As discussed in the main text, the cutting process generates

uneven wood surfaces: EW regions have open tracheids, while LW regions have mainly closed tracheids (i.e. blocked lumens, influencing adsorption of liquids in the wood).

Stylus Profilometry

The surface roughness of wood cross-section after RMC and CSC are characterized by stylus profilometry. In general, EW is much rougher than LW, therefore, EW contributes more to the overall (an area consists of both EW and LW) surface roughness parameters.

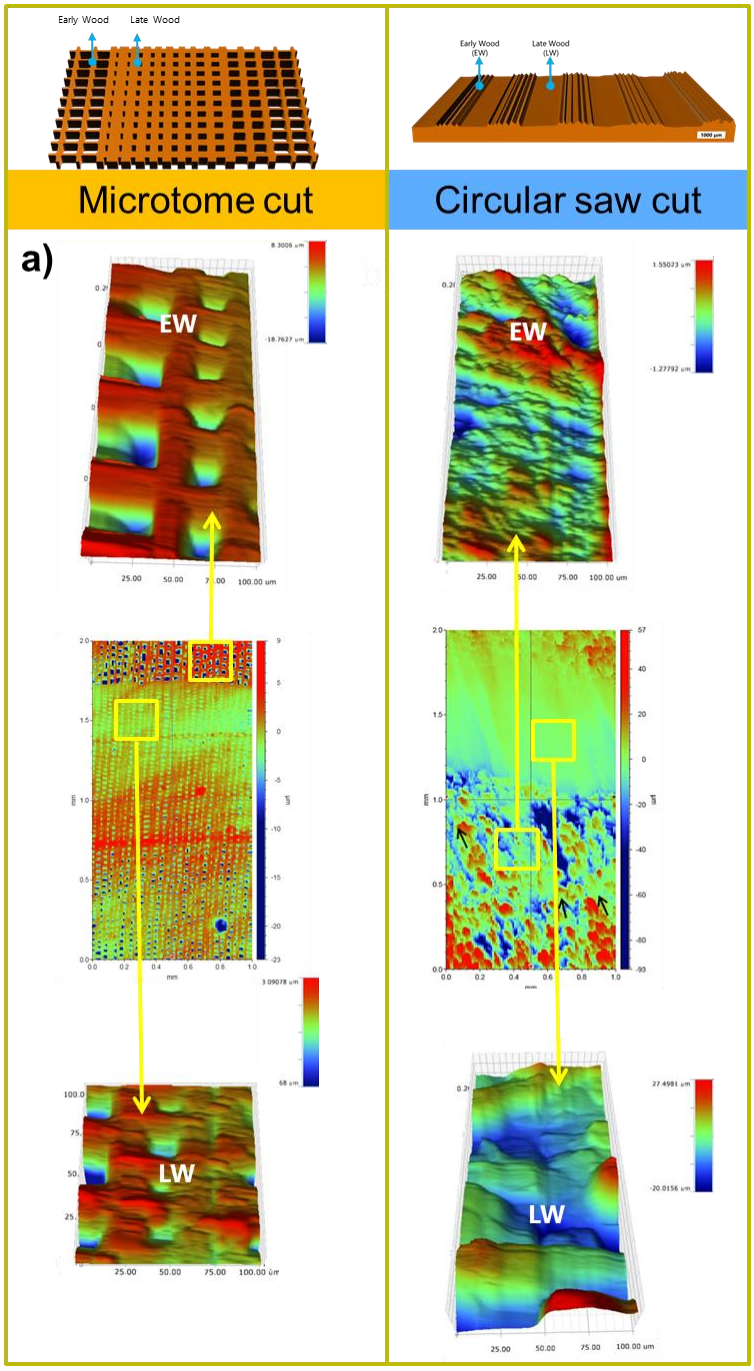

Figure S4: 3D profiles of wood cross-section by two different cutting methods.

Table S1: roughness values in micrometers from the mapping images shown in Figure S4.

	CSC process			RMC process		
	EW + LW	**EW**	**LW**	**EW + LW**	**EW**	**LW**
Sp	57.162	27.498	1.55	9.315	8.301	3.091
Sv	-92.959	-20.016	-1.278	-23.448	-18.763	-11.187
Sz	150.121	47.514	2.828	32.763	27.063	14.278
Sa	9.141	5.879	0.311	1.754	2.876	0.936
Sq	13.37	7.614	0.382	2.697	4.061	1.424

ZnO distribution mechanism analysis

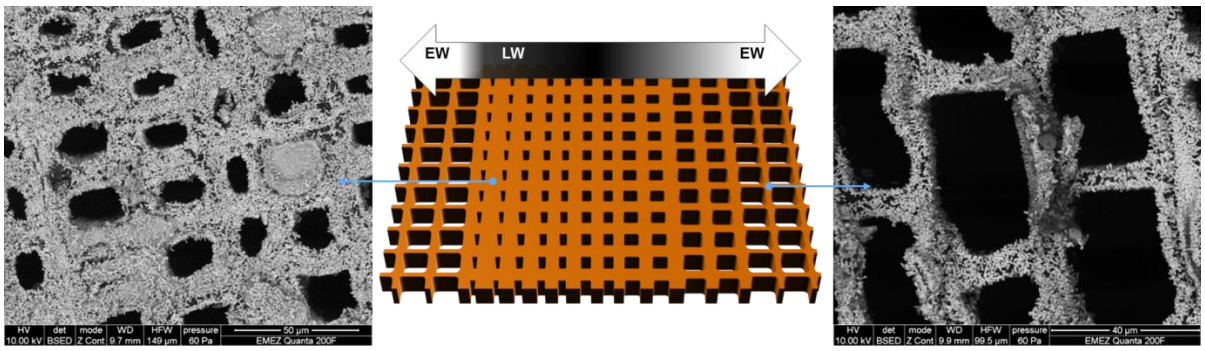

Figure S5: Distribution of ZnO rods on wood cross-sections cut by microtome cut. SEM micrographs of the LW and EW scaffolds after treatment (ZnO growth) show the densely arranged ZnO rods in both areas.

We applied the same modification on a CSC wood cross-section which presents a fully open porous structure on both EW and LW (Figure S5). According to the SEM images there is not obvious ZnO rods density difference in between EW and LW regions, and therefore no preferential growth.

Wettability characterization

Figure S6: Top view images of ultrasmall water droplets deposited on ZnO-W LW at 0, 4, and 5 seconds.

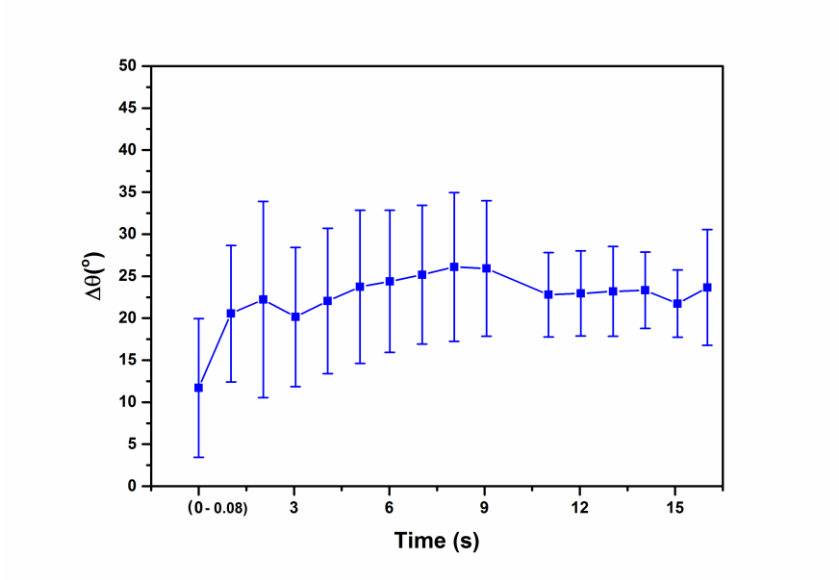

Figure S7: The contact angle differences (Δθ) observing from perpendicular and parallel directions of the large droplets sitting on ZnO-LW.

Movie S1: Progressive wetting of the droplet in the LW.

Movie link: https://pubs.acs.org/doi/suppl/10.1021/acssuschemeng.7b03104

2.3 Beech wood cross-sections as natural templates to fabricate superhydrophobic surfaces

Yaru Wang[†‡], Selin Vitas[†‡], Ingo Burgert[†‡], Etienne Cabane*[†‡]

[†]Wood Materials Science, ETH Zürich, Stefano-Franscini-Platz 3, CH-8093 Zürich, Switzerland

[‡]Applied Wood Materials, EMPA-Swiss Federal Laboratories for Materials Science and Technology, Überlandstrasse 129, CH-8600 Dübendorf, Switzerland

KEYWORDS

templating, superhydrophobicity, polydimethylsiloxane, wood anatomy, surface structuration

ABSTRACT

Inspired by the hierarchical and porous wood microstructure, we fabricated polydimethylsiloxane (PDMS) positive replicas of beech (*Fagus sylvatica)* cross-sections, with superhydrophobic properties. Microtomed transverse sections of beech wood were directly used as templates, and we obtained an accurate replication of the anatomic wood features (vessels and fibers). The resulting PDMS positive replicas show an arrangement of pillars, contributing to surface structuration. By adjusting the PDMS pre-curing time, we could control the extent of PDMS penetration inside the wood capillaries, inducing the formation of pillars with various aspect ratios. We studied the wettability of the templated surfaces as a function of the different pillars heights, and identified the optimal pillar aspect ratio to enhance the hydrophobicity of the PDMS structured surfaces (reaching a water contact angle of 156°). *Fagus sylvatica* wood cross-sections are therefore simple, scalable, and inexpensive templates to manufacture structured surfaces, with the possibility to adjust wettability according to application needs.

INTRODUCTION

Controlling surface wettability is of great interest in a wide range of applications, including anti-icing,[1] anti-bio adhesion,[2] water collection,[3] liquid transportation,[4] and water purification.[5] In this regard, the extraordinary wetting phenomena observed on the surfaces of biological materials are an important source of bioinspiration for surface functionalization.[6, 7, 8, 9] Biological surfaces with special wettabilities or directional water droplet roll off can be found in various organisms; in the plant kingdom – lotus leaves,[10] rice leaves,[11] or cactus spines[12] – and in the animal kingdom – butterfly wings,[13] water strider legs,[14] cicada wings,[15] dessert beetle back,[16] or gecko toe pads.[17] Most of these surfaces display highly complex hierarchical structures, a property known to contribute to surface wettability, together with the surface energy. The Wenzel equation predicts that the increase of roughness on a hydrophobic surface enhances its hydrophobic character. Certain roughness features can also help to trap air, and create a composite surface able to repel a wide range of liquids (Cassie-Baxter mode).[18]

The precise fabrication of material surfaces with controlled surface topography along various length scales is therefore of high importance. A number of fabrication techniques can be used to fabricate microsized structures on surfaces. Processes include soft lithography,[19] photolithography,[20] inorganic particle growth,[21] electrospinning,[22] templating,[23] or 3D-printing.[24] These approaches are often sophisticated multistep processes, requiring a high energy input and non-renewable resources, and are generally costly. In comparison, templating methods can be seen as relatively straightforward and low cost. Templates can be manufactured from breath figure arrays,[25] electrochemical etching,[26] assembly of colloidal particles, lithography and woven material surfaces,[27] or biological materials such as plant leaves,[28] or insect wings,[29,30] can be used directly. Natural templates have several advantages: low cost, limited processing, abundance, biodegradability, and an intrinsic hierarchical structure. However, for practical reasons many replication attempts from biological templates have been limited. When using natural templates, there is a limitation in terms of design, since the surface features are imposed by the biological material. For example, the papillae on lotus leaf surface are several micrometers in diameter and in height,[31] and the protrusions on cicada wings have diameters of around 100 nm, with maximum heights around 450 nanometers.[15] The features display a rather low aspect ratio, and it is not possible to adjust it to match with the requirements needed for certain applications. In many other cases, another challenge resides in the difficulty to access large surfaces. Although the replica may show excellent properties, the final surface areas may not be suitable for large scale applications.

Looking for an alternative biological template, we found wood, a wildly available porous material. The wood structure results from the alignment of hollow elements with high aspect ratios (fibers, and vessels in the case of hardwoods). While fibers typically do not exceed a few millimeters in length and up to tens of micrometers in diameter, single vessels (assembled from a multitude of vessel elements) can run along the tree trunk over several meters, and have diameters ranging from tens to hundreds of microns.[32]

The wood elements can be approximated as capillaries, facilitating the transport of fluids. When wood is cut perpendicular to the fiber direction, the cross-section can be described as a flat surface with a dense distribution of holes or pores, the opening of these capillaries. Our approach is to take advantage of these unique features. The wetting of the porous wood material with a curable polymer precursor should allow for the production of pillars with high aspect ratio. The replication of the microstructures of wood using polymer micro-casting has been studied by Parmak et al.,[33] Uraki et al.,[34] and Kitin et al.,[35] for different purposes. In their reports, accurate replica with evenly distributed pillars were not obtained or not aimed, and the control over the pillar heights was not shown. In addition, they did not characterize the wettability properties of their surfaces.

In this work, we chose *Fagus sylvatica* cross-sections as templates, and a PDMS kit (with cure processing controlled by temperature) to show the feasibility of this concept. An interesting way to obtain surface pillars with different heights, is to adjust the viscosity of the polymer solution entering the wood capillaries. With this approach, we show that it is possible to obtain an exact replica of the beech wood template, and to achieve control over the height of the pillars. According to our measurements, with an optimized pillar aspect ratio, it is possible to obtain highly structured pure PDMS surfaces with a superhydrophobic behavior. With the direct use of wood, we propose an extremely convenient and facile approach to obtain superhydrophobic surfaces.

EXPERIMENTAL SECTION

Materials**.** The templates were obtained from European beech (*Fagus sylvatica*). We used wood cubes (10 × 10 × 4 mm^3, radial × tangential × longitudinal) with microtome trimmed surfaces. We used the Sylgard® 184 Silicone Elastomer Kit (Dow Corning, USA), as a curable polymer.

Methods**.** The PDMS casting process on beech wood is described in Scheme 1. The PDMS based is mixed with the curing agent (10:1 ratio by weight) in a Petri dish, pre-cured in an oven

at 65 °C for different times (ranging from 5 to 20 minutes) before cooling at room temperature (RT). The microtome cut beech wood cross-sections are then deposited on the PDMS (4g of PDMS, in a Petri dish with Ø = 35 mm). The cross-section is facing down to allow the viscous PDMS mixture to penetrate into the beech wood cells for 3h at RT and ambient pressure. The stamped PDMS and beech wood are placed in an oven for the final curing step at 65°C for 30 min. Finally, the cured PDMS is peeled off the wood template.

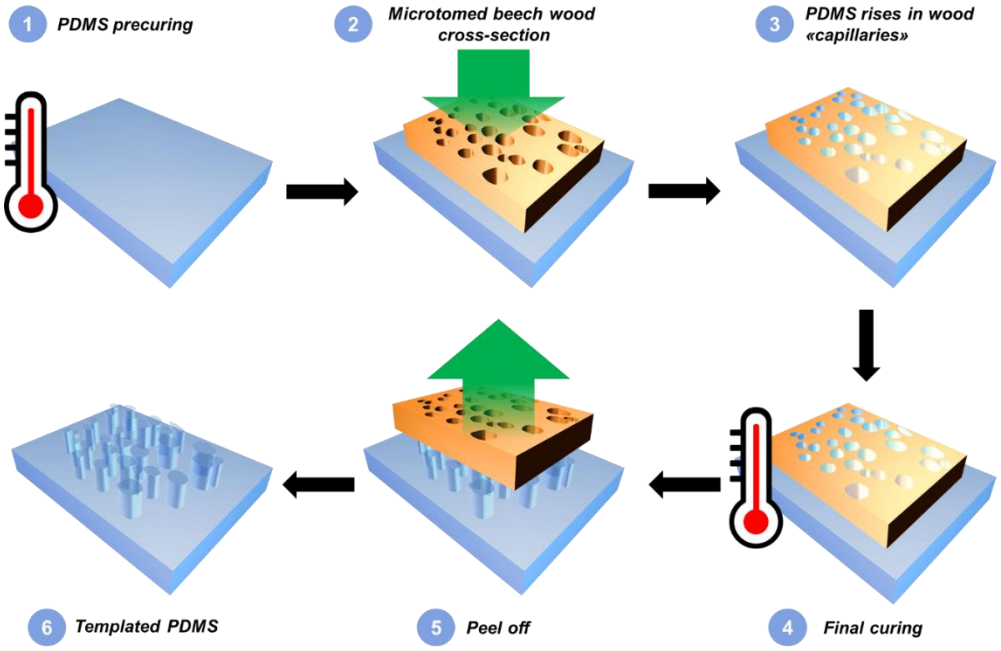

Scheme 1: casting process for the fabrication of surface-structured PDMS materials using a wood cross-section as templating material.

PDMS replicas from beech wood transverse sections were labeled as "TS-pillar height". TS-0 represents directly cured PDMS without stamping. The replicas from wood radial section were labeled "RS".

In principle, other species with different porosities could also be used for this process, with adjusted experimental conditions. Optical microscopy images of stained wood cross sections with different pore sizes and distributions are shown in Figure S1.

Characterization**.** Pore analysis of *Fagus sylvatica* cross-sections: basic quantities characterizing the beech pore distributions were acquired through image analysis. SEM images of beech wood cross-sections were analyzed by ImageJ (1.52a) to obtain the average diameter of the vessels and fibers, as well as the average distance in between two neighboring vessels or fibers. The contrast is adjusted to yield a binary image. For vessel counting, areas smaller than 10 pixels were removed in order to exclude the fibres. In the case of *Fagus sylvatica*, the cell

diameter threshold to differentiate between a vessel and a fiber is set to 18 µm.[36] The pitch P is defined as the distance between the center of two neighboring cells (see Figure S2).

The surface structures of native wood and PDMS replica were characterized with scanning electron microscopy (SEM), atomic force microscopy (AFM), and stylus profilometry. SEM images were acquired with a scanning electron microscope (SEM; FEI Quanta 200F, Hillsboro, OR, USA). AFM images were obtained from an atomic force microscope (AFM, Nano Wizard 4, JPK Instruments AG, Berlin, Germany) in Quantitative Imaging (QI) mode at 20 °C and 65% relative humidity. Image processing was done in the JPK image processing software (JPK Instruments AG). The height of the pillars were measured from the cross-section profiles obtained by SEM (results averaged over 20 pillars). Stylus profilometry, Bruker Dektak XT equipped with a 2 µm radius tip, was used as a complementary technique to measure the surface roughness and surface profiles.

Contact angles (CA) were measured with a Krüss drop shape analyzer (DSA 100) using the sessile drop method. 2 µl water drops were used for all the PDMS samples.

RESULTS & DISCUSSION

Anatomical features

Beech wood is a diffuse-porous hardwood: it has a highly and rather regular porous structure. According to calculations, our samples are characterized by a pore density of approximately 3500 pores/mm^2. The wood pores are best seen on the cross sectional cuts shown in Figure 1. As proposed by Plötze et al.,[37] the pores in beech wood might be classified in various groups, from micropores (radius < 80 nm) to macropores (radius > 2 µm). The pores of interest for this study belong to the macropore class, and correspond to the vessels and fibers luminal areas. The vessel diameters typically range from 50 to 200 µm (variations according to the hardwood species), and the length of a single vessel element ranges from 100 to 1200 µm.[32] Fibers have a smaller diameter, and their length is usually two to ten times longer than individual vessel elements.[32] According to our image analysis, beech wood is characterized by an average vessel diameter of 41.5 ± 9.9 µm, and an average fiber diameter of 5.8 ± 9.5 µm. These numbers are consistent with literature values reported for beech wood.[38, 39]

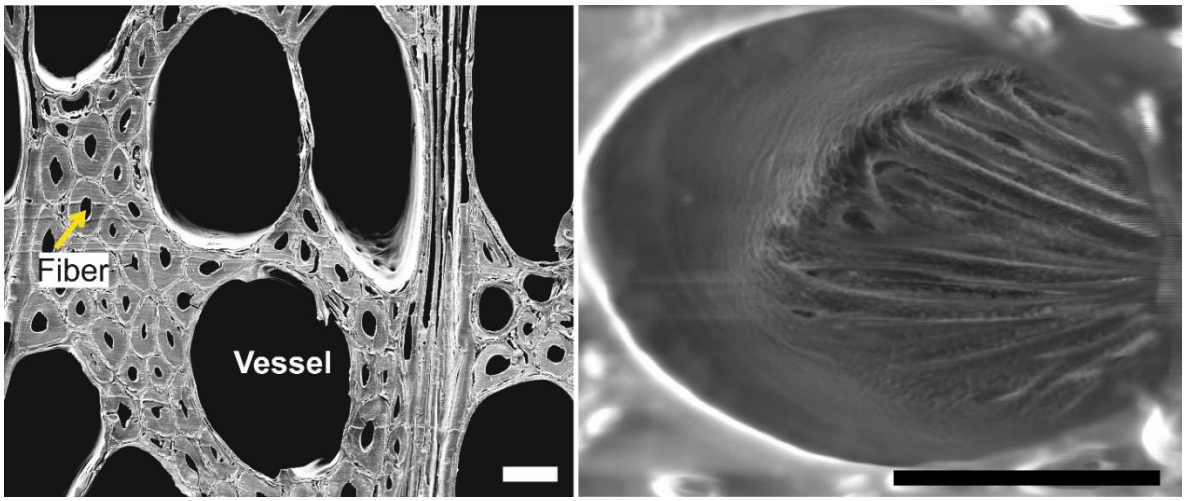

Figure 1: SEM images of native beech wood cross sections showing the distribution of vessels and fibers, and a perforation plate (scale bars: 20µm).

The above-mentioned wood elements may all be approximated as linear tubes, running perpendicular to the cross-section plan (i.e. they are all parallel to each other). From the image analysis, we found out that in average, two vessels are about 79.4 µm apart, while fibres are about 16.9 µm apart. These values correspond to the distance between the geometric centers of two neighboring cells (i.e. pitch P, see Figure S2).

PDMS templating

In this study, the primary goal of the PDMS micro-casting was to replicate the macroporous structures of wood (i.e. vessels, fibers). According to the SEM images shown in Figure 2a-c, the wood PDMS templating was successful, with the creation of PDMS pillars with dimensions corresponding to vessel and fiber lumina (vessel pillars and fiber pillars). As seen in Figure 2d, the PDMS pillars have concave tips (shown by the dotted yellow line following the curvature). This shape reflects the meniscus created upon the capillary rise of the liquid PDMS inside the wood pores. The concave shape was also confirmed by surface topography measurements with stylus profilometry (see Figure S3).

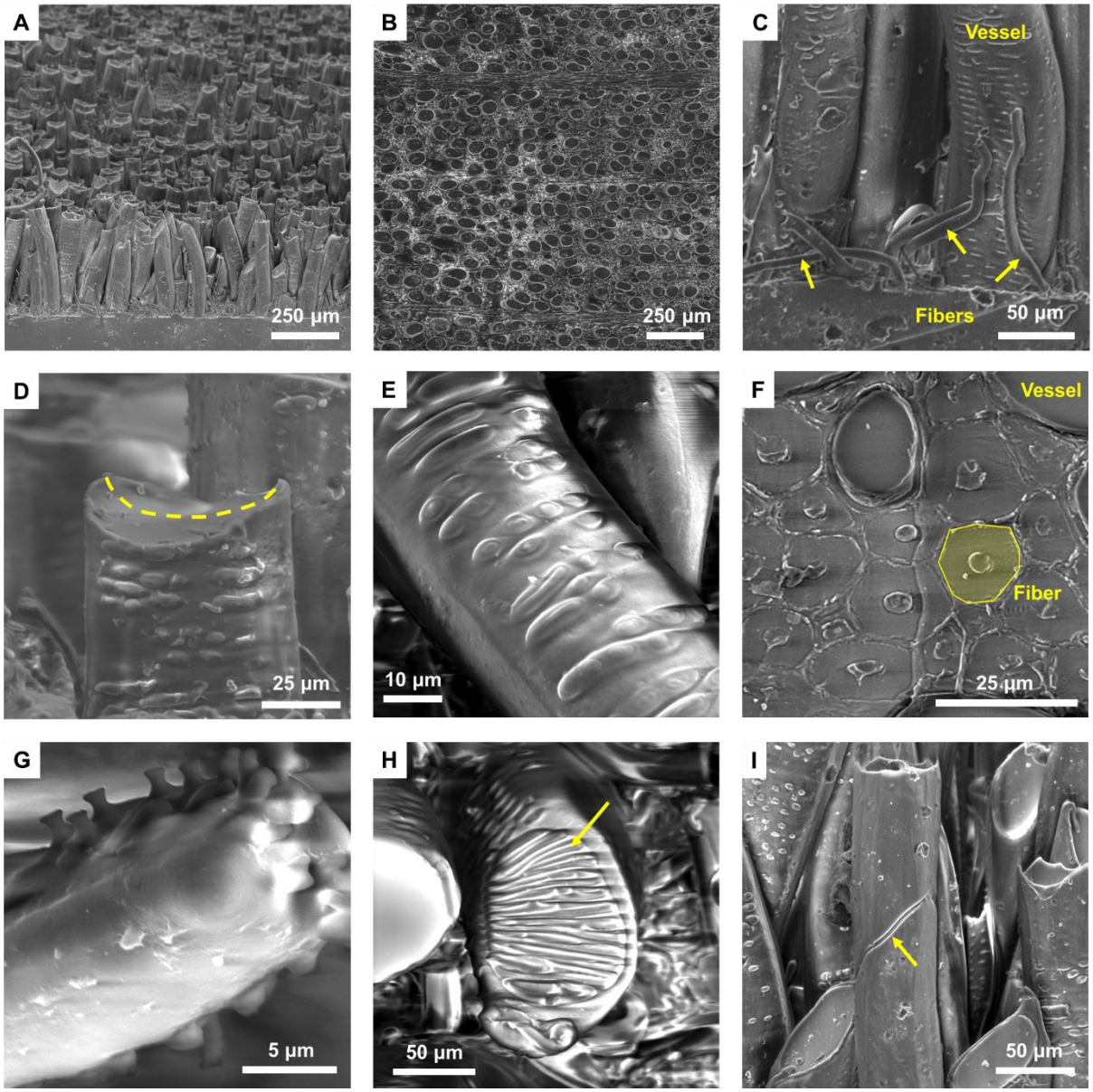

Figure 2: SEM images of PDMS replica from a beech wood scaffold. A) side view showing PDMS pillars replicated from vessel elements. B) top view of vessel pillars. C) zoomed image showing thin PDMS pillars replicated from fibers (indicated by arrows) and vessel pillars in the background. D) example of a concave pillar tip. E) Surface of a vessel-templated pillar showing pits. F) top view of the area between neighboring vessel-templated pillars showing detailed replication of the fiber cross-sections. G) protrusions on the surface of the PDMS pillar replicated from vessel. H) Top view showing a perforation plate structure replicated at the tip of a vessel pillar (indicated by the arrow). I) side view of a replicated vessel with the arrow showing the junction between two individual vessel elements.

In addition, the SEM of the templated PDMS show precise replication of various anatomical features. Besides replicating vessel and fiber lumina (large features, tens of microns), the SEM images clearly show smaller details, such as pits and perforation plates (microns and submicrons sizes, Figure 2e). The precise contours of individual fiber cell walls are seen in

Figure 2f. The protrusions decorating a replicated vessel shown in Figure 2g correspond to the exact replication of inter-vessel pits, indicating that PDMS was able to penetrate inside these open pits (a similar micro-casting of open pits was obtained from the radial section, Figure S4). Figure 2h shows the replication of a scalariform perforation plate on the top of a vessel pillar. This shows that in this case, the PDMS was stopped by this natural "barrier", and did not flow into the next vessel element. Finally, in the microcast of a vessel shown in Figure 2i, the arrow points at the cell wall feature of a simple perforation in between two vessel elements.

Surface topography of the PDMS replicas

As opposed to pre-fabricated molds having holes or cavities with finite length, with the utilization of wood as a template we face a technical challenge associated to the open structure of vessels and fibres. However, this was aimed to produce a PDMS surface with various pillar heights obtained from the same mold. To do this, we needed to control the penetration depth of the PDMS mixture inside the wood elements. The capillary flow of a liquid inside a porous material (assumed to be a bundle of parallel capillary tubes) can been described with the Lucas-Washburn law:

$$L^2 = \frac{\gamma r t \cos(\theta)}{2\eta} \qquad \text{(Eq. 1)}$$

Where L is the liquid penetration distance into the capillary, γ is the surface tension of the liquid, θ its contact angle with the material, r is the capillary tube radius, η is the dynamic viscosity of the liquid, and t is the time. In our system, by changing the pre-curing time, we could vary the extent of crosslinking in between PDMS chains, hence the viscosity of the PDMS mixture could be adjusted.[40,41, 42] Through this setup, we got control over the PDMS penetration depths into wood cells. Alternatively, if we keep a fixed pre-curing time, we can control the penetration depth by adjusting the contact time between our wood templates and the PDMS mixture.

The PDMS structured surfaces peeled off beech wood cross-sections are shown in Figure 3, arranged according to increasing pillar heights. The pillar heights values were estimated from SEM images and AFM measurements (see Figure S5).

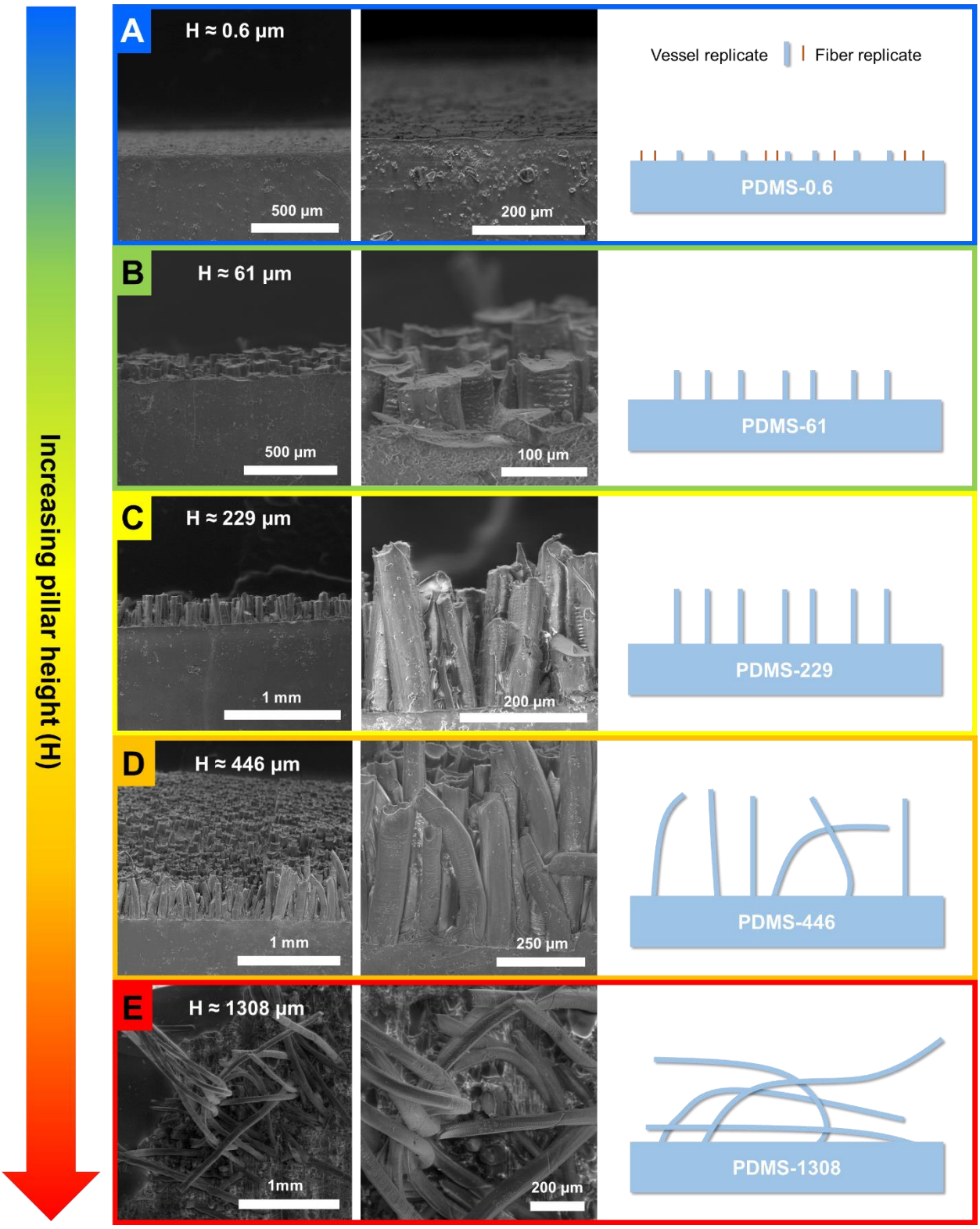

Figure 3: SEM images of beech wood replicated PDMS surfaces with different pillar heights. Corresponding SEM images in top view are given in Figure S6.

The surface shown in Figure 3a was obtained with the longest PDMS pre-curing time. The highly viscous PDMS pre-mix barely entered the lumina of both vessels and fibers, giving rise to shallow bumps with heights below one micrometer. With decreasing pre-curing time, the

PDMS pre-mix could start to flow deeper in capillaries, and we obtained surfaces with larger pillar heights. In Figure 3b and c, the images show two surfaces with rather well defined and straight pillars, with heights approximately 61 ± 8.2 and 229 ± 28.3 μm, respectively.

When the pre-curing time was further decreased (lower viscosity), the PDMS penetrated deeper in the vessel lumina, yielding pillars with higher aspect ratios (see Figure 3d). Eventually, as shown in Figure 3d and e, the aspect ratio was such that pillars started to bend (this is also shown in Figure S6). This was expected due to the mechanical properties of the silicone elastomer (PDMS). In the extreme case shown in Figure 3e, most of the PDMS pillars did not resist the peel off process: large contact area between PDMS and the wood cell walls gives large friction when peeling off PDMS, therefore the majority of the pillars broke, and the SEM images show a clear fracture pattern at the base of the pillars (see Figure S6). The remaining very high pillars (H = 1308 μm) suggest that the PDMS mixture is capable of flowing in the vessel elements over long distances, possibly crossing structural features, such as scalariform perforation plates (the perforation plates are likely teared off upon peeling, and remain embedded inside the PDMS pillars). According to the x-axis error bars in Figure 4, the shorter the pillars, the more uniform the pillar height. This may be the result of two factors. First, to obtain a higher pillar, the rising PDMS is more likely to encounter perforation plates inside the vessels. The presence of a perforation plate can retard the PDMS flow, when compared to the portion of a vessel that does not contain any perforation. This could contribute to increasing the pillar size distribution. Secondly, long pillars are more likely to break while peeling off, which would lead to the formation of segments of pillars, again increasing the size distribution.

According to the SEM images, it appears that the PDMS samples essentially replicate the vessel elements. As shown by various images (see Figure 2c and Figure S6), PDMS can also enter the fiber lumina, and fiber microcasts are obtained. However, we believe that most of the replicated fibers are broken during the peel off process and remain in the wood cube, due to their extremely high aspect ratio. The few remaining replicated fibers are bent. In the case of PDMS templated surfaces with high pillar heights (TS-229 and TS-446), the replicated fibers are too few and shorter than the vessels (due to bending), and they most likely do not contribute to the surface wettability. For very short vessel pillars (TS-0.6), the presence of fiber pillars is likely to play a more significant role for the final contact angle, since the solid/air fraction will be clearly affected.

Wettability study

The contact angles of the different PDMS surfaces are given in Figure 4. For an ideal flat PDMS surface (i.e. no templating), we measured a CA of 107.8°, which will be used as the Young's contact angle for PDMS. As the average pillar height goes from 0 to 229 µm, the surface roughness increases, along with the CA values (from 107.8 to 156°). However, further increase of pillar heights to 446 µm makes the CA drop off to 141.3°. In accordance with the SEM images shown in Figure 3 and Figure S6, this is likely due to the bending of PDMS pillars. For the highest pillar heights (ca. 1308 µm), all the pillars are bent and collapsed on the surface: when a water droplet sits on the surface, replicated vessels wrap around it. As shown in Figure 4A, the water droplet still keeps a spherical shape, but it is difficult to define the CA value for this surface.

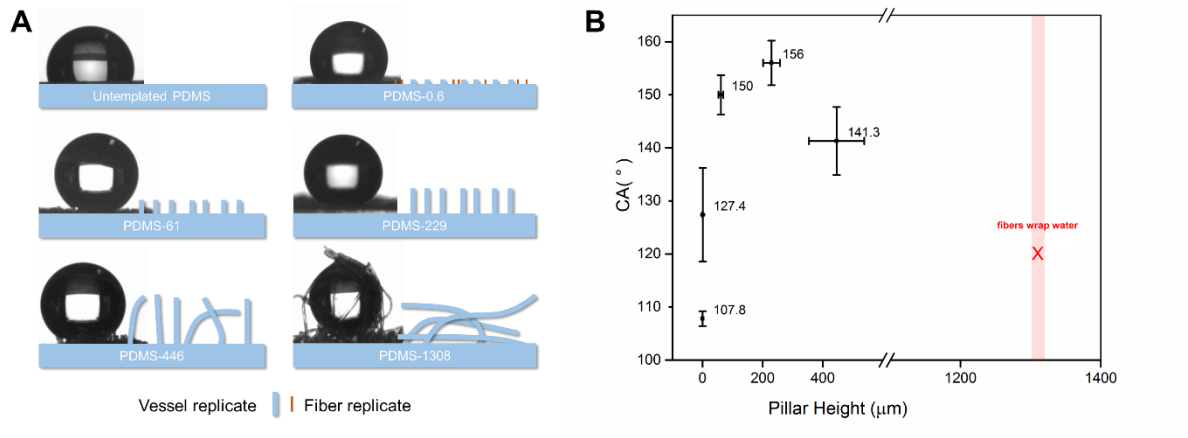

Figure 4: A) Contact angle images on the PDMS replicas with different pillar heights; B) plot showing the corresponding measured CAs as a function of pillar height. The legend "fibers wrap water" describes the behavior of the highest pillars (1308 µm) in the presence of a water drop.

To better understand our experimental results, we calculated the theoretical contact angle values that would fit a regular array of PDMS pillars having the dimensions of our samples. To perform these calculations, we used the pitch values (P) and pillar diameters (D) determined by image analysis, and the estimated pillar heights (H) (see values in Table 1). We also made the following assumptions: i) the PDMS surfaces accurately replicate the wood scaffold (pore distribution = pillar distribution, and pore diameter = pillar diameter), ii) PDMS without wood templating is considered as an ideal surface, and the CA measured can be taken as the Young's CA for flat PDMS, iii) all pillars are cylindrical, of the same height, and regularly distributed, iv) for TS-0.6, the surface roughness is given by the fiber microcasts, while in all other cases, only the vessel microcasts are considered.

As described by Wenzel,[43] texturing a surface to increase the surface roughness can make the surface more hydrophobic if the material is intrinsically hydrophobic. This is described by Equation 2:

$$\cos\theta^* = r\cos\theta_Y \quad \text{(Eq. 2)}$$

Where θ_Y is the Young's contact angle in ideal condition, θ^* is the apparent contact angle with, and r is the roughness (ratio between the real surface area, and the projected surface area).

Later, Cassie and Baxter analyzed wetting phenomena on porous surfaces, and proposed the following equation:[18]

$$\cos\theta^* = f\cos\theta_Y + (f-1) \quad \text{(Eq. 3)}$$

Where θ_Y is the Young's contact angle, θ^* is the apparent contact angle, and f is the solid fraction of the surface (surface present at the top of the protruding structures, to be opposed to the air fraction corresponding to the air pockets on the surface). Along with the theoretical CA values calculated with the Wenzel or Cassie-Baxter equations, it is possible to predict which wetting mode should be favored, through the calculation of the critical angle θ_c according to the surface parameters *f* and *r*:

$$\cos\theta_c = \frac{f-1}{r-f} \quad \text{(Eq. 4)}$$

If $\theta_Y > \theta_c$, then the Cassie-Baxter mode (CB) should be favored, and vice versa. The experimental and calculated CA values are summed up in Table 1.

Table 1: Experimental and theoretical data for contact angles on wood-templated surfaces.

Sample ID	H(µm)[a]	P(µm)[b]	D(µm)[c]	r[d]	f(%)[e]	θ_C(°)[f]	Predicted wetting mode	θ_{CB}(°)[g]	θ_W(°)[h]	θ(°)[i]
TS-0	Smooth surface			1	100	180	Ideal	107.8	107.8	107.8
TS-0.6	0.624	16.9	5.8 ± 9.5	1.04	9.2	163.6	W	159.4	108.5	127.4 ± 8.8
TS-61	61.0 ± 8.2	79.4	41.5 ± 10.0	2.26	21.4	112.6	W	148.3	133.7	150.0 ± 3.7
TS-230	229.6 ± 28.3	79.4	41.5 ± 10.0	5.75	21.4	98.2	CB	148.3	-	156.0 ± 4.2
TS-446	446.0 ± 92.0	79.4	41.5 ± 10.0	10.22	21.4	94.5	CB	148.3	-	141.3 ± 6.4
TS-1308	1308	79.4	41.5 ± 10.0	29.53	21.4	91.5	CB	148.3	-	-

[a]Height of the PDMS pillars in µm (all pillar heights were estimated from SEM and profilometry, except TS-0.6 measured by AFM). [b]Pitch in µm: average distance between two neighboring pillars (center to center distance). [c]Pillar diameter in µm. [d]Roughness, $r = \frac{area+\pi\times D\times H\times n}{area}$. [e]Solid fraction in percent, $f = \frac{n\times\pi(D/2)^2}{area}$. [f]Critical contact angle. [g]Calculated Cassie-Baxter contact angle. [h]Calculated Wenzel contact angle. [i]Experimental contact angle.

In theory, TS-0.6 and TS-61 should fit to the Wenzel mode, while TS-229, TS-446, and TS-1308 should fit the Cassie-Baxter mode. As predicted, the experimental and Wenzel theoretical values are similar in the case of the TS-0.6 sample. However, for TS-61, the experimental CA value of 150.0° is closer to the Cassie-Baxter CA (148.3°) than the Wenzel mode (133.7°). This may result from the assumptions mentioned above. In this case, the deviation from the expected CA might be due to the contribution of the fiber microcasts that we neglected in this calculation. For TS-229 and TS-446, the experimental values are close to the expected CA values, calculated from the Cassie-Baxter model. The CA difference observed for TS-229 and TS-446 is explained by the bending of PDMS pillars on the latter surface. The pillar collapse increases the solid fraction, which, according to Eq. 3, will decrease the contact angle. Finally, the comparison between calculated and experimental data is not conclusive for TS-1308, because we cannot provide a definite value for the experimental CA. However, the comments related to pillar bending and collapse, can be applied to this surface as well.

CONCLUSION

In summary, we show a facile and low cost strategy to produce structured PDMS surfaces using wood as a template. With this simple microcasting technique, we were able to replicate the porous structure of beech wood cross-sections with high precision, over a large surface area (1 square centimeter). The method can be used to enhance the surface wettability of PDMS surfaces, through structuration with pillar arrays. By "growing" pillar arrays of different aspect ratios ranging from 0.1 to 33.3, different contact angles were achieved: it was possible to obtain superhydrophobic surfaces when a compromise between pillar size and mechanical stability was found.

The possibilities offered by the wood template are numerous. In the future, we will explore the diversity of wood species, which can provide a wide range of templates (see some examples in Figure S1). We used *Fagus sylvatica* in this work, but we believe that many other wood species could be used to generate other surface features offering solutions to design and control the pillar size and distribution. Since the method can yield pillars with high aspect ratio, it could also be interesting to use other casting materials, with which we could form more rigid structures and avoid collapsing. Wood also provides a direct answer to up-scaling issues: large cross-sections can easily be obtained from wood stems, through circular saw cutting followed by polishing. In addition, polymer surfaces having well-defined regions with different wettabilities can be created with wood templates, since wood cross-sections can be easily processed by different techniques, including etching, engraving, or marking with chemicals, laser or mechanical tools. For these reasons, we believe that our approach is very promising, and could be an advantageous technique for various applications where a simple, scalable and inexpensive structuration technique is needed. Nevertheless, the anatomical structures might vary within one wood species due to the different growing environments. One must be aware that the replica surface topographies from two wood templates of the same wood species can be rather different. Furthermore, the upscaling challenges, including a homogeneous trimming of large wood surfaces, the homogenous curing of polymers as well as potentially large friction in the demolding require further investigation.

ACKNOWLEDGMENTS

The authors would like to thank the China Scholarship Council (CSC) for funding, Stéphane Croptier and Thomas Schnider from the Wood Materials Science group in ETH Zürich for discussions on wood

species and for their help in wood samples preparation, respectively. We are grateful to the Scientific Center for Optical and Electron Microscopy (ScopeM) at ETH Zürich for the SEM studies.

REFERENCES

1. Kreder, M. J.; Alvarenga, J.; Kim, P.; Aizenberg, J., Design of anti-icing surfaces: smooth, textured or slippery? *Nature Reviews Materials* **2016,** *1* (1), 15003.
2. Sun, T.; Tan, H.; Han, D.; Fu, Q.; Jiang, L., No platelet can adhere—largely improved blood compatibility on nanostructured superhydrophobic surfaces. *Small* **2005,** *1* (10), 959-963.
3. Hao, B.; Lin, W.; Jie, J.; Ruize, S.; Yongmei, Z.; Lei, J., Efficient Water Collection on Integrative Bioinspired Surfaces with Star-Shaped Wettability Patterns. *Adv. Mater.* **2014,** *26* (29), 5025-5030.
4. Ghosh, A.; Ganguly, R.; Schutzius, T. M.; Megaridis, C. M., Wettability patterning for high-rate, pumpless fluid transport on open, non-planar microfluidic platforms. *Lab on a Chip* **2014,** *14* (9), 1538-1550.
5. Sai, H.; Fu, R.; Xing, L.; Xiang, J.; Li, Z.; Li, F.; Zhang, T., Surface modification of bacterial cellulose aerogels' web-like skeleton for oil/water separation. *ACS Appl. Mater. Interfaces* **2015,** *7* (13), 7373-7381.
6. Bhushan, B.; Jung, Y. C.; Koch, K., Micro-, nano- and hierarchical structures for superhydrophobicity, self-cleaning and low adhesion. *Philosophical Transactions of the Royal Society A: Mathematical, Physical and Engineering Sciences* **2009,** *367* (1894), 1631-1672.
7. Bixler, G. D.; Bhushan, B., Biofouling: lessons from nature. *Philosophical Transactions of the Royal Society A: Mathematical, Physical and Engineering Sciences* **2012,** *370* (1967), 2381-2417.
8. Gorb, S. N., *Functional surfaces in biology: little structures with big effects*. Springer Science & Business Media: 2009; Vol. 1.
9. Darmanin, T.; Guittard, F., Superhydrophobic and superoleophobic properties in nature. *Mater. Today* **2015,** *18* (5), 273-285.
10. Cheng, Y. T.; Rodak, D.; Wong, C.; Hayden, C., Effects of micro-and nano-structures on the self-cleaning behaviour of lotus leaves. *Nanotechnology* **2006,** *17* (5), 1359.
11. Wu, D.; Wang, J. N.; Wu, S. Z.; Chen, Q. D.; Zhao, S.; Zhang, H.; Sun, H. B.; Jiang, L., Three‐Level Biomimetic Rice‐Leaf Surfaces with Controllable Anisotropic Sliding. *Adv. Funct. Mater.* **2011,** *21* (15), 2927-2932.
12. Ju, J.; Bai, H.; Zheng, Y.; Zhao, T.; Fang, R.; Jiang, L., A multi-structural and multi-functional integrated fog collection system in cactus. *Nature communications* **2012,** *3*, 1247.
13. Zheng, Y.; Gao, X.; Jiang, L., Directional adhesion of superhydrophobic butterfly wings. *Soft Matter* **2007,** *3* (2), 178-182.
14. Gao, X.; Jiang, L., Biophysics: water-repellent legs of water striders. *Nature* **2004,** *432* (7013), 36.
15. Sun, M.; Watson, G. S.; Zheng, Y.; Watson, J. A.; Liang, A., Wetting properties on nanostructured surfaces of cicada wings. *J. Exp. Biol.* **2009,** *212* (19), 3148-3155.
16. Parker, A. R.; Lawrence, C. R., Water capture by a desert beetle. *Nature* **2001,** *414* (6859), 33.
17. Autumn, K.; Hansen, W., Ultrahydrophobicity indicates a non-adhesive default state in gecko setae. *Journal of Comparative Physiology A* **2006,** *192* (11), 1205.
18. Cassie, A.; Baxter, S., Wettability of porous surfaces. *Transactions of the Faraday society* **1944,** *40*, 546-551.
19. Baquedano, E.; Martinez, R. V.; Llorens, J. M.; Postigo, P. A., Fabrication of Silicon Nanobelts and Nanopillars by Soft Lithography for Hydrophobic and Hydrophilic Photonic Surfaces. *Nanomaterials* **2017,** *7* (5), 109.
20. Öner, D.; McCarthy, T. J., Ultrahydrophobic Surfaces. Effects of Topography Length Scales on Wettability. *Langmuir* **2000,** *16* (20), 7777-7782.

21. Guo, H.; Peter, F.; Kirstin, C.; Benjamin, M.; Munish, C.; Harald, H.; E., R. Y.; Ingo, B., Bio-Inspired Superhydrophobic and Omniphobic Wood Surfaces. *Advanced Materials Interfaces* **2017,** *4* (1), 1600289.
22. Miyauchi, Y.; Ding, B.; Shiratori, S., Fabrication of a silver-ragwort-leaf-like super-hydrophobic micro/nanoporous fibrous mat surface by electrospinning. *Nanotechnology* **2006,** *17* (20), 5151.
23. Yan, Z.; Liang, X.; Shen, H.; Liu, Y., Preparation and basic properties of superhydrophobic silicone rubber with micro-nano hierarchical structures formed by picosecond laser-ablated template. *IEEE Transactions on Dielectrics and Electrical Insulation* **2017,** *24* (3), 1743-1750.
24. Yang, Y.; Li, X.; Zheng, X.; Chen, Z.; Zhou, Q.; Chen, Y., 3D‐Printed Biomimetic Super‐Hydrophobic Structure for Microdroplet Manipulation and Oil/Water Separation. *Adv. Mater.* **2018,** *30* (9), 1704912.
25. Zander, N. E.; Orlicki, J. A.; Karikari, A. S.; Long, T. E.; Rawlett, A. M., Super-Hydrophobic Surfaces via Micrometer-Scale Templated Pillars. *Chem. Mater.* **2007,** *19* (25), 6145-6149.
26. Lee, K.; Lyu, S.; Lee, S.; Kim, Y. S.; Hwang, W., Characteristics and self-cleaning effect of the transparent super-hydrophobic film having nanofibers array structures. *Appl. Surf. Sci.* **2010,** *256* (22), 6729-6735.
27. Roach, P.; Shirtcliffe, N. J.; Newton, M. I., Progess in superhydrophobic surface development. *Soft matter* **2008,** *4* (2), 224-240.
28. Mele, E.; Girardo, S.; Pisignano, D., Strelitzia reginae leaf as a natural template for anisotropic wetting and superhydrophobicity. *Langmuir* **2012,** *28* (11), 5312-5317.
29. Zhang, X.; Ji, D.; Lei, T.; Zhao, B.; Song, K.; Hu, W.; Wang, J.-Y.; Pei, J.; Wang, Y., Integration of antireflection and light diffraction in nature: a strategy for light trapping. *Journal of Materials Chemistry A* **2013,** *1* (36), 10607-10611.
30. Wang, H.; Yao, Q.; Wang, C.; Fan, B.; Sun, Q.; Jin, C.; Xiong, Y.; Chen, Y., A simple, one-step hydrothermal approach to durable and robust superparamagnetic, superhydrophobic and electromagnetic wave-absorbing wood. *Scientific reports* **2016,** *6*, 35549.
31. Nosonovsky, M.; Bhushan, B., Lotus-Effect and Water-Repellent Surfaces in Nature. *Multiscale Dissipative Mechanisms and Hierarchical Surfaces: Friction, Superhydrophobicity, and Biomimetics* **2008**, 181-197.
32. Rowell, R. M., *Handbook of wood chemistry and wood composites*. CRC press: Florida, USA, 2012.
33. Parmak, E. D. S., Fabrication of microstructured polymers by a simple biotemplate embossing method and their characterization. *Materials Testing* **2016,** *58* (3), 246-251.
34. Uraki, Y.; Nemoto, J.; Sano, Y., A novel preparation of microcast for wood micromorphology using polydimethylsiloxane without digesting cell wall. *Journal of Wood Science* **2006,** *52* (2), 163-166.
35. Kitin, P.; Sano, Y.; Funada, R., Analysis of cambium and differentiating vessel elements in Kalopanax pictus using resin cast replicas. *IAWA Journal* **2001,** *22* (1), 15-28.
36. Sass, U.; Eckstein, D., The variability of vessel size in beech (Fagus sylvatica L.) and its ecophysiological interpretation. *Trees* **1995,** *9* (5), 247-252.
37. Plötze, M.; Niemz, P., Porosity and pore size distribution of different wood types as determined by mercury intrusion porosimetry. *European Journal of Wood and Wood Products* **2011,** *69* (4), 649-657.
38. Steppe, K.; Cnudde, V.; Girard, C.; Lemeur, R.; Cnudde, J.-P.; Jacobs, P., Use of X-ray computed microtomography for non-invasive determination of wood anatomical characteristics. *Journal of structural biology* **2004,** *148* (1), 11-21.
39. Kiaei, M.; Samariha, A., Fiber dimensions, physical and mechanical properties of five important hardwood plants. *Indian Journal of Science and Technology* **2011,** *4* (11), 1460-1463.
40. Flowers, G.; Switzer, S. T. *Background material properties of selected silicone potting compounds and raw materials for their substitutes*; Mason and Hanger-Silas Mason Co., Inc., Amarillo, Tex.(USA): 1978.
41. Bello, M.; Welch, C.; Goodwin, L.; Keller, J. *Sylgard® Mixing Study*; Los Alamos National Laboratory (LANL), Los Alamos, NM (United States): 2014.

42. Sylgard 184: viscosity increase during cure. https://www.sandia.gov/polymer-properties/E1-viscosity.html.
43. Wenzel, R. N., Resistance of solid surfaces to wetting by water. *Industrial & Engineering Chemistry* **1936,** *28* (8), 988-994.

2.3.1 Supplementary information

Optical microscopy pictures of cross-sections of different wood species

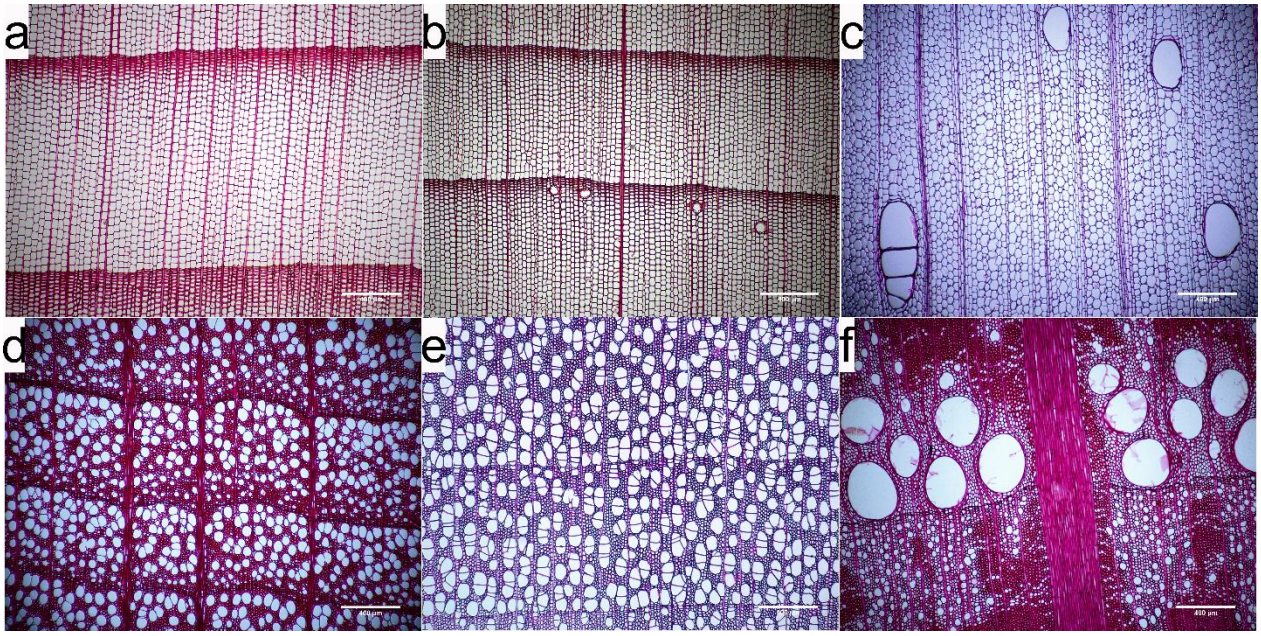

Figure S1: Optical images of wood cross-sections stained with Safranin, showing the diversity of wood microstructures. a) Silver fir (Abies alba Mill.); b) Spruce (Picea abies Karst.); c) Balsa (Ochroma lagopus Sw.); d) Beech (Fagus sylvatica L.); e) White poplar (Populus alba L.); f) Oak (Quercus petraea Liebl.). All images were taken with an optical microscope (Olympus BX 51).

Pore counting

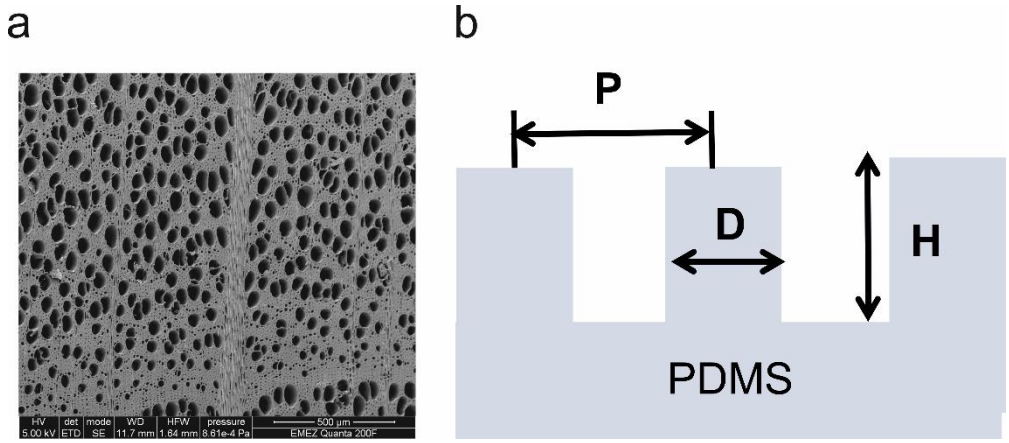

Figure S2: a) SEM picture used for data processing, and b) scheme showing the quantities obtained from the image analysis and applied to the PDMS microcast (P is the pitch, D the diameter of a casted vessel or fiber). H is the height of a vessel or fiber pillar, measured after the demolding process.

Surface roughness

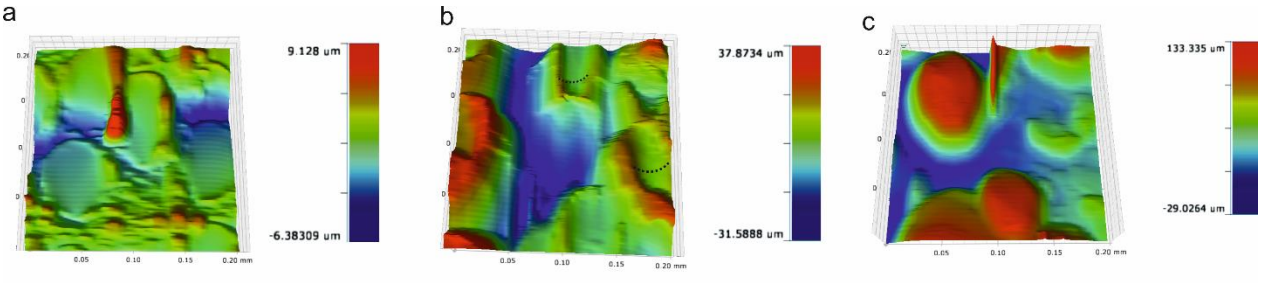

Figure S3: stylus profilometry images of PDMS replicas: a) TS-0.6; b) TS-61; c) TS- 230. The black curves show the concave tips of the pillars.

Due to the moving of the long pillars during tip tapping, PDMS-446 and PDMS-1360 could not be measured. The corresponding roughness values are shown below.

Table S1: The surface roughness measured by stylus profilometer.

Sample	Sa (µm)	Sq (µm)
TS-0.6	2.6	3.3
TS-0	0.3	0.5
TS-61	11.3	14.2
TS-230	13.0	16.0
TS-446	Unmeasurable, pillar bent with the lowest set point (1 µg)	
TS-1308		

Radial section replica

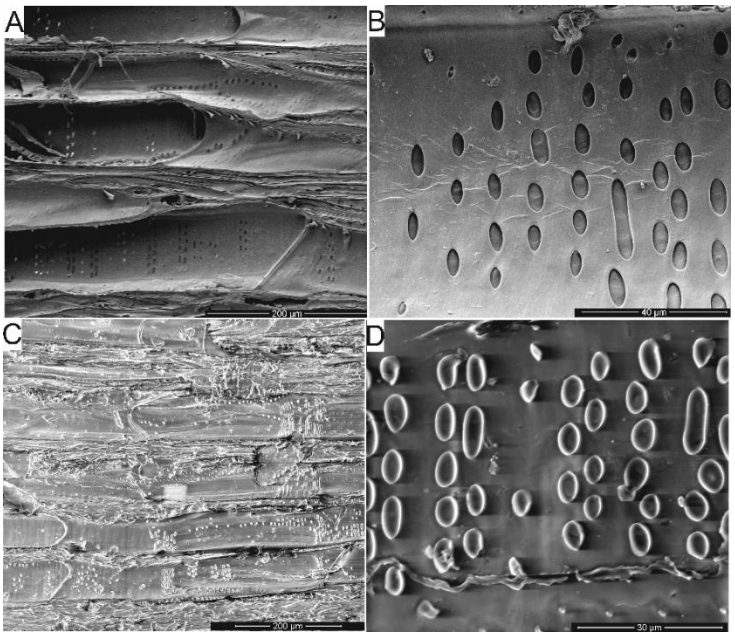

Figure S4: templating from beech wood radial section. A) and b) native wood, c and d) PDMS replicas.

AFM measurements

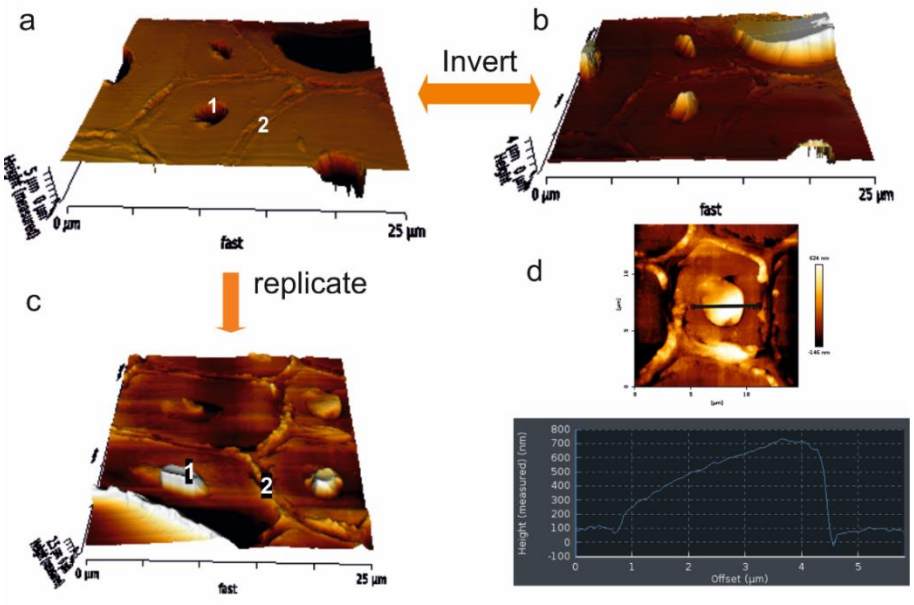

Figure S5: AFM height image of a) native wood, and b) the inverted image processed by JPK data processing software (JPK instruments, Germany). c) TS-0.6 replica with fiber microcast (label 1) and middle lamella (cell contour, label 2); d) the height profile of a fiber pillar.

Top view SEM images of the PDMS replicas

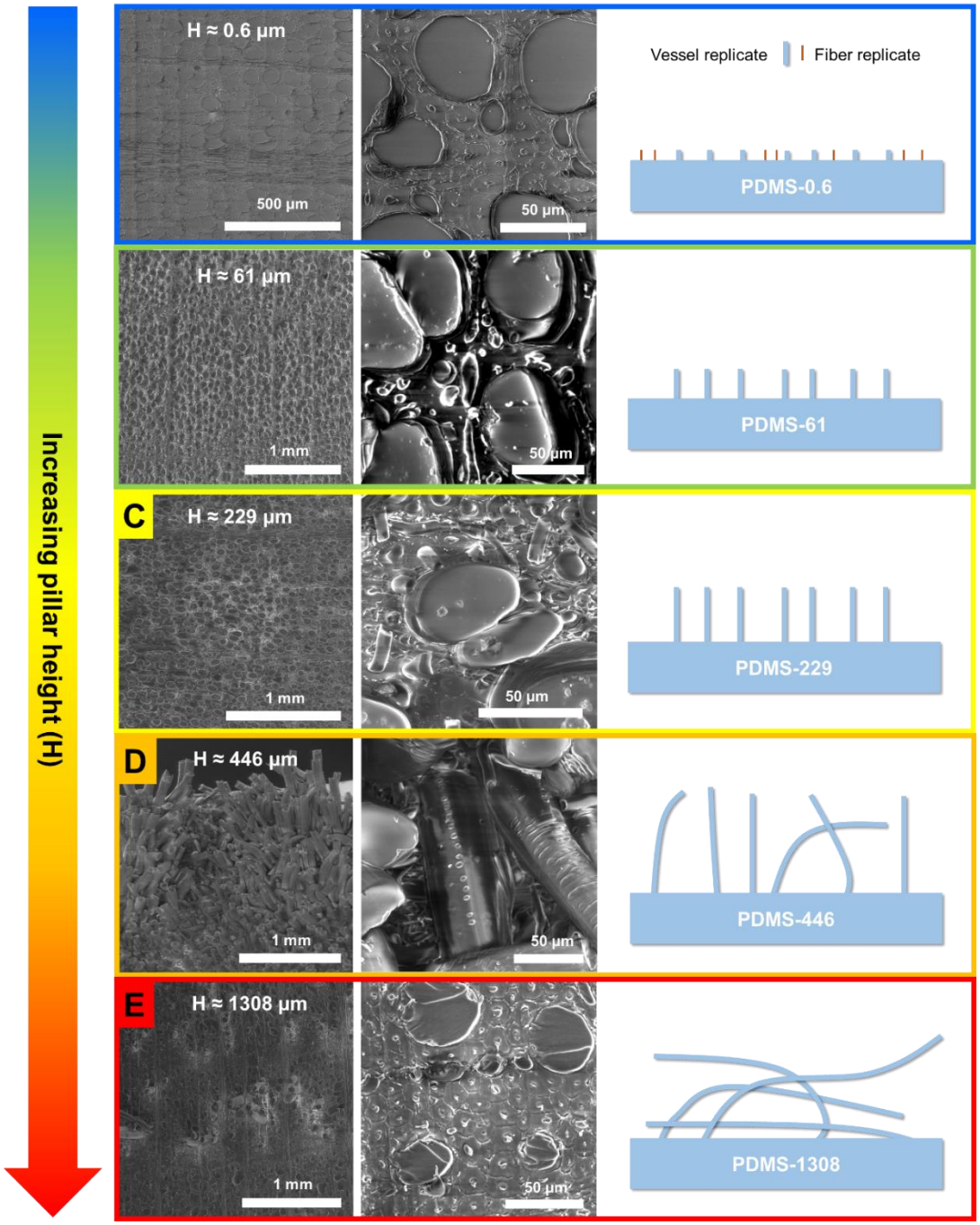

Figure S6: SEM images of beech wood replicated PDMS surfaces with different pillar heights (top view).

3. General discussion and outlook

The main focus of this thesis has been to develop functional wood-based and wood-templated materials with special wettabilities, based on the understanding of natural biological wetting models, as well as of wood structure and chemistry. The aim of this chapter is to further discuss the results of the publications presented in Chapter 2. In the outlook, scientific and potential industrial relevance are highlighted.

3.1 General discussion

In this thesis, the wettability of wood-based and wood-templated materials was studied based on four biological role models of special wettabilities. In this subchapter, the important roles of bioinspiration in creating special wettability are discussed firstly. In the second part of this chapter, some specific aspects related to the wettability of wood surfaces are presented. Afterwards, several key aspects such as a comprehensive comparison of the pitcher plant and lotus leaf wetting models and the materials manufacturing process (the wood cutting, wood species selection, and selection of chemicals) are reviewed one by one. Finally, the limitations of our protocols developed in Chapter 2 are discussed.

3.1.1 Bioinspired materials with special wettability

Surfaces with special surface wettability such as slippery surface, wettability patterns, directional flow of liquids and superhydrophobicity have raised much research interest due to their advantageous control of the interaction between the liquid and the solid.[1] Coincidentally, in nature, there exist many excellent examples of creatures with special surface wettabilities to serve for their living need or to adapt to the habitat. Surface characterization showed that these special wetting phenomena (such as the superhydrophobicity of lotus leaf, the slippery surface of pitcher plant, the wettability patterns of desert beetle's back and the directional flow of water on rice leaf) are not only based on the chemical composition of the surface but also originate most importantly from the unique micro- and nano- surface structures.[1] Biomimetic work of transferring the special wettability from natural organisms to manmade materials allows equipping engineered surfaces with similar functions as known for the biological role models. For example, inspired by pitcher plant, many materials surfaces such as glass,[2] porous teflon membranes,[3] aluminum, and polyamide[4] have been developed into slippery liquid-infused porous surfaces. During the fabrication process, various lubricants such as perfluorinated fluids[3]

or silicone oil[2] can be infused into substrates of porous networks,[4] achieving dewetting, antifouling, anti-bacterial, or anti-icing surfaces. Using the protocol in Subchapter 2.1, we obtained a stable slippery surface by covalently attached linear PDMS on a more complex surface – wood. Compared to silicon wafers or glass slides which are commonly used for surface grafting of lubricant molecules,[5] wood surfaces comprise many "imperfections" - chemical inhomogeneity and micro-/nanoscale roughness. Nevertheless, after modification, the slippery wood surface is endowed with water repellency, anti-smudge, and antifouling properties, and also with improved resistance to bacterial attachment. This modification protects wood through the liquid-like layer which is distinguished from the traditional treatment with solid modifiers. However, the (long-term) stability compared to the solid modifiers still need to be improved (The limitations of liquid-like coating are elaborated in subchapter 3.1.6.). For superhydrophobic surfaces, a facile replication of biological materials such as lotus leaf[6] and cicada wing[7] to produce manmade materials can lead to well-designed hierarchical surface roughness and therefore, prominent water repellency. Superhydrophobic surfaces can have a wide range of applications in self-cleaning surfaces, antifogging surfaces, anti-corrosion, and drag reduction. In Subchapter 2.3, wood is exploited as a natural biological mask for superhydrophobic surfaces fabrication. Comparing to other biological templates such as lotus leaf, cicada wings or butterfly wings, the wood template is a 3D mask consisting of micro-capillaries which allows the viscous polymer precursor to flow into them. By controlling the penetration depth of the polymer precursor, one wood template can offer the replica of various pillar heights.

Not only superhydrophobicity, but also wettability patterns (integration of both (super)hydrophobic and (super)hydrophilic regions on the same surface) inspired by desert beetle can provide the possibility of efficient fog water harvesting and microfluidic manipulation. A common fabrication procedure of wettability patterns includes creating a homogenous rough structure on the surface, coating the surface with low surface energy chemicals which can be degraded by UV, applying a photomask on top of this coating and irradiating UV. After removing the photomask, the UV exposed region on the surface will be decomposed and become hydrophilic. The mask shielded regions stay hydrophobic.[8] In our study, the surface topography of wood itself plays a critical role in building up wettability patterns. In Subchapter 2.2, the natural surface topographical patterns from wood growth rings were used to dictate the final wettability patterns. This approach works on wood cross-sections but is not suitable for other biomass-based material surfaces such as some aerogels/films.

3.1.2 Aspects of wettability of wood and its measurement

As summarized in Subchapter 1.6.1, the wettability of wood is complex and depends on a wide range of factors such as wood species, wood machining, chemical treatments, and measurement conditions. Consequently, compared to artificial materials, wood surface wetting tests require more considerations about the following specificities: fast absorption of liquid by wood, wood anisotropic structure inducing anisotropic wetting, and measurement accuracy.

Since wood has a high water permeability, the water CAs on native wood surfaces rapidly change over time.[9] Water penetration into the wood pores results in decreased drop size, while the spreading of water on the wood surface leads to a fast decrease of contact angles.[9] Due to the remarkable evolution of CAs on native wood over time, the exact time when the CA is measured should always be mentioned.

The wood structure is anisotropic. The same wood can have different CAs when measuring on different planes (sections). Wood cells are aligned in parallel along the stem: the surfaces of wood on radial and tangential planes present grooved structures, which lead to the anisotropic wetting by water. The wood surface plane and the measurement direction need to be mentioned in this case.

Lastly, the wood surface roughness resulting from anatomical features after cutting, make the baseline for the liquid drop profile fitting difficult to judge. An inaccurate location of the baseline at the droplet/wood interface can induce a large error in the measurements.

3.1.3 Comparison between two biological wetting models

Lotus leaf and pitcher plant are two notable anti-wetting models existing in nature. Superhydrophobic surfaces and SLIPS inspired by the two biological models differ from material fabrication techniques, anti-wetting mechanisms, featured contact angles, and liquid repellent ranges. A comparison and deep understanding of the performances of these two surface models provide important information on their advantages and shortcomings and guided us to select an appropriate strategy for application purposes. Here we focus the discussion on the durability of these two models in terms of long-lasting water repellency: the underwater durability refers to the thermodynamic stability, and the anti-abrasive stability reflects the mechanical robustness of water repellent surfaces.

The thermodynamic durability can be judged from the “critical pressure” at which the surface starts to lose the original wettability or from how long the surfaces maintain the performance in a water environment, so-called “longevity”.[10] Superhydrophobic surfaces are usually not

thermodynamically stable or durable,[11] i.e. the property does not persist in long-term when the surface is immersed in water environments or impacted by water droplets. When superhydrophobic surfaces are subjected to a large hydrostatic pressure or stay in a water environment for an extended time period, the air trapped in the microstructures might be replaced by water. This results in the transition from the Cassie-Baxter state to the Wenzel state (theory discussed in Subchapter 1.3.2), consequently leading to a water repellency failure. For example, Herminghaus[12] observed that the air plastron disappeared from lotus leaf surfaces when the leaves were submerged in water at a depth of 20 cm for a few seconds, and the leaves were wet after retracting from water. This was also observed with the quick failure of the superhydrophobic wood surfaces during underwater tests reported in Subchapter 2.1. However, one can enhance the stability of the air-water-solid interface by creating hierarchical structures with specific geometries.

The mechanical robustness of superhydrophobic surfaces is related to the anti-abrasion properties of the modifying coatings. The usual failure of superhydrophobic surfaces originates from the destruction of the delicate hierarchical structure (e.g. the surface features lack hardness, or weak interfaces between coating and substrates cause the loss of these features upon abrasion). The mechanical durability is also a major challenge for superhydrophobic wood. The mechanical robustness of superhydrophobic surfaces can be enhanced by either improving the mechanical properties of the coatings to limit their removal, or performing a bulk modification to maintain the structure after surface is worn away.[13]

By contrast, SLIPS is both thermodynamically stable (pressure resistant) and mechanically stable, it exhibits self-healing ability, and is tolerant to substrate defects.

In slippery surfaces, a smooth and stable interface is created, which minimizes the danger of water impalement into micro-/nanostructures. Wong *et al.*[3] reported that SLIPS on a porous matrix can stand an extremely high pressure of ~676 atm while the highest pressure reported for superhydrophobic surfaces is only ~ 7 atm.[14] The thermodynamic stability of SLIPS is independent of the actual size of structures.[15] However, a certain roughness and porosity on the matrix are still required to immobilize the lubricant on the surface. [3, 15] The thickness of the lubricant layer and the affinity of lubricant to the matrix are critical to retain the liquid-repellent stability. If the lubricant film is too thin, or has insufficient affinity to the substrate, the supporting solid might be exposed to the liquids to be repelled, which might result in inferior repelling performance.

Besides, the slippery surface has a certain mechanical stability. On one hand, it is defect tolerant, which ensures the stability of the repellency performance on damaged samples. For example,

by designing an interconnected honeycomb wall structure matrix, damaged (containing defects) samples can support a metastable SLIPS coating to maintain the liquid repellency.[15] On the other hand, the lubricating layer can heal itself by wicking into defect sites in the substrates, maintaining the liquid-repellent function.[3]

Some common concerns about a liquid or liquid-like layer are based on a low thermal stability and the possible leaching of the lubricant. In terms of thermal stability, SLIPS can still retain the slippery properties even after undergoing extreme thermal conditions such as rapid cooling down by liquid nitrogen temperatures (-196 °C) and heating up to 200 °C.[16] Additionally, the lubricant layer on SLIPS is stably held which would not have the drainage problem just by tiling the surface because the gravity is much smaller than the high pressure tested in the previous report[3] which cannot splash the lubricant away and eliminate the lubricating effect. However, application in a real environment with strong UV irradiation, exposure to rain water, ice and dust contamination and frequent change of temperatures in long term would probably undermine the excellent performance of the slippery surface, but still, this need to be investigated systematically.

Superhydrophobic surfaces can also offer some superior properties over slippery surfaces. For example, a report[2] showed that superhydrophobic surfaces tend to accumulate hydrophobic dust at the air/water interface, which can be easily picked up and taken away by water drops rolling on the surface. On the opposite, hydrophobic dust particles might adhere to SLIPS surfaces and water cannot take them away completely.[2]

Based on these considerations, we selected different approaches to modify the wood wettability. In Subchapter 2.1, we were interested in the development of a stable hydrophobic coating of wood. We therefore modified wood surfaces with a method similar to the SLIPS technology, by fixing the lubricant molecules on wood through covalent bonds. We showed in Subchapter 2.1 that the slippery wood surface has a better underwater durability than that of superhydrophobic wood. The slippery wood surfaces were penetrated by water after several days, while the superhydrophobic surfaces (inspired by the lotus leaves) encountered a quick failure due to the transition from Cassie-Baxter to Wenzel wetting state (further discussion shown in 3.2.2). In Subchapter 2.2, our idea was to create wettability patterns through a selective wood modification. We chose to create the different wetting zones through structuration (mimicking the lotus leaf). Hydrophobization of EW was achieved through surface structuration via sol-gel-derived ZnO particle growth. Though the technique of creating SLIPS patterns is reported,[15] this would not be possible through the implementation of SLIPS: the wetting patterns can hardly be obtained on wood cross-section because the lubricants,

usually extremely low surface tension liquids, would spread homogeneously on both EW and LW. Therefore, for creating wettability patterns on wood, (super)hydrophobization provides a more facile route than SLIPS.

3.1.4 The critical role of wood cutting methods

The cutting process strongly affects the wood surface morphology, which might not only influence chemical treatment processes, but also the final performances and applications of wood. Wood species, anatomical planes, and cutting parameters such as blade sharpness or speed[17, 18, 19] can all influence the wood surface morphology. In the following discussion, we take spruce cross-sections as an example to compare the different effects.

Microtome cuts are usually used in the laboratory for small sample surface trimming or slicing. The clean cuts generate smooth surfaces that are suitable to study the wood anatomy. Grinding through multi-sandpapers of different grit sizes can polish the wood, leading to wood surface topography similar to microtome cut. A proper grinding can preserve well-defined EW and LW anatomical structures.[20] Circular saw cutting gives EW and LW surface different morphologies resulting from the density and mechanical property differences between EW and LW. The spruce EW structure is destroyed: the cell walls are torn and shredded, covering part of the lumina, while on the LW, the cell walls are smeared and compressed, covering all the LW lumina, forming a micro-level smooth solid layer. Different band saw cuts yield extremely rough surfaces, with highly damaged fibers pulled out, laying above lumina across the EW and LW regions. The EW and LW are barely recognizable because the anatomical features of cells are all covered by fiber fragments (SEM pictures shown in Subchapter 2.2, supplementary information part). Furthermore, wood surfaces can be treated with sanding (different from grinding, here the sanding refers to only using a rough sandpaper). Meijer *et al*.[21] reported that sanding damage the spruce EW where tracheids are compressed and cell walls are damaged, while the LW remains rather unchanged. We observed that sanding of wood surfaces results in surface roughness homogenization at the microscale. The different surface morphology observation might be due to the different polishing conditions such as the sanding speed and the grit size of the sandpaper.

The above-discussed techniques should be chosen with care to prepare the material surfaces for the targeted final application. For example, contact angle hysteresis is related to the surface roughness and heterogeneity.[22] The low sliding angle of slippery surfaces results from the chemical homogeneity and physical smoothness of the liquid-liquid interface.[3]

For the slippery surface developed in Subchapter 2.1, a smooth surface after the lubricant attachment is needed to avoid the high contact angle hysteresis. Extremely low sliding angles are unlikely to be established on slippery wood surfaces because the intrinsic wood anatomy generates microscale surface roughness. Though the microtome cut cannot eliminate the anatomical roughness, but it causes a low cutting-induced roughness. Therefore, in theory, microtome-cut would improve the performance of the contact hysteresis compared with other cutting/machining processes. However, in practice, microtome cut is limited to small samples with a certain thickness and is difficult to conduct on veneer. This microtome-cut veneer might be prepared through trimming a bulk wood radial section through microtome and then splitting a thin slice of veneer off the bulk wood. Grinding can also give nice trimmed wood surface for slippery surface preparation purpose. However, sanding wood veneers is technically difficult. Grinding will remove a certain thickness of wood surface through abrasion, veneer is too thin and can be easily damaged in this process.

For wettability patterns on wood cross-sections (Subchapter 2.2), the fact that EW is predominantly modified is assumed to be related to the transport of the chemicals inside the wood structure. The purpose of cutting is to generate different roughness on EW and LW (rough EW and smooth LW are favored for the wettability patterning purpose). After circular saw cutting, the EW fibers remain open (favoring transport of fluids), while the LW lumina are sealed (preventing liquid transport). The microtome cut is not the most appropriate cut because it does not provide enough additional surface topography contrast beyond the intrinsic anatomy difference: both EW and LW have an open porous surface. Sanding of wood surfaces leads to surface roughness homogenization at the microscale which is also not favored. Thus, the circular saw cutting is the best option in this case.

In Subchapter 2.3, the wood cutting is critical for wood templating applications: the cut cells from the cross-section need to be fully open, allowing for fluid penetration. Parmak[20] tried to emboss polymers by applying pyrolyzed wood cross-sections with and without a surface grinding step. Without grinding, the beech wood cross-sections are covered by the cell wall fibers, forming a flat solid layer. The templated polymer from unground beech sample showed a relatively flat surface with few pillar features, while with emery paper ground samples, the embossing texture corresponding to wood anatomical structure appeared. Therefore, microtome cutting or grinding would be the best candidates compared to sawing and sanding.

3.1.5 Choosing the appropriate chemistry and wood scaffold

For the materials fabrication strategies developed in this thesis, toxicity and environmental impact have to be considered: wood, minerals, PDMS and green solvents (water and ethanol) are involved. Wood composed of biopolymers is naturally "green". ZnO can be mined as zincite, SiO_2 is found in nature as sand, quartz, and in various living organisms.[23] PDMS is inert, nontoxic[24] and has been widely used in contact lenses and medical devices.[25] Nevertheless, there are many possibilities to substitute these chemicals or to use other wood species. As discussed in the following sections, these alternatives could be used to achieve similar functional properties or to enlarge the scope of properties and applications.

Alternative wood species

We conducted our research on beech and spruce wood, which are typical hardwood and softwood species widely available in Switzerland. However, other wood species can be also appropriate to develop materials according to the strategies described in this thesis.

Different wood species share a very similar chemical composition (cellulose, hemicellulose, and lignin). However, wood species are also characterized by the presence of a vast variety of extractives and ashes, usually constituting less than 10% of the wood.[26] They might interfere with the penetration and reactivity of chemicals during the wood modification process.[27] The specific influence of extractives on our chemical processes was not investigated. Nevertheless, it is thought that inorganics and organic small molecules can have an influence of some reactions. In the case of ZnO, the morphology can be controlled by the metal ions which can have electrostatic interaction with the ZnO crystal face,[28] and also by citrates due to the coordination with Zn^{2+} ions of the (0001) surface.[29] However, to our knowledge, the influence of wood extractives on the growth of ZnO on wood is still not reported. Still, the influence from extractives can be eliminated through Soxhlet extraction before any chemical process. Based on this, the chemical modifications targeting the hydroxyl groups on wood surfaces should be generally applicable to other woods.

We consider that the slippery surface strategy for wood protection developed in Subchapter 2.1 is a universal approach for all wood species. However, the performances of the various modified species are expected to exhibit some differences in wettability and antifouling performance due to the different wood anatomical features. For example, the maximum softwoods tracheid size is around 30 µm in diameter, while hardwood vessels typically have diameters between 50-200 µm.[30] Therefore, on the wood radial section, the distance from peak to valley and the distance between groove edges will be smaller for softwoods when compared to hardwoods. As reported

by Zhang *et al.*,[31] the groove width can influence the contact behavior of the water droplets and the sliding performance.

The preparation of wood with wettability patterns in Subchapter 2.2 was conducted on spruce wood, and these patterns heavily rely on the wood anatomical structure and surface morphology resulting from machining. Softwoods usually display clear EW and LW regions, with an abrupt or gradual transition from EW to LW, which represents a good opportunity for patterning based on growth rings. For hardwoods (such as beech), Merk *et al.*[32] observed that $CaCO_3$ precipitates easily in large beech wood vessels, and suggested that the deposition pattern of $CaCO_3$ might be generated from the varying efficiency of fluid transport through the porous structure. This indicates that the patterning strategy might also be suitable to ring-porous hardwoods, which have patterns formed by large pores in EW. For diffuse-porous hardwoods, the EW and LW are sometimes difficult to distinguish because there are no clear pore size distribution changes across the growth ring. Therefore, our protocol for wettability patterning would probably not be suitable for the diffuse porous woods.

In Subchapter 2.3, the pillar diameters and the distance between each pillar is dictated by the wood cell structure and distribution. In principle, any wood species can be templated. To create a superhydrophobic PDMS surface, usually one needs to target the Cassie-Baxter wetting state (can be judged from the wetting transition shown in Subchapter 1.3.2). In the case of an array of pillars, this can be expressed by the following equation:

$$150° \leqslant \cos^{-1}\left[\frac{\pi D^2}{4P^2}\left(\cos\theta_Y + 1\right) - 1\right] < 180° \qquad \textit{eq. 1}$$

Where D is the diameter of the pillar (the diameter of the lumen), P is the distance between two nearest pillars (the distance between two adjacent lumina), and θ_Y is the Young's contact angle of the material.

Through wood species selection, researchers can partly dictate a certain polymer surface microstructure, though the pillar diameter (lumen size) and the pitch (the distance between the two nearest pillars) cannot be chosen independently. The lumen size and distance between neighboring lumina satisfying the above equation should produce a superhydrophobic surface in principle. However, one also needs to note that the capillaries of different diameters will lead to different fluid penetration depths, according to the Lucas-Washburn law. The experimental conditions should be adjusted according to the specific wood structure and the desired pillar heights.

Alternative chemicals for patterning

The porosity related wood accessibility to chemical treatments lead to the result that the less dense EW may be capable of accommodating more modifiers.[33] The ZnO on EW plays the double role of changing both the surface roughness and surface chemistry. Due to the hydrophobic nature of the synthesized ZnO and the extra roughness created on EW, the modified wood exhibited a hydrophobic EW while the LW remains hydrophilic.

To enlarge the scope of modifiers, one can try to establish other inorganic particles on the surface, such as sol-gel derived TiO_2 or SiO_2 to substitute the ZnO. $CaCO_3$ might also be a candidate because it was observed that the $CaCO_3$ precipitates more in the large lumen of spruce EW cells than the LW.[34, 35] A preferred distribution of these inorganic particles on EW can increase its roughness, but might not be sufficient to create hydrophobicity An intrinsic hydrophobic nature of the added metal oxides is also required. Indeed, hydrophilic particles will make the EW more hydrophilic, yielding EW and LW with similar hydrophilicity.

Patterning of surfaces using polymers has been reported.[36, 37, 38] In the case of wood modification, control over the distribution of polymers has only been shown for targeting the modifications in wood lumina, at the lumen-cell wall interface, and in the cell walls.[39] To our knowledge, rare work claimed that the polymer modification generates patterns between EW and LW. Therefore, it is difficult to predict if polymerization under controlled conditions can achieve wettability patterns as shown in Subchapter 2.2.

Overall, the different accessibilities of the treating reagents to the EW and LW wood sites are critical to chemical patterning. Further work on the specific chemical diffusion processes inside the wood structure is needed to clarify the distribution of the added chemicals.

In Subchapter 2.2, we also showed further chemical patterning potential based on ZnO modified wood: SiO_2 and PEI-PDA (polydopamine/polyethyleneimine) aqueous solutions were deposited on ZnO-W. The patterning takes the advantage of the different wettabilities obtained on the ZnO-W: the EW is water resistant (CA ≈ 128°) while LW can be wetted. When a ZnO-W cross-section comes into contact with aqueous solutions, the Cassie wetting state[40] forms on EW (preventing water penetration), while the LW immediately absorbs the water containing chemicals. However, this might not be observed for any solution. The addition of chemicals to water can change the surface tension of the new solution, and liquids of low surface tension will wet both EW and LW.

Alternative polymers for templating

The PDMS kit (*Sylgard*® 184) can be substituted by other curable polymer mixtures. As an example, photochemically cross-linked perfluoropolyether-based elastomers (PFPE)[41] are commonly used in templating techniques.[42, 43] These fluoropolymers can not only facilitate the demolding process but also improve the CA of the replica due to the low surface energy of fluoropolymers. Irgarcure® photo-initiated polymerization of polystyrene (PS) and poly(methyl methacrylate) (PMMA) are also potential candidates. In general, polymers with better tensile strength and higher Young's modulus when compared to elastomers (such as PDMS) might be excellent candidates to obtain standing straight pillars with high aspect ratios. However, the demolding of rigid polymers from wood would be difficult. In this case, the wood template could be destroyed through delignification,[44] to disassemble the wood scaffold after templating, or wood cell walls could be pre-coated with low energy compounds to ease the demolding process.

3.1.6 Limitations of the developed approaches

From an ideal surface to a wood surface

We followed the strategy of liquids repelling another immiscible liquid to design anti-wetting wood substrate.[2] Our method was inspired by the work by Wang and Mc.Carthy,[45] reporting on covalently attached PDMS chains as the immobilized lubricant on glass and silicon wafer to achieve a more stable SLIPS property. However, this strategy cannot be directly transferred to wood: the expected effect (water sliding away on modified wood) could not be accomplished with the same protocol.[45] Glass and silicon wafers are close to ideal surfaces, which should be flat, smooth, and clean. Native wood is never flat at micro or nanoscale (due to the intrinsic anatomical structure). A thin layer consisting of PDMS brushes is not thick enough to compensate for the roughness or even defects: it cannot generate a smooth surface on the unideal wood surface.

Hence, we adopted the repeated dip-coatings with concentrated solutions. This will certainly introduce loosely bonded PDMS chains, which are entangled with the covalently bonded PDMS chains on the wood surface. These free polymer chains can actually provide an enhanced slippery effect on this lubricating system. On one hand, the enhanced coating density of PDMS will increase the surface steric hindrance,[46] preventing other substances to penetrate and settle, ensuring the antifouling property (steric repellency among the dense polymer chains will resist the incorporation of other substances such as large proteins). On the other hand, the unbonded

PDMS chains make the PDMS layer more slippery. This minor change in the protocol also ensured the low contact angle hysteresis of 24° reported in Subchapter 2.1: it is likely that the thick PDMS layer attenuates defects which can pin the water droplets. With only a thin PDMS monolayer, the droplet of the same volume cannot slide down with even tilting the plate to 90°. An aspect worth mentioning is that the expected oil repellency was not observed with the liquid-like PDMS lubricant modified wood, probably due to micro- and nano- level roughness from the wood anatomical structures and the defects from the liquid-like layer.

Pre-imposed patterns

Wood anatomy structure is critical in building up wettability patterns and in wood templating techniques, since the patterns or polymer surface topographies result from the wood anatomical structures. In Subchapter 2.2, the wettability patterns on wood cross-sections are created based on the confinement of wood growth rings. Selecting wood substrates with growth rings of different curvatures can provide wood materials with arc-shape wetting patterns or even loop-shape wetting patterns. However, more complex shapes would be challenging to achieve through the protocol we developed in Subchapter 2.2. Other strategies such as photo masking[8] or inkjet printing[47] could be applied to wood surfaces to provide more possibilities of wettability pattern shapes.

Furthermore, in Subchapter 2.3, the pillar sizes and pitches are pre-imposed by wood species, which provides little freedom for surface microstructure design and geometry optimization. Nevertheless, the wide range of wood species can offer the researchers a certain selection range.

Bending and peeling off issues for long pillars

High aspect-ratio micropillar arrays possess many interesting properties, such as large mechanical compliance, large surface area, and a topography that is separated from the underlying substrates.[48] These properties have been used to explore and fabricate biomimetic adhesives, superhydrophobic surfaces, superoleophobic surfaces, and mechanical sensors.[48]

In Subchapter 2.3, we fabricated a series of pillars of different aspect ratios. As pointed out, there is a critical pillar aspect ratio above which the pillars start to bend, which makes the CA difficult to predict. Ultralong pillars face two major issues: pillars bend due to the low Young's modulus of PDMS (1.32 - 2.97 MPa, varying according to the curing temperature for Sylgard® 184 kit),[49] and the pillars might break during demolding due to the poor mechanical strength of PDMS (ultimate tensile strength of cured Sylgard® 184 is 7.65 MPa[49]) and the large friction between the cell walls and the polymer. Intact long polymer pillars might be obtained by choosing polymers with higher tensile strength such as PMMA (ultimate tensile strength 70

MPa[50]) or PS (ultimate tensile strength 40 MPa[50]). However, this would require breaking down the wood templates (delignification or dissolution of wood in ionic liquid) to release the replica.

3.2 Outlook

3.2.1 Industrial relevance

The utilization of wood materials provides ecological benefits to the sustainable development of societies.[51] Wood-based products are extensively applied in construction, but unfortunately face multiple issues of dimensional instability, deterioration by microorganisms, surface weathering, and flammability. Modifications are applied in order to prevent these issues and to better utilize this economical construction material. To reach the market requirement, modified wood materials should be durable, safe (no leaching of toxic chemicals), fabricated through cost-effective and facile procedures and keep the native wood aesthetic appearance.

The modification of wood by SiO_2 and PDMS in Subchapter 2.1 shows a strong potential for up-scaling. In the modification protocols, wood veneers are alternatively dipped into tetraethyl orthosilicate (TEOS) and ammonium solutions, which is a quite straightforward procedure that could be implemented for industrial production. Moreover, the SiO_2 obtained from the reduction of the TEOS precursor is pre-absorbed by wood, hence the homogeneity of this surface modification is possibly not much influenced when scaling up, which should also ensure the quality of large size products. The second step (growing PDMS) is completed through dip-coating and heating up. Additionally, during the whole reaction, only water and ethanol were applied as solvents. This process goes along the European commission's requirements for the limitation of organic hazardous air pollutants from wood coatings.[52] Finally, the coating is transparent, which retains the aesthetics of wood. However, the long-term stability of the liquid-like coating on wood (including chemical stability of the covalent bonding and the mechanical stability) still need to be improved. Especially for outdoor conditions, environmental factors such as UV, rain water, and abrasion can possibly undermine the performance. A long- term test in a natural outdoor environment need to be launched to further investigate the performance of the coating.

For Subchapter 2.2, the modification of creating wettability patterns is difficult to be implemented for large wood cross-sections. The protocol follows a two-step surface modification: the preparation of ZnO seeds layer on wood surface through sol-gel approach, the growth of ZnO seeds into ZnO micro-rods through hydrothermal reactions. Multiple factors might hinder a transfer from this laboratory stage into a large scale production. Firstly, the typical non-linear scale-up problem (when a reaction system increases proportionally, the

changes of reaction kinetics and thermodynamics, and fluid mechanics are significantly different from the laboratory scale or do not increase linearly, respectively)[53] may induce a different ZnO microrods distribution on the wood cross-sections. Consequently, wettability patterns generated from the chemical patterns might be insufficient or disappear. Secondly, the process involves applying vacuum and hydrothermal reaction which are expensive, sophisticated to manipulate and need specially designed industrial autoclaves. Therefore, presently, this protocol is still at the lab scale.

Superhydrophobic surfaces have a wide range of applications in industry, including anti-fog glass, anti-freeze surfaces, oil/water separation, anti-bacterial surfaces, and medical applications.[54] The superhydrophobic PDMS surfaces obtained by wood templating method in Subchapter 2.3 have great potential for scale up. This method circumvents the sophisticated templates fabrication procedures and does not involve toxic fluorine-based chemicals. Moreover, large surfaces are accessible (wood trunk sections of several tens of centimeters can be used) which make large-scale templating possible. However, the up-scaling might lead to problems in the manufacturing process such as the challenge of a homogeneous trimming of wood template surfaces, inhomogeneous curing of polymers, and difficulties in demolding.

3.2.2 Scientific relevance

Bio-inspired wood materials

The complexity of chemical compositions, hierarchical structures, and multifunctionality in biological materials are extremely challenging to transfer to artificial materials. The fabrication methods usually involve intensive consumption of energy, sophisticated control, and expensive raw materials, consequently facing the challenge of upscaling.[39] One approach to circumvent these issues is to directly adopt the natural abundant material wood, which is of low cost, gives direct access to large-scale, possesses hierarchical structure, is multifunctional and offers accessibility for further functionalization. Some pioneering reports[32, 39, 55, 56] based on directly using wood as a scaffold are encouraging further utilization of wood and the transfer of design/functions of biological models to wood materials. This dissertation contributes to this emerging field of research, with a focus on questions related to wettability.

The study of the wettability of wood

The study of wood surface wetting by various liquids is important for wood gluing and wood surface treatments.[57] The surface wettability of wood can determine the flow-ability of the coating, the spreading and penetrating of the coating materials onto/into the wood surfaces.[58] Multiple factors such as chemical composition, the anatomical structure, and the machining process are interrelated and make the wetting process complex. Though there are different techniques for wettability measurements as illustrated in Chapter 1.4.3, the accurate data acquisition for wood surfaces is still challenging due to the inhomogeneity of the surface chemistry, hierarchical surface roughness, fast liquid sorption and swelling effects during the measurement.[58]

In the experimental parts in Chapter 2, the wettability testing protocols were set up for measuring different wettabilities. The influence of droplet sizes, the CA evolution over time, or the sample history (the sample has been dried, or has been kept at room temperature or in water environment) are all considered in Chapter 2. For example, regarding the droplet size choice during the CA measurement in Subchapter 2.2, the droplet should be large enough to spread sufficiently on LW and to reach the EW/LW boundaries. As a consequence, the water droplet spreading can be stopped by the EW from both sides, which results in a distorted droplet form with anisotropic CAs.

These testing protocols can be set as references for other work where measurements of special wood surface wetting are required.

Water repellency in wood protection research

Wood absorbs and loses moisture from the air according to the changes of the relative humidity. This brings wood the serious issue of dimensional instability as engineer material. Furthermore, a non-uniform drying of wood can result in splitting and cracking of wood.

Targeting this issue, a lot of hydrophobization techniques have been proposed. [59, 60, 61, 62] Firstly, one needs to keep in mind that dimensional stability and water repellency are not necessarily correlated. An example of wood treatment for dimensional stability is to bulk wood with polyethylene glycol (PEG). Though PEG is a hydrophilic polymer, the PEG treated wood would not dramatically swell while absorbing moisture.[63]

Secondly, water repellency for wood is a rate phenomenon while dimensional stability involves an equilibrium.[63] Wood is very sensitive to water vapor, not only liquid water. A traditional repellency to the water in liquid form can alleviate but cannot thoroughly solve the problem. A water-repellent wood still absorbs moisture and finally reaches an equilibrium moisture content

depending on the relative humidity in the environment. After absorbing moisture, a water-repellent wood will exhibit a decreased CA and a dimensional change. Therefore, a long term dimensional stability protection working in humid environment requires bulk wood modifications.

As shown in Figure 1a, a typical superhydrophobization of wood cannot work in long-term in this case. Inhomogeneous covering of the wood surface with modifiers can generate prominent defects for water to penetrate and accumulate inside wood (Figure 1a).

Creating a liquid surface in principle might be a good solution to solve the above-mentioned issues, because liquid surfaces can be smooth down to molecular level, and intrinsically defect-free, providing self-repair by flowing, repel immiscible liquids with great stabilities. The penetration of water vapor/moisture through the lubricant layer would be extremely difficult (Figure 1b).

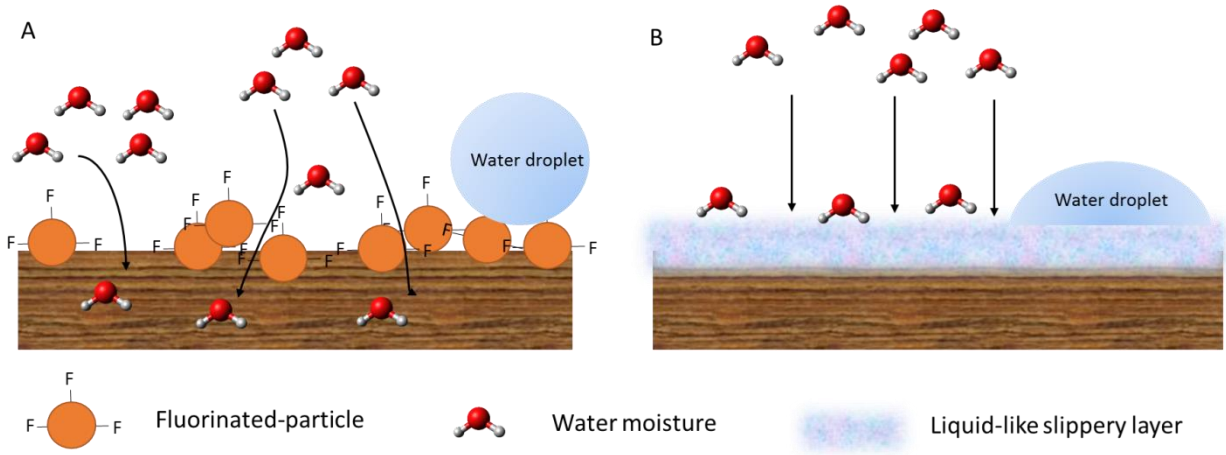

Figure 1. The permeability of water through the protection layers by superhydrophobization and slippery surface. Arrows indicate the pathway.

Guo *et al.*[64] have applied the SLIPS technique on wood, however, one drawback of SLIPS is that liquid on the solid surface might be depleted leading to the loss of surface properties. Our work in Subchapter 2.1 shows a different strategy, with the aim to create a more stable liquid-like "slippery" surface which is covalently attached on the solid surface and present thermal stability at a temperature as high as 100 °C (this liquid layer would not evaporate).[5] Compared to Wang and McCarthy's work,[45] we applied this strategy on a wood surface with more complex surface, with a rough topography and inhomogeneous chemical composition. On one hand, we demonstrated the antifouling, anti-smudge and self-healing properties which were not shown in their work. On the other hand, this report showed that the covalently attached liquid-like polymers cannot achieve the exact same performances (failure in repelling oil, large CA hysteresis[65, 64]) on an unideal surface.

However, as analyzed in subchapter 3.1.5 in practice, a fully functioning slippery surface is challenging on wood. More work is needed for a systematical evaluation of the imperfections and defects of slippery strategies implied on the wood surface.

Overall, the contribution of this work to the science community is to demonstrate the potential of slippery surface in wood protection, to provide a reference for researchers working on transferring SLIPS strategy onto other unideal surfaces such as fabrics, mats or rough films, and to trigger future work on a further improved "slippery surface" for wood protection.

Utilization of wood structure

The anatomical structure of wood has been extensively studied to understand its influence on the appearance of cut wood, its density, its sorption behavior, mechanical properties, and some other physical properties.[66]

In the wood materials science community, many researchers are now focusing on new utilization concepts of the wood scaffold. This is illustrated by the studies reporting on the deposition or grafting of inorganic and organic chemicals in the scaffold.[67, 68, 69, 70] Yet, the full utilization of the anisotropic structure of wood and its anatomical features still need to be explored. Previous reports about utilizing wood pits to filter out the bacteria *E. coli* from water,[71] taking advantage of wood cell channels for wastewater treatment, [72] exploiting wood structure in solar-driven water extraction and desalination[73] and utilizing the anisotropic structure of wood to generate anisotropic magnetic behavior[74] have all shown a close correlation of materials function and wood structure utilization. Our works on wood templating and utilizing wood growth rings to generate chemical patterns also point toward this direction.

References for Chapter 3

1. Sun, T.; Feng, L.; Gao, X.; Jiang, L., Bioinspired surfaces with special wettability. *Acc. Chem. Res.* **2005,** *38* (8), 644-652.
2. Cao, M.; Guo, D.; Yu, C.; Li, K.; Liu, M.; Jiang, L., Water-repellent properties of superhydrophobic and lubricant-infused "slippery" surfaces: A brief study on the functions and applications. *ACS Appl. Mater. Interfaces* **2015,** *8* (6), 3615-3623.
3. Wong, T.-S.; Kang, S. H.; Tang, S. K.; Smythe, E. J.; Hatton, B. D.; Grinthal, A.; Aizenberg, J., Bioinspired self-repairing slippery surfaces with pressure-stable omniphobicity. *Nature* **2011,** *477* (7365), 443-447.
4. Yong, J.; Chen, F.; Yang, Q.; Fang, Y.; Huo, J.; Zhang, J.; Hou, X., Nepenthes inspired design of self‐repairing omniphobic slippery liquid infused porous surface (SLIPS) by femtosecond laser direct writing. *Advanced Materials Interfaces* **2017,** *4* (20), 1700552.
5. Wang, L.; McCarthy, T. J., Covalently attached liquids: instant omniphobic surfaces with unprecedented repellency. *Angew. Chem.* **2016,** *128* (1), 252-256.
6. Yuan, Z.; Chen, H.; Zhang, J., Facile method to prepare lotus-leaf-like super-hydrophobic poly(vinyl chloride) film. *Appl. Surf. Sci.* **2008,** *254* (6), 1593-1598.
7. Liu, Y.; Song, Y.; Niu, S.; Zhang, Y.; Han, Z.; Ren, L., Integrated super-hydrophobic and antireflective PDMS bio-templated from nano-conical structures of cicada wings. *RSC Advances* **2016,** *6* (110), 108974-108980.
8. Hao, B.; Lin, W.; Jie, J.; Ruize, S.; Yongmei, Z.; Lei, J., Efficient Water Collection on Integrative Bioinspired Surfaces with Star-Shaped Wettability Patterns. *Adv. Mater.* **2014,** *26* (29), 5025-5030.
9. Boehme, C.; Hora, G., Water absorption and contact angle measurement of native European, North American and tropical wood species to predict gluing properties. *Holzforschung-International Journal of the Biology, Chemistry, Physics and Technology of Wood* **1996,** *50* (3), 269-276.
10. Samaha, M. A.; Vahedi Tafreshi, H.; Gad-el-Hak, M., Sustainability of superhydrophobicity under pressure. *Physics of Fluids* **2012,** *24* (11), 112103.
11. Roach, P.; Shirtcliffe, N. J.; Newton, M. I., Progess in superhydrophobic surface development. *Soft matter* **2008,** *4* (2), 224-240.
12. Herminghaus, S., Roughness-induced non-wetting. *EPL (Europhysics Letters)* **2000,** *52* (2), 165.
13. Bayer, I. S., On the durability and wear resistance of transparent superhydrophobic coatings. *Coatings* **2017,** *7* (1), 12.
14. Lee, C.; Kim, C.-J., Underwater restoration and retention of gases on superhydrophobic surfaces for drag reduction. *Phys. Rev. Lett.* **2011,** *106* (1), 014502.
15. Vogel, N.; Belisle, R. A.; Hatton, B.; Wong, T.-S.; Aizenberg, J., Transparency and damage tolerance of patternable omniphobic lubricated surfaces based on inverse colloidal monolayers. *Nature communications* **2013,** *4*, 2176.
16. Lu, Y.; He, G.; Carmalt, C. J.; Parkin, I. P., Synthesis and characterization of omniphobic surfaces with thermal, mechanical and chemical stability. *RSC Advances* **2016,** *6* (108), 106491-106499.
17. Arnold, M. In *Planing and sanding of wood surfaces-Effects on surface properties and coating performance*, PRA's 7th International Woodcoatings Congress" Reducing the Environmental Footprint, 2010.
18. Costes, J.-P.; Larricq, P., Towards high cutting speed in wood milling. *Annals of Forest science* **2002,** *59* (8), 857-865.
19. Kminiak, R.; Gaff, M., Roughness of surface created by transversal sawing of spruce, beech, and oak wood. *BioResources* **2015,** *10* (2), 2873-2887.
20. Parmak, E. D. S., Fabrication of microstructured polymers by a simple biotemplate embossing method and their characterization. *Materials Testing* **2016,** *58* (3), 246-251.
21. De Meijer, M.; Thurich, K.; Militz, H., Comparative study on penetration characteristics of modern wood coatings. *Wood Science and Technology* **1998,** *32* (5), 347-365.
22. Wang, B.; Zhang, Y.; Shi, L.; Li, J.; Guo, Z., Advances in the theory of superhydrophobic surfaces. *J. Mater. Chem.* **2012,** *22* (38), 20112-20127.

23. Schröder, H. C.; Wang, X.; Tremel, W.; Ushijima, H.; Müller, W. E., Biofabrication of biosilica-glass by living organisms. *Natural product reports* **2008,** *25* (3), 455-474.
24. Hu, Y.; Ge, J.; Yin, Y., PDMS rubber as a single-source precursor for templated growth of silica nanotubes. *Chem. Commun.* **2009,** (8), 914-916.
25. Abbasi, F.; Mirzadeh, H.; Katbab, A. A., Modification of polysiloxane polymers for biomedical applications: a review. *Polym. Int.* **2001,** *50* (12), 1279-1287.
26. Imamura, H., Contribution of extractives to wood characteristics. In *Natural Products of Woody Plants*, Springer: 1989; pp 843-860.
27. Rowell, R. M., Commonwealth Forestry Bureau. *Oxford, England* **1983,** *6* (12), 363-382.
28. Joo, J.; Chow, B. Y.; Prakash, M.; Boyden, E. S.; Jacobson, J. M., Face-selective electrostatic control of hydrothermal zinc oxide nanowire synthesis. *Nature materials* **2011,** *10* (8), 596.
29. Cho, S.; Jang, J.-W.; Jung, S.-H.; Lee, B. R.; Oh, E.; Lee, K.-H., Precursor effects of citric acid and citrates on ZnO crystal formation. *Langmuir* **2009,** *25* (6), 3825-3831.
30. Rowell, R. M., *Handbook of wood chemistry and wood composites*. CRC press: Florida, USA, 2012.
31. Zhang, P.; Liu, H.; Meng, J.; Yang, G.; Liu, X.; Wang, S.; Jiang, L., Grooved organogel surfaces towards anisotropic sliding of water droplets. *Adv. Mater.* **2014,** *26* (19), 3131-3135.
32. Merk, V. Mineralization of wood cell walls for improved properties. ETH Zurich, 2016.
33. Rowell, R. M., Penetration and reactivity of cell wall components. *The Chemistry of Solid Wood* **1984,** *207*, 175-210.
34. Merk, V.; Chanana, M.; Gaan, S.; Burgert, I., Mineralization of wood by calcium carbonate insertion for improved flame retardancy. *Holzforschung* **2016,** *70* (9), 867-876.
35. Merk, V.; Chanana, M.; Keplinger, T.; Gaan, S.; Burgert, I., Hybrid wood materials with improved fire retardance by bio-inspired mineralisation on the nano-and submicron level. *Green Chemistry* **2015,** *17* (3), 1423-1428.
36. Zahner, D.; Abagat, J.; Svec, F.; Fréchet, J. M.; Levkin, P. A., A facile approach to superhydrophilic–superhydrophobic patterns in porous polymer films. *Adv. Mater.* **2011,** *23* (27), 3030-3034.
37. Schneider, M. H.; Willaime, H.; Tran, Y.; Rezgui, F.; Tabeling, P., Wettability Patterning by UV-Initiated Graft Polymerization of Poly(acrylic acid) in Closed Microfluidic Systems of Complex Geometry. *Anal. Chem.* **2010,** *82* (21), 8848-8855.
38. Telford, A. M.; Thickett, S. C.; Neto, C., Functional patterned coatings by thin polymer film dewetting. *J. Colloid Interface Sci.* **2017,** *507*, 453-469.
39. Burgert, I.; Cabane, E.; Zollfrank, C.; Berglund, L., Bio-inspired functional wood-based materials–hybrids and replicates. *Int. Mater. Rev.* **2015,** *60* (8), 431-450.
40. Cassie, A.; Baxter, S., Wettability of porous surfaces. *Transactions of the Faraday society* **1944,** *40*, 546-551.
41. Hu, Z.; Finlay, J. A.; Chen, L.; Betts, D. E.; Hillmyer, M. A.; Callow, M. E.; Callow, J. A.; DeSimone, J. M., Photochemically Cross-Linked Perfluoropolyether-Based Elastomers: Synthesis, Physical Characterization, and Biofouling Evaluation. *Macromolecules* **2009,** *42* (18), 6999-7007.
42. Zhang, X.; Ji, D.; Lei, T.; Zhao, B.; Song, K.; Hu, W.; Wang, J.-Y.; Pei, J.; Wang, Y., Integration of antireflection and light diffraction in nature: a strategy for light trapping. *Journal of Materials Chemistry A* **2013,** *1* (36), 10607-10611.
43. Rolland, J. P.; Hagberg, E. C.; Denison, G. M.; Carter, K. R.; De Simone, J. M., High‐resolution soft lithography: enabling materials for nanotechnologies. *Angew. Chem. Int. Ed.* **2004,** *43* (43), 5796-5799.
44. Segmehl, J. S. Wood and wood-derived cellulose scaffolds for the preparation of multi-functional materials. ETH Zurich, 2017.
45. Wang, L.; McCarthy, T. J., Covalently attached liquids: instant omniphobic surfaces with unprecedented repellency. *Angewandte Chemie International Edition* **2016,** *55* (1), 244-248.
46. Yang, W.; Zhou, F., Polymer brushes for antibiofouling and lubrication. *Biosurface and Biotribology* **2017**.
47. Zhang, L.; Wu, J.; Hedhili, M. N.; Yang, X.; Wang, P., Inkjet printing for direct micropatterning of a superhydrophobic surface: toward biomimetic fog harvesting surfaces. *Journal of Materials Chemistry A* **2015,** *3* (6), 2844-2852.

48. Chandra, D.; Yang, S., Stability of High-Aspect-Ratio Micropillar Arrays against Adhesive and Capillary Forces. *Acc. Chem. Res.* **2010,** *43* (8), 1080-1091.
49. Johnston, I.; McCluskey, D.; Tan, C.; Tracey, M., Mechanical characterization of bulk Sylgard 184 for microfluidics and microengineering. *Journal of Micromechanics and Microengineering* **2014,** *24* (3), 035017.
50. Tensile Property Testing of Plastics. http://www.matweb.com/reference/tensilestrength.aspx (accessed 09. 11. 2018).
51. Schultz, T. P.; Nicholas, D. D.; Preston, A. F., A brief review of the past, present and future of wood preservation. *Pest management science* **2007,** *63* (8), 784-788.
52. Commission, E., Surface Treatment Using Organic Solvents (including Wood and Wood Products Preservation with Chemicals). 2007.
53. 8 Key Challenges To Pilot Plant Scale-Up. https://www.epicmodularprocess.com/blog/8-key-challenges-to-pilot-plant-scale-up#nonlinear (accessed 22. 04. 2019).
54. Darband, G. B.; Aliofkhazraei, M.; Khorsand, S.; Sokhanvar, S.; Kaboli, A., Science and Engineering of Superhydrophobic Surfaces: Review of Corrosion Resistance, Chemical and Mechanical Stability. *Arabian Journal of Chemistry* **2018**.
55. Rüggeberg, M.; Burgert, I., Bio-inspired wooden actuators for large scale applications. *PloS one* **2015,** *10* (4), e0120718.
56. Burgert, I.; Keplinger, T.; Cabane, E.; Merk, V.; Rüggeberg, M., Biomaterial Wood: Wood-Based and Bioinspired Materials. In *Secondary Xylem Biology*, Elsevier: Amsterdam, 2016; pp 259-281.
57. Kudela, J.; Wesserle, F., Wood wetting with various liquids. *Annals of Warsaw University of Life Sciences-SGGW. Forestry and Wood Technology* **2013,** *83*.
58. Sedighi Moghaddam, M. Wettability of modified wood. KTH Royal Institute of Technology, 2015.
59. Wang, S.; Liu, C.; Liu, G.; Zhang, M.; Li, J.; Wang, C., Fabrication of superhydrophobic wood surface by a sol–gel process. *Appl. Surf. Sci.* **2011,** *258* (2), 806-810.
60. Liu, C.; Wang, S.; Shi, J.; Wang, C., Fabrication of superhydrophobic wood surfaces via a solution-immersion process. *Appl. Surf. Sci.* **2011,** *258* (2), 761-765.
61. Wang, S.; Shi, J.; Liu, C.; Xie, C.; Wang, C., Fabrication of a superhydrophobic surface on a wood substrate. *Appl. Surf. Sci.* **2011,** *257* (22), 9362-9365.
62. Wang, C.; Piao, C.; Lucas, C., Synthesis and characterization of superhydrophobic wood surfaces. *J. Appl. Polym. Sci.* **2011,** *119* (3), 1667-1672.
63. Rowell, R. M.; Banks, W. B., *Water repellency and dimensional stability of wood*. Forest Products Laboratory, Department of Agriculture, Forest Service, Forest Products, 1985.
64. Guo, H.; Fuchs, P.; Casdorff, K.; Michen, B.; Chanana, M.; Hagendorfer, H.; Romanyuk, Y. E.; Burgert, I., Bio‐Inspired Superhydrophobic and Omniphobic Wood Surfaces. *Advanced Materials Interfaces* **2017,** *4* (1), 1600289.
65. Wang, Y.; Yan, W.; Frey, M.; Vidiella del Blanco, M.; Schubert, M.; Adobes‐Vidal, M.; Cabane, E., Liquid‐Like SiO2‐g‐PDMS Coatings on Wood Surfaces with Underwater Durability, Antifouling, Antismudge, and Self‐Healing Properties. *Advanced Sustainable Systems* **2018**, 1800070.
66. Desch, H. E.; Dinwoodie, J. M., *Timber: structure, properties, conversion and use*. Macmillan International Higher Education: 2016.
67. Keplinger, T.; Cabane, E.; Berg, J. K.; Segmehl, J. S.; Bock, P.; Burgert, I., Smart Hierarchical Bio‐Based Materials by Formation of Stimuli‐Responsive Hydrogels inside the Microporous Structure of Wood. *Advanced Materials Interfaces* **2016,** *3* (16), 1600233.
68. Cabane, E.; Keplinger, T.; Künniger, T.; Merk, V.; Burgert, I., Functional lignocellulosic materials prepared by ATRP from a wood scaffold. *Scientific reports* **2016,** *6*, 31287.
69. Ermeydan, M. A.; Cabane, E.; Hass, P.; Koetz, J.; Burgert, I., Fully biodegradable modification of wood for improvement of dimensional stability and water absorption properties by poly (ε-caprolactone) grafting into the cell walls. *Green Chemistry* **2014,** *16* (6), 3313-3321.
70. Fu, Q.; Medina, L.; Li, Y.; Carosio, F.; Hajian, A.; Berglund, L. A., Nanostructured Wood Hybrids for Fire-Retardancy Prepared by Clay Impregnation into the Cell Wall. *ACS Appl. Mater. Interfaces* **2017,** *9* (41), 36154-36163.

71. Boutilier, M. S.; Lee, J.; Chambers, V.; Venkatesh, V.; Karnik, R., Water filtration using plant xylem. *PloS one* **2014,** *9* (2), e89934.
72. Vidiella del Blanco, M.; Fischer, E. J.; Cabane, E., Underwater Superoleophobic Wood Cross Sections for Efficient Oil/Water Separation. *Advanced Materials Interfaces* **2017,** *4* (21), 1700584.
73. Zhu, M.; Li, Y.; Chen, G.; Jiang, F.; Yang, Z.; Luo, X.; Wang, Y.; Lacey, S. D.; Dai, J.; Wang, C., Tree‐inspired design for high‐efficiency water extraction. *Adv. Mater.* **2017,** *29* (44), 1704107.
74. Merk, V.; Chanana, M.; Gierlinger, N.; Hirt, A. M.; Burgert, I., Hybrid wood materials with magnetic anisotropy dictated by the hierarchical cell structure. *ACS Appl. Mater. Interfaces* **2014,** *6* (12), 9760-9767.

Acknowledgement

This thesis represents the end of the journey of my doctoral study. I wish to express my sincere gratitude and thanks to my Professor Ingo Burgert who gave me the opportunity to do research in his group, continuously supported me for more than three years and imparted me the knowledge about wood materials. I am also thankful to my advisor Etienne Cabane for his guidance, suggestions and supports during the various stages of my doctoral study, and especially for his encouragement when I was not confident. I am very thankful to Prof. Christoph Neinhuis and Prof. Cordt Zollfrank for being my co-examiners for the dissertation and the defense. I extend my appreciation to Prof. Nicolas Spencer for his generous offer of the access to the drop shape analyzer in the Laboratory of Surface Science and Technology and his helpful discussion. I would like to thank Dr. Karsten Kunze in ScopeM, ETH Zürich for his training and advising on SEM operation. Special thanks to all my colleagues for all the help and discussions, to all the coauthors of my papers for participating in my work. I also feel grateful to work with, Kunkun Tu, Marta Vidiella del Blanco, Selin Vitas, and Pavel Iliev who created so much joy and happiness during my doctoral study. I feel lucky to have Rui Xiong, Wenqing Yan, Philippe Grönquist, Ahmed Latif and Caifa Zhou who supported me so much during my Ph.D. study. Last but not least, I would like to thank my mother for being always supporting and encouraging.

Thank you!

Declaration

I, Yaru Wang, declare that this thesis is my own work and has not been submitted in any form for another degree or diploma at any university or other institute.
Information derived from the published and unpublished work of others has been acknowledged in the text and a list of references is given in the bibliography.